Roland Lachmayer · Dietmar Kracht ·
Volker Wesling · Henning Ahlers *Editors*

Generative Manufacturing of Optical, Thermal and Structural Components (GROTESK)

Generative Manufacturing of Optical, Thermal and Structural Components (GROTESK)

Roland Lachmayer · Dietmar Kracht ·
Volker Wesling · Henning Ahlers
Editors

Generative Manufacturing of Optical, Thermal and Structural Components (GROTESK)

Springer

Editors
Roland Lachmayer
Institute of Product Development
Leibniz University Hannover
Garbsen, Germany

Volker Wesling
Clausthal Centre for Material Technology
Clausthal University of Technology
Clausthal-Zellerfeld, Germany

Dietmar Kracht
Laser Zentrum Hannover e.V. (LZH)
Hannover, Germany

Henning Ahlers
Hochschule Hannover
Hannover, Germany

Preface

Additive Manufacturing is based on a layer-by-layer fabrication, opening up new possibilities for the creation of nearly arbitrary 3D objects from digital data by exploiting an unprecedented degree of design freedom. Within recent years, Additive Manufacturing has established for the industrial-grade production of complex mechanical parts giving rise for technological innovation and an individualized production under economic conditions. A field in which Additive Manufacturing is only slowly gaining popularity but offering enormous potential is the integration of optical systems, which are typically composed of a multitude of discrete optical elements in a rather complex optomechanic assembly. However, 3D printing of function-integrated optical systems has not matured yet as realizing macroscopic multi-material components with high precision remains a challenge.

Manufacturing optical systems using 3D printing—this is the goal of the innovation network "GROTESK—Generative Production of Optical, Thermal and Structural Components". The team is composed of partners from the Gottfried Wilhelm Leibniz University Hannover (LUH), the Clausthal Center for Material Technology (CZM), the University of Applied Sciences and Arts in Hannover (HsH) and the Laser Zentrum Hannover e.V. (LZH). By exploiting this multi-disciplinary research environment, a complete process chain for the production of integrated optical systems has been developed, which covers the following essential aspects in the context of Additive Manufacturing:

– Simulation and design of optical systems with a focus on the requirements analysis for materials and workpieces (sGROTESK, oGROTESK)
– Tailored materials and corresponding process development for the reliable production of superior multi-material components (wGROTESK)
– Additive Manufacturing of glass materials for functional optics (oGROTESK)
– Development of a novel machine concept for the processing of multiple materials in a single production environment (mGROTESK, wGROTESK)
– Concepts for function integration in sophisticated optomechanic systems to realize a material-, time- and cost-effective fabrication (wGROTESK, sGROTESK)

The objective of this book is to present the latest results in the context of 3D-printed optomechanical systems and additively deposited glass-based optics, as well as the future prospects in both fields. In order to demonstrate the capabilities of the Additive Manufacturing approach, a solid-state laser system including multi-material structural (e.g., optomechanics with integrated alignment options) and thermal components (e.g., laser crystal heat sink with integrated sensors for thermal monitoring) is 3D-printed and characterized.

Additive Manufacturing of fused silica glass materials, which are particularly interesting for 3D printing of high-quality optics, has gained interest in recent years due to the beneficial material properties. Chapter "Additive Manufacturing of Glass Materials for the Production of Optical, Thermal and Structural Components" addresses possibilities and limitations for the laser glass deposition technique in the context of optics manufacturing. Next to the fabrication and characterization of different functional glass optics, a process chain is presented including a discussion about automation of necessary pre- and post-processes.

Based on the combination of Additive Manufacturing with innovative construction design, Chapter "Additively Manufactured Polymer Optomechanics and Their Application in Laser Systems" determines the possibilities and limitations of 3D-printed optomechanics using polymers. Not only the extent to which commercial optics can be integrated stress-free into optomechanics was investigated, but also how integrated optomechanical systems consisting of several functional components can be manufactured additively. To demonstrate the capabilities, the sophisticated optical system of a solid-state laser is created from conventional and additively manufactured components and the properties of both systems are compared.

Chapter "Additive Manufacturing of Optics and Optomechatronics: Multiphysics Simulation Environments for Process, Materials and Design Analysis" of this book introduces a multiphysics simulation environment for modeling Additive Manufacturing processes. In particular, the laser glass deposition technique is being examined regarding a proper process parameter window. In addition, properties of functional elements of the mentioned solid-state laser system are simulatively characterized to define the requirements for new materials for the Additive Manufacturing.

Additive Manufacturing of multi-functional components like heat sinks for laser crystals require tailored materials with adapted thermal properties such as melting point and thermal expansion coefficient, since mechanical stress induced by thermal gradients can lead to damage of the crystalline structure. Chapter "Molybdenum Copper MMC for Additive Manufacturing of Thermal and Structural Components" presents novel molybdenum copper pseudo-alloys, which are suitable materials for laser crystals mounts being created in an Additive Manufacturing process, whereby the adaption of the material properties, as well as the appropriate bonding between alloy and crystal is considered.

Those novel pseudo-alloys are tailored to be processed by the well-developed Additive Manufacturing technique of laser metal deposition. Chapter "Additive Manufacturing of Optical, Thermal and Structural Components by Laser Metal Deposition" describes the challenges in 3D printing those materials and derives the matching process parameter. In addition, an intelligent process control is presented to enable the 3D printing directly onto a laser crystal.

Chapter "Development of System Technology for Coaxial Laser Material Deposition of Optical, Thermal and Structural Components" presents a novel machine concept for the combined laser-based processing of glass materials in fiber form as well as metal materials in wire and powder form. This machine environment is particularly interesting for the Additive Manufacturing of optical, thermal and structural multi-material components of optical systems. Not only the requirements of the different material classes on the laser beam source are taken into account, but also the appropriate process technology for material feeding and changing.

The book documents the current possibilities for the Additive Manufacturing of optical and optomechanical components with a focus to the production of combined and multi-material components. At the same time, it addresses the future research fields in order to further increase the achieved potentials.

Garbsen, Germany   Roland Lachmayer
Clausthal-Zellerfeld, Germany   Volker Wesling
Hannover, Germany   Henning Ahlers
Hannover, Germany   Dietmar Kracht

Contents

Editors and Contributors

About the Editors

Univ.-Prof. Dr.-Ing. Roland Lachmayer is the founding director and head of the Institute for Product Development at Leibniz University Hannover (IPeG). He is senator of the Leibniz University, speaker of the graduate school "Tailored Light", member of the scientific directorate of the Laser Zentrum Hannover e.V. (LZH), managing director of the Wissenschaftliche Gesellschaft für Produktentwicklung e.V. and since 2018 speaker of the EFRE-funded research network GROTESK. Since 2019, Prof. Lachmayer leads the task group Additive Manufacturing of the cluster of excellence PhoenixD. His publications to date include work on development methodology as well as numerous publications on additive manufacturing.

Dr. rer. nat. Dietmar Kracht is an Executive Director and the Speaker of the Board of the Laser Zentrum Hannover e.V. (LZH). He is a member of the Clusters of Excellence PhoenixD and QuantumFrontiers, the Clausthal Center for Materials Technology (CZM) and of the Board of Directors of the Hannover Centre for Optical Technologies. His main research interests are optical technologies, laser beam sources and their applications.

Univ.-Prof. Dr.-Ing. Volker Wesling is director of the Institute of Welding Technology and Separating Manufacturing Processes at Clausthal University of Technology (ISAF). Furthermore, he is a member of the executive board of the Clausthal Center for Materials Technology (CZM). He is a senator of the Clausthal University of Technology, a member of the scientific directorate of the Laser Zentrum Hannover e.V. (LZH) and board representative of the scientific society for joining technology e.V. (WGF). Within the scope of his research activities, he is primarily concerned with materials-oriented manufacturing technology.

Prof. Dr.-Ing. Henning Ahlers is Professor of Machining and Laser Manufacturing Technology, Machine Tools and Assembly Technology at Hannover University of Applied Sciences and Arts and Managing Director of LZH Laser Akademie GmbH in Hannover. He is head of the mGROTESK sub-project within the ERDF-funded GROTESK research network. He is a sub-project leader in the EU blueprint project Skills4AM and in several ERASMUS+ projects on the topic of additive manufacturing.

Contributors

Henning Ahlers Hochschule Hannover University of Applied Sciences and Arts, Hannover, Germany

Alexander Barroi Laser Zentrum Hannover e.V. (LZH), Hannover, Germany

Robert Bernhard Clausthal Center of Materials Technology, Clausthal University of Technology, Clausthal-Zellerfeld, Germany

Jana Budde Laser Zentrum Hannover e.V. (LZH), Hannover, Germany

Tobias Grabe Institute of Product Development (IPeG), Leibniz University Hannover, Garbsen, Germany

Jörg Hermsdorf Laser Zentrum Hannover e.V. (LZH), Hannover, Germany

Moritz Hinkelmann Laser Zentrum Hannover e.V. (LZH), Hannover, Germany

Christian Hoff Laser Zentrum Hannover e.V. (LZH), Hannover, Germany

Peter Jäschke Laser Zentrum Hannover e.V. (LZH), Hannover, Germany

Stefan Kaierle Laser Zentrum Hannover e.V. (LZH), Hannover, Germany

Dietmar Kracht Laser Zentrum Hannover e.V. (LZH), Hannover, Germany

Fabian Kranert Laser Zentrum Hannover e.V. (LZH), Hannover, Germany

Roland Lachmayer Laser Zentrum Hannover e.V. (LZH), Hannover, Germany;
Institute of Product Development, Leibniz University Hannover, Garbsen, Germany;
Cluster of Excellence PhoenixD (Photonics, Optics, and Engineering—Innovation Across Disciplines), Hannover, Germany

Marius Lammers Hochschule Hannover University of Applied Sciences and Arts, Hannover, Germany;
Laser Zentrum Hannover e.V. (LZH), Hannover, Germany

Philipp Neef Clausthal Center of Materials Technology, Clausthal University of Technology, Clausthal-Zellerfeld, Germany

Jörg Neumann Laser Zentrum Hannover e.V. (LZH), Hannover, Germany

Katharina Rettschlag Laser Zentrum Hannover e.V. (LZH), Hannover, Germany

Julian Röttger Institute of Product Development (IPeG), Leibniz University Hannover, Garbsen, Germany

Volker Wesling Clausthal Center of Materials Technology, Clausthal University of Technology, Clausthal-Zellerfeld, Germany;
Institute of Welding and Machining, Clausthal University of Technology, Clausthal-Zellerfeld, Germany

Henning Wiche Clausthal Center of Materials Technology, Clausthal University of Technology, Clausthal-Zellerfeld, Germany

Additive Manufacturing of Glass Materials for the Production of Optical, Thermal and Structural Components

Katharina Rettschlag, Fabian Kranert, Moritz Hinkelmann, Peter Jäschke, Stefan Kaierle, and Roland Lachmayer

1 Introduction and Motivation

One material that significantly influences and is indispensable to life in the modern age is glass. Glass is used primarily in everyday life in the form of window panels or drinking glasses, but also in special areas such as optics and laser technology in the form of lenses or special optical components for beam shaping and guiding.

By means of additive manufacturing it is possible to produce components with an almost unlimited complexity, which cannot be produced with conventional methods or only with a very high expenditure of time and money. Additive manufacturing opens up unimagined possibilities, especially in tool or prototype construction. For materials such as polymers and metals, sophisticated systems are already commercially available. [1, 2] For specially developed materials or materials with particularly challenging material properties, the processes must be adapted.

Processing glass using additive manufacturing technologies provides outstanding new possibilities for optics manufacturing, enabling a high novel potential of flexibility. An almost limitless degree of freedom would mean a revolution in optics manufacturing.

K. Rettschlag (✉) · F. Kranert · M. Hinkelmann · P. Jäschke · S. Kaierle · R. Lachmayer
Laser Zentrum Hannover e.V. (LZH), Hollerithallee 8, 30419 Hannover, Germany
e-mail: k.rettschlag@lzh.de

K. Rettschlag · R. Lachmayer
Institute of Product Development, Leibniz University Hannover, An der Universität 1, 30823 Garbsen, Germany

K. Rettschlag · F. Kranert · M. Hinkelmann · S. Kaierle · R. Lachmayer
Cluster of Excellence PhoenixD (Photonics, Optics, and Engineering—Innovation Across Disciplines), Hannover, Germany

Parts and components with specially designed optical properties can be manufactured faster, with lower material consumption and in a more targeted manner compared to the previously established manufacturing technology.

In this chapter, a process developed at the Laser Zentrum Hannover e.V., Laser Glass Deposition (LGD), is applied and adapted to the additive manufacturing of functional glass optics. For this purpose, different optical components are fabricated and investigated for their optical, stress-optical and geometrical properties. In addition, measurements are performed for the reproducibility of the glass components and for monitoring the manufacturing process. Following successful adaptation of the fiber extrusion process, a process chain will be created with a description of what pre-, in- and post-process stages are necessary to obtain functional additively manufactured glass optics. If possible, the manufactured optics should no longer undergo manual post-processing, which must be taken into account in the process chain.

At the beginning, the essential basics of the materials used and the process applied are described. This also includes a description of the main process parameters and monitoring systems. In the following Sect. 3, the experiments carried out for the different optical components are presented. In Sect. 4, the results obtained are highlighted and the components are examined for their properties and functionalities. Finally, the process chain is presented based on these findings and the chapter is summarized.

2   State of the Art

Below is a comprehensive overview of potential materials used in optics due to their outstanding material properties. In addition, different processes are presented with which additive manufacturing of glass can be realized. Likewise, the selection of a suitable process and a detailed explanation is given in this section.

2.1   Glass in Optics and Laser Technology

Glass materials have been used in optics and optical technology for decades to centuries. With the use of developments from laser technology, the demand for high-precision optics in wavelength ranges from the far UV to the far IR became ever greater. Materials engineering responded by developing specialty glasses for use in high-precision optics. [3] Today's commercial optical glasses from which lenses are made include N-BK7 (boron crown glass), fused silica, and N-SF11 (flint glass). In addition, a wide variety of other materials are used for optics, including germanium, zinc selenite, potassium fluoride, or silicon. [4]

Many special glasses contain substances that are harmful to health, which can evaporate during processing and cause subsequent damage to health. For this reason, materials such as germanium, zinc selenide, and even the fluorides are not selected for processing.

Fused silica has advantages over other glasses due to its outstanding optical properties, but also its thermomechanical resistance and high heat transfer coefficients. Likewise, fused silica is the most commonly used glass material, and silica sand is the most important glass raw material in optical fiber fabrication. [5] For these reasons, process development and adaptation will be carried out starting with fused silica.

2.2 Properties of Fused Silica

Fused silica is one of the standard materials in laser technology and photonics. In contrast to other commonly used glasses, this glass material does not contain any added components of sodium carbonate and calcium oxide, but consists almost exclusively of pure silicon dioxide. Almost exclusively, because depending on the manufacturing process or the starting material impurities can occur. The outstanding properties of the material are particularly interesting for laser technology and photonics. Fused silica is optically transparent in the range from 170 nm to 5 μm [6], which means that it is used for the majority of optical applications with different doping levels. In addition, fused silica has a low coefficient of thermal expansion of 0.54×10^{-6} K^{-1} [6] and high thermal shock resistance compared to other glasses. A third key property is high chemical resistance to acids with the only exceptions being hydrofluoric acid and phosphoric acid. [7]

The property that challenges the processing of fused silica is the comparatively high processing temperature (compared to other glasses). For pure fused silica, this is definitely above 2000 °C. Depending on the degree of impurity or doping, the processing temperature can still be lowered, but usually settles around 2000 °C. [6]

2.3 Technologies for Additive Manufacturing of Glass

Similar to the additive manufacturing of metals, additive glass manufacturing can also be implemented with different process strategies. Almost all of these processes are still at the research and development stage, with a few exceptions such as the Glassomer technology. All processes for additive glass manufacturing can be divided in a first subdivision into processes with bonding materials and processes without bonding materials.

At the beginning, the processes with binders are presented. Each of these processes includes a subsequent process step from the outset, in which the binder material must be baked out and removed. In the case of the Glassomer already mentioned, for example, this process step is always necessary. The binder material, which is contained in the glassomer starting material, is cured layer by layer in the desired form using a stereolithography or

a two-photon polymerization system for polymers. Afterwards, the polymer is heated out of the structure. Almost transparent glass components with a high resolution in the range of tens of micrometers can be manufactured with this process. For the design of the components, however, shrinkage must be taken into account beforehand. The production of individual parts requires production times of up to 24 h and more. A further limitation is the small design space of the processes used. [8, 10]

Another possible process is the stereolithography with glass pastes. Here, the glass particles are embedded in a polymer matrix. As with the Glassomer process, additive manufacturing is used to cure the polymer to create the shape, which is subsequently heated out again. The result is glass components with high resolution. However, the process limits its potential use in optics, due to the risk of defect formation and inclusion formation. [9]

Further processes are carried out without bonding materials. This category of additive glass manufacturing can be divided into three types of processes. Starting with Glass 3D Printing: Here, the glass material to be processed is heated so that the viscosity is low enough to allow it to flow. The low-viscosity glass is placed in a container on the axis unit of the system and then processed. Using a funnel, the glass is deposited layer by layer onto a substrate, similar to polymer-based fused deposition modeling. The resolution of Glass 3D Printing is limited by the opening of the funnel, which defines the layer thickness of the applied layers. The layer structure of the manufactured components is clearly visible and the resolution is not small enough for complex structural components. However, it has already been shown that transparent design objects can be finished using this process. [11, 13]

There are also powder-based processes for additive glass manufacturing. These are based on Selective Laser Sintering (SLS) or Laser Powder Bed Fusion (LPBF). This process is based on the principle of SLS of polymers or LPBF of metals. The material in a powder bed is fused in layers laser-based and the structure is built up. The resolution that can be achieved with this process is limited by the particle size used, but high-resolution components can be manufactured. Due to the many voids between the individual glass powder particles, only glass components that are very milky or porous can be produced up to now, whereby the transparency is strongly influenced. The enclosed cavities and defects are difficult or impossible to bake out without affecting the structure or function of the manufactured component. [12]

The third process technology is the fiber-based extrusion process, also known as LGD. For this process, glass fibers or rods of different properties and thicknesses are used as starting materials and applied laser-based in single layers [14, 15]. The exact mode of operation of the process technology is explained in more detail in the following Sect. 2.4.

2.4   Laser Glass Deposition

As already mentioned in Sect. 2.3, the LGD method is applied for the work described here. The advantages of this process especially lie in the starting material. Glass fibers or glass rods with different diameters are used. This allows pure glass material to be processed without additional bonding materials. Only the polymer coating of the glass fibers is necessary to guarantee a break-free feeding of the fiber into the process zone. This coating is evaporated without leaving any residues due to the prevailing high process temperatures of over 2000 °C [16]. This could also be proven in [17] with the aid of SEM investigations.

Figure 1 schematically illustrates the functional principle of the LGD process. All relevant process parameters and components are marked in this illustration. The adjustable parameters are considered in more detail in the following Sect. 2.5.

The basic principle of the process is based on laser deposition welding of wires or fibers, as is already widely established for metal processes. For the processing of glass, the process has to be adapted to the changed material properties and the resulting process characteristics. The LGD process is a CO_2 laser-based process (10.6 µm wavelength), for melting the glass fibers and applying them layer by layer. The fibers to be processed are fed laterally under an angle into the process zone and the laser radiation is emitted coaxially to the glass substrate. The introduced laser radiation is focused via a lens. In order to achieve a homogeneous energy input into the fiber and the glass substrate and no vaporization of the material, a defocused beam with a diameter of approx. 4 mm is used. For positioning and generation of a direction-independent deposition a 3-axis system with an additional rotation axis is used. With this setup, a direction-independent manufacturing
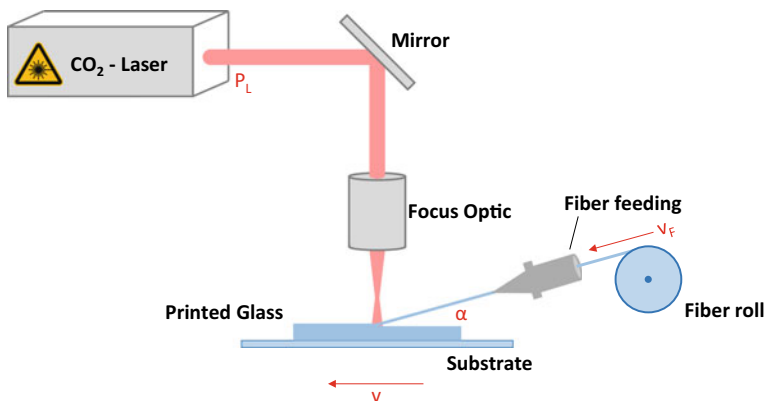

Fig. 1 Schematic drawing of the experimental principle of laser glass deposition with identification and naming of the main process parameters

of optical and structural components in a continuous process is possible. In first works, a successful processing of the glass material could be demonstrated. [18, 19]

The fused silica fibers used in this work are coreless fibers or core fibers with a glass material diameter of 400 µm and a polymer coating of 50 µm. These fibers are printed in different shapes and structures on fused silica substrates with different thicknesses between 2 and 5 mm.

2.5   Process Parameters

The following process parameters will become relevant during the manufacturing process of the oGROTESK project (optics systems by generative manufacturing of OTS components). An essential adjustment parameter is the laser power P_L, which is varied for changes in the energy input. The high-power CO_2 system used (Rofin DC 045) allows a maximum optical output power of 4.5 kW. However, for the work described here, only power levels up to 200 W are required, necessitating heavy throttling of the system. [17–21]

Two further parameters are the speed rates of the axes v and the feeding speed of the fiber v_F. These and the correlation between them are investigated for the different components to be printed, such as waveguides, sphere lenses and volume components. In addition to the possibility of varying the energy input via the laser power, adjustments can also be made by changing the speeds. Which parameters were determined for which manufactured components will be considered in detail in the following sections.

3   Experiments

Within the oGrotesk project, three different components are investigated, waveguides, spherical lenses and volume components. For this purpose, basic parameter studies are carried out at the beginning. Based on these studies, specific parameter sets are selected in order to be able to manufacture functional optical components. The properties of these components are subsequently investigated and evaluated in order to verify their functionality and to be able to adjust the parameters.

3.1   Parameter Studies

For a better understanding, the parameter studies are split up into the components to be manufactured within this chapter. Thus, the studies are described starting with the waveguides, and then move to the spherical lenses and finally the volume components.

Waveguides: Preliminary work on the process development of LGD has already been carried out at the Laser Zentrum Hannover e.V. (LZH) consisting of a laser welding process of glass [14]. In addition to the LZH investigations, initial investigations have also been carried out using the fiber extrusion process from [22], showing highly promising results. Based on these preliminary investigations, parameter studies for a manufacturing of functional waveguides are carried out. A major difference between the process and the preliminary investigations is the fiber geometry, i.e. the fiber cross-section. This must remain almost completely intact for a functional waveguide. However, the fiber must be heated sufficiently to ensure a bond with the silica glass substrate. For this purpose, a study was carried out to narrow down the range of suitable parameter sets. This was done for both coreless fibers (HSQ300 Fibers) and core fibers (Optran® WF), since a change in the fiber coating also results in a change in the suitable parameter set due to the changed polymer properties of the coating. Results in a power range of 90–120 W and a velocity ratio of 1:1 for a deposition of functional waveguides.

Following the printing process, the waveguide ends must be cleaved in order to obtain an optical end face. The setup and execution of this cleave process is described in detail in [17]. This is necessary to be able to couple in and out of the fiber without losses (except for the Fresnel losses). This process step was carried out in cooperation with the sGROTESK subproject.

Sphere lenses: Based on the parameter studies for waveguides, experiments for the manufacturing of glass sphere lenses are carried out. For these studies, another parameter is crucial, the distance of the fiber feed nozzle to the substrate surface h. In addition, the deposition process differs from that of the single fibers. The radiation of the CO_2 laser softens the fiber end. A viscous glass sphere is formed at the fiber end via a constant material flow. This glass sphere is deposited on the substrate surface (Fig. 5). The height h defines the time of deposition and thus the size of the deposited spherical lens. For this lens production, the same parameter sets are used as for the waveguides and the nozzle height h is varied over a range of 4 mm.

Volume parts: The volume components were manufactured after the waveguides and spherical lenses. Thus, it was possible to base on the previously gained experience from the deposition of single layers. For an investigation of the deposition of several layers, a further parametric study was carried out. Using a statistical design of experiments and the knowledge from previous investigations, a number of 25 tests were performed in a limited parameter range. These tests serve to further narrow down the parameter range and to define possible quality levels of the printed components. For this purpose, wall structures consisting of twelve glass layers with a length of 35 mm were manufactured. The structure length was calculated for the dimensions of the substrates. To determine the quality levels, the wall structures were tested for the fusion of the individual layers with each other. These tests and the evaluation of the manufactured samples result in the quality levels shown in Fig. 2 below. [21]

	135 W	141 W	146 W	152 W	158 W
90 mm/min	2	3	4	4	5
108 mm/min	1	2	3	4	4
120 mm/min	1	2	3	4	4
144 mm/ min	1	2	3	3	4
180 mm/min	1	2	2	3	3

Number	Definition
1	Low fusion Detaching of the fiber
2	Slight fusing Partially optically transparent Nearly Regular surface
3	Optically transparent Fusion of the layers Regular surface
4	Strong fusion Optically transparent Unregular surface
5	Sublimation

Fig. 2 According to [21] parameter sets for preliminary study for volume components with marked quality zones (left); Definition of the different defined quality zones (right)

3.2   Waveguides

The coreless fibers described above are currently being used for initial investigations into the production of functional waveguides. For this purpose, the fiber is guided laterally into the process zone at an angle of $\alpha = 40°$. The fibers are deposited on substrates with thicknesses of 2–3 mm. To guarantee a constant material flow in the process zone, the axis speed and the fiber feeding speed are set to the same value of 90 mm/min. In order to guarantee subsequent processing of the fiber ends, the deposition process is started 5 mm before and after the substrate so that the overhanging fiber can be cleaved and the fiber ends can be polished with a CO_2 laser. The laser power is set to 130 W. [17]

Thus, coreless waveguides could be manufactured in straight and curved shapes. The curved waveguides were made in an S-curve with radii of 6, 8, 10, 50 and 60 mm. [17, 20]
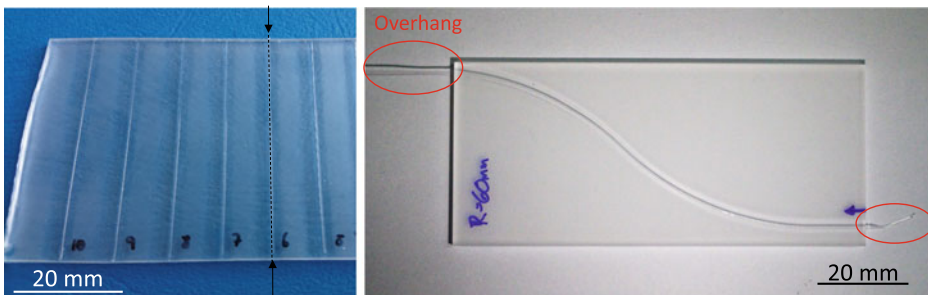

Fig. 3 Left: Six printed coreless straight waveguides side by side with a length of 50 mm [17]. Right: Printed coreless curved waveguide with a curvature radius of 60 mm [20]
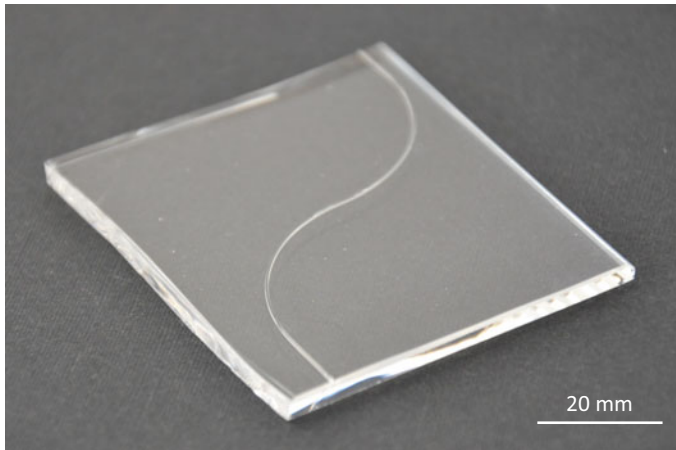
Fig. 4 LGD printed functional waveguide with a fiber core and a radius of curvature of 19 mm. The fiber ends were subsequently cleaved and polished in cooperation with sGROTESK

Figure 3 shows examples of printed straight coreless waveguides with a length of 50 mm [17] and curved coreless waveguides with a radius of curvature of 60 mm [20].

Subsequent to the coreless fibers, core fibers were also deposited by means of LGD in order to reduce the possible losses occurring and to take advantage of the light-conducting properties of the starting fiber. The core fibers were manufactured with the same parameters as the coreless fiber. Only the process gas had to be changed from compressed air to oxygen in order to be able to completely burn the coating, since that of the core fibers is more temperature-resistant than the one of the coreless fibers. The core fibers were also printed in straight and curved form. Here, the lengths are between 50 and 80 mm. The radii of curvature of the manufactured S-curves are 19 mm. Figure 4 shows a curved core fiber printed on a 3 mm thick substrate.

3.3 Sphere Lenses

For the manufacturing of functional spherical lenses, the feed angle of the fiber feeder α is kept constant at 45° to the substrate. The starting material used for these experiments was the coreless glass fiber HSQ300 fiber from Heraeus GmbH & Co. KG. The glass substrate used is GE 214 from Schröder Spezialglas GmbH with dimensions of $100 \times 100 \times 3$ mm^3. The laser power and the axis and fiber conveying speeds are kept the same as the values for the production of waveguides, as previously described in 3.2. Only the nozzle height h is varied in order to adjust the diameter of the sphere lenses and thus the focal length of the optics.
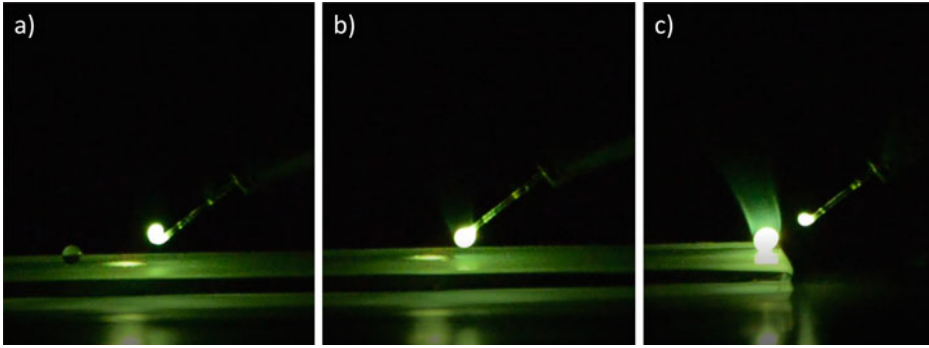
Fig. 5 Deposition process of glass sphere lenses: **(a)** Initial forming of a viscous glass sphere at the fiber end. Pulling up of the fiber due to the prevailing surface forces caused by the laser irradiation from the top; **(b)** Completely viscous glass sphere at the fiber end; **(c)** Deposition of the glass sphere on the substrate and formation of a new sphere at the fiber end

At the end of the input fiber, the glass sphere to be deposited is formed in the process zone (Fig. 5a). This glass drop is completely viscous. As soon as the sphere surface and the substrate surface are in contact, the sphere is pulled off the fiber end (Fig. 5c). The prevailing surface forces create a nearly round spherical shape. In this shape, the glass sphere cools immediately after leaving the process zone. As soon as a glass sphere is deposited on the substrate, a new viscous sphere is formed at the fiber end due to the continuously irradiated laser radiation. [19]

From first parameter studies [18], the height of the fiber nozzle to the substrate could be narrowed down to the range of 6–9 mm. For the following described results, $P_L = 147$ W was chosen for the laser power and v, $v_F = 90$ mm/min for the axis and fiber feeding speed. The distance h was varied between 6 and 9 mm in 0.5 mm steps. These parameter sets were used to investigate the reproducibility of the glass sphere within a process run and in comparison of the process runs to each other (seven in total). Here, the height $h = 6$ mm represents the lower limit at which just initial spheres can be formed, but lines can still be printed sequentially. With $h = 9$ mm, the upper limit is defined, in which the spheres can no longer be formed larger, since the gravity force for pulling the sphere off the fiber is predominant. [19]

In order to obtain the same initial conditions for each process run, the fiber is cut off before each process run and a defined stickout of 5 mm is set. This is to ensure that the spheres are always deposited in almost the same position. [19]

3.4   Volume Components

Based on the preliminary investigations described in 3.1, further experiments will be carried out to additively manufacture wall structures from fused silica. An essential focus for the evaluation is placed on the height of the individual layers, since the surface properties of the walls are defined by the layer geometry. In addition, the layer height can be used to determine the process speed. The height of the layer can be adjusted on the one hand by moving the Z-axis, but also by the rate of fusion during the printing process. For this, the process parameters must be well adjusted to each other. [21]

Before printing a wall structure, the height of a single printed layer is defined for the individual parameter sets. Based on this, the theoretical wall height is determined for a defined number of layers, which is compared with the real wall height. Within a manufacturing process, the set layer height and thus the travel distance of the Z-axis is kept constant after each layer is deposited. All structures are printed in a dragging manner, which means that the direction of deposition of the fiber corresponds to the direction of movement of the axis. [21]

A comparison is also made between a wall structure manufactured with a material input at a speed ratio of 1:1 and a wall structure manufactured with a disproportionate material input. For these investigations, the parameter sets shown in Table 1 were selected. [21]

The evaluation of the manufactured walls shows clear differences, especially when considering different material inputs. In the following Fig. 6, for example, walls are shown with a 1:1 material input on the left and with a twice as high material input on the right. [21]

Especially in the bonding of the individual layers to each other and in the transparency of the samples, clear differences in the qualities can be observed.

Table 1 Parameter sets for the manufacturing of different wall structures. 1–3 with a material input of 1:1; 1–6 with a disproportionate material input

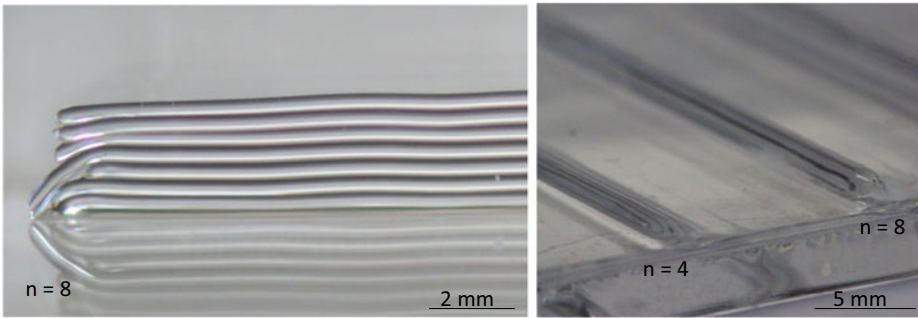| Parameter set	Laser power [W]	Axis speed [mm/min]	Fiber feeding speed [mm/min]	Number of layers
1	135	90	90	1, 2, 4, 8
2	141	90	90	
3	146	90	90	
4	158	90	180	1, 4, 8, 16
5	163	90	180	
6	169	90	180	

Fig. 6 Left: Image of a printed wall structure of parameter set 2 consisting of eight layers. Right: Illustration of printed wall structures of parameter set 5 consisting of four layers on the left and eight layers on the right [21]

3.5   Process Monitoring

A pyrometer (MAURER KTR 1550 1) is integrated into the system design for inline process monitoring. The measuring spot of this pyrometer is directed to the process zone in order to detect and evaluate the temperature profile during a process run. The arrangement of the pyrometer within the system is shown in Fig. 7.
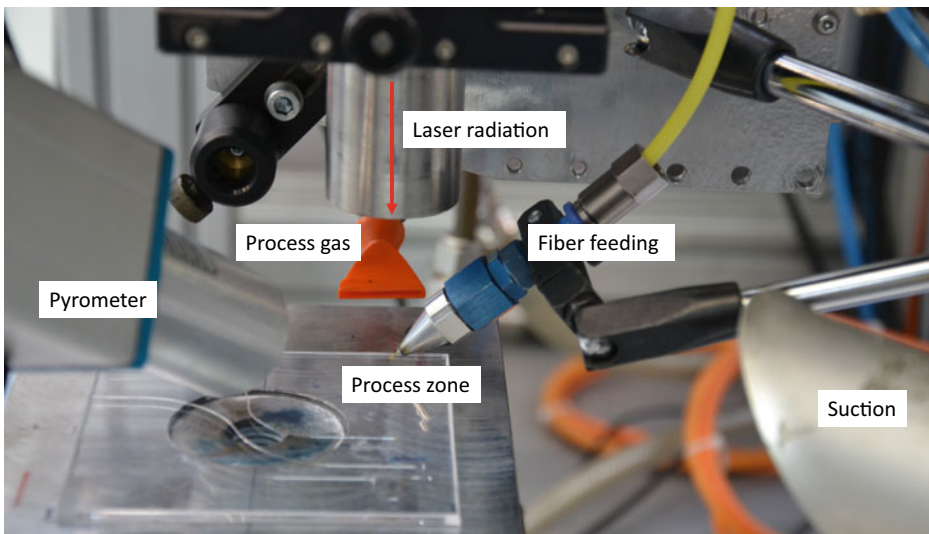

Fig. 7 Image taken from the process zone of the current process setup for additive glass manufacturing with the individual components named

The pyrometer used can accommodate a temperature range from 300 to 2500 °C. This wide temperature range is necessary to record the entire process of printing fused silica, since the softening temperatures are in the range of 1600–1710 °C and the processing temperatures beginning at 2000 °C as described in Sect. 2.2. The spot diameter of the pyrometer is 1.5 mm. The recorded temperatures are therefore an average of the temperature values detected in this spot. To increase the accuracy of the measurements, the optics of the pyrometer can be exchanged to create a smaller spot.

Furthermore, the inline measurement of the pyrometer can be used to actively control the process. By measuring the temperatures within the process zone, the viscosity of the glass and thus the quality of the deposited layer can be determined. With an active control of the laser power via the measured temperatures, components with consistent qualities can be manufactured.

4 Results and Sample Evaluation

In the following sections, the different evaluation methods for the manufactured components are presented and the main results are described. The tests were carried out for the waveguides, spherical lenses and volume components. In order to avoid presenting all measurement methods for each of the components, selected measurements are shown for explanation. In the course of the oGROTESK project, a large number of measurements were carried out, which cannot be all explained in detail here.

4.1 Temperature Detection

The temperatures of the individual process runs are recorded for subsequent comparison among the individual manufacturing processes and comparison with the constructed simulation (comparison Chap. 3 "Additive Manufacturing of Optics and Optomechatronics: Multiphysics Simulation Environments for Process, Materials and Design Analysis"). For the waveguides, a characteristic curve is formed quickly; at the beginning of the process, the temperature rises sharply to a maximum value and then remains constant throughout the entire deposition of the fiber (Fig. 8). If unevenness or outliers occur within the graphical progression of these measurements, it is an unstable process run, which can also be seen in the printing result.

The graphical temperature profile of the spherical lenses shows some differences compared to the waveguides. Likewise, each process run is detected also for different sphere sizes. The graphically prepared measurements of the smallest spheres, i.e. with a distance h of the fiber nozzle to the substrate surface of 6 mm, and of the parameter set with $h = 7$ mm are exemplarily shown in the Fig. 9. For both processes, the laser power of 147 W and traversing speeds of 90 mm/min are identical. [19]
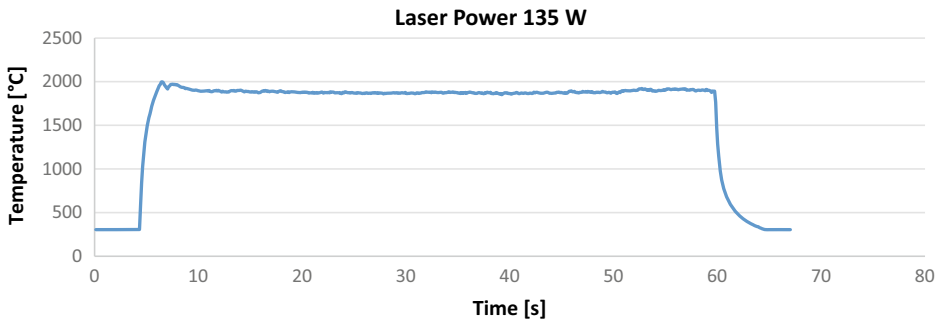
Fig. 8 Exemplary temperature curve of a deposited straight waveguide at a preset power of 135 W
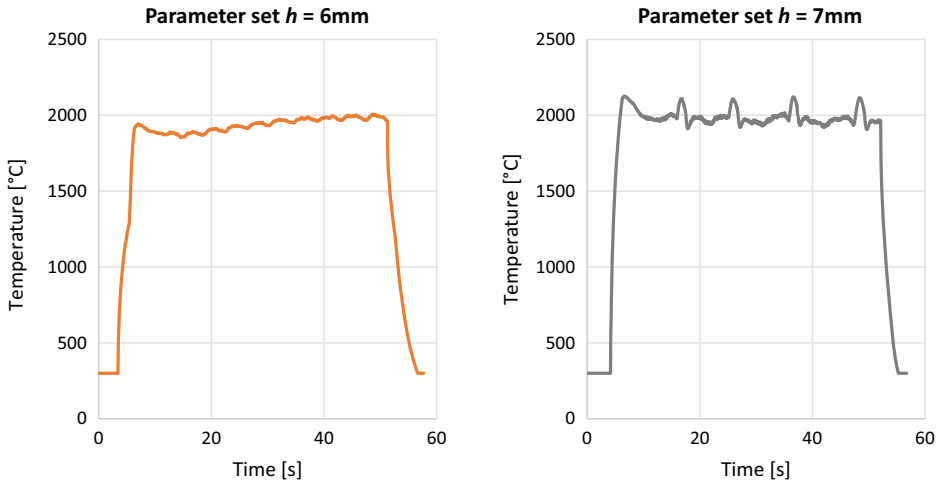

Fig. 9 Left: Graphical illustration of the measured temperature for the fiber nozzle height of 6 mm. Right: Graphical illustration of the measured temperature for the fiber nozzle height of 7 mm [19]

It is noticeable from these profiles that there is no constant temperature during the process, as is the case with the waveguides, but that individual slight waves (Fig. 9 left) or clear peaks (Fig. 9 right) occur. The number of waves or peaks corresponds to the number of glass spheres deposited during the process. The height of the waves and peaks also varies with the size of the deposited spheres, the waves representing the smaller spheres and the peaks the larger ones. One assumption about the occurrence of these patterns is that during the formation process of the spheres for the period of deposition, more material is available in the process zone into which the laser radiation is coupled in.

This results in a larger area of viscous glass material within the measuring spot of the pyrometer, which means that for a short time the averaged temperature is a significantly

higher value than before. This larger amount of material during sphere deposition can be clearly seen in Fig. 5c on the right. [19]

For the volume components, the temperature measurement curve is similar to that of individual fiber deposits, except that after each deposited fiber, the separation process takes place, causing the temperature to rise briefly, and then the system returns to the starting point, causing the temperature to drop until the new layer is printed.

4.2   Reproducibility

The reproducibility is also investigated in order to compare the manufactured components with each other. When manufacturing waveguides, it is crucial that no defects occur within the structures or that the fiber is too deliquesced, otherwise the optical properties cannot be maintained.

For the production of spherical lenses, reproducibility is even more decisive, since the optical properties such as the focal length are defined with the shape of the sphere and the sphere diameter. In order to be able to predict which sphere diameter can be produced with which parameter sets and output fibers and how uniform this production is, each individual deposited sphere is measured. The diameter is measured both horizontally and vertically in relation to the top view. The measurement of the individual glass spheres shows irregularities. The diameters of the glass spheres manufactured in one process run show partly strong variations, as can be seen for a selected parameter sets in the Fig. 10. There, the averaged diameters over a process run are plotted with the associated standard deviation. [19]

With the coreless fiber with a diameter of 400 μm, spheres with diameters between 1.3 and 1.5 mm can be produced for the set nozzle heights between 7 and 8 mm. If the diameters of the starting fibers are varied, it is expected that other sphere diameters can also be manufactured with good reproducibility. The formation process of the spheres will probably be the same for each starting fiber, only the diameter of the viscous glass sphere for deposition can be changed. Within the parameter sets, the diameters of the manufactured glass spheres vary strongly, so that deviation up to 4% belongs to the best results. This tolerance is clearly too high for precise manufacturing of optics. Possible error indicators still have to be determined and the influences eliminated. In addition, a change of the feed angle α between 30° and 50° could not achieve any improvement. Another assumption is that the surface condition of the substrate has a great influence on the deposition strategy of the sphere, respectively on the possibility of adhesion of the glass spheres. The substrates used for these investigations are gas flame polished and have a slight waviness but smooth surfaces. This makes it difficult for the sphere to adhere. Possible improvements could be achieved here by roughening the surface. [19]
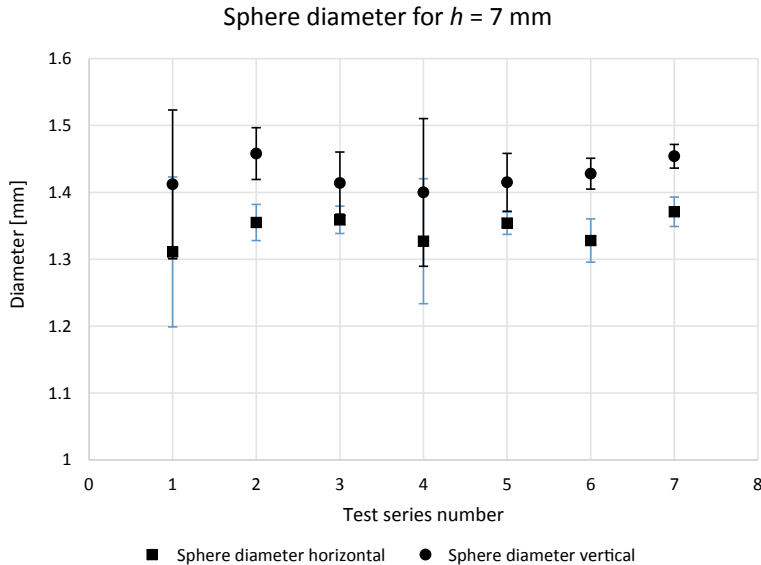
Sphere diameter for *h* = 7 mm

Fig. 10 Graphical representation of average sphere diameters of individual process runs for the parameter set with nozzle height h = 7 mm. The diameters were measured in horizontal and vertical direction related to the top view [19]

4.3   Stress Measurements

All manufactured samples are evaluated with a polarimeter (StrainMatic M4/140, ilis GmbH) in order to investigate the internal stresses generated by the process and to detect possible differences. Likewise, this measurement method is well suited to check whether post-processing methods achieve a reduction of the internal stresses.

Processing glass at very high temperatures creates stresses in the material after the components have been cooled, which cause a change in the optical properties, i.e. refractive index variations. During the production of functional waveguides, only individual fibers, i.e. single layers, are deposited. After depositing just one fiber, stresses of up to 15.5 MPa are present in the glass [20].

Due to the process, the material for the production of the spherical lenses is also irradiated only once, as in the case of the waveguides, which also results in stresses of up to 15.5 MPa. These stresses generate an optical path difference of up to 105 nm. [18]

Applying several layers for the manufacturing of volume components means multiple light exposure of the substrate and already deposited material, thus higher stresses are expected after the printing process. Measurements have shown that these components have internal stresses of up to 17 MPa and higher. [21]

Initial post-annealing processes have shown that a reduction of stresses is feasible, but so far no complete tempering (laser-based) was possible. Further investigations on this will follow.

4.4 Measurement of Optical Transparency

Waveguides: One of the most decisive evaluation methods is the optical evaluation also explicitly for the waveguides in order to be able to verify the optical function of the components. This allows to test whether the function of the fiber is maintained after the deposition process. A theoretical maximum transmission through fused silica fiber is 93%, since 3.5% Fresnel reflections have to be considered at each end face. For the coreless waveguides, a review of the optical properties was performed in [18] for straight shapes and in [20] for curved shapes. For the straight waveguides, it was detected that up to 86% of the coupled radiation can be transmitted through the straight waveguides [18].

In the case of the curved waveguides in the form of S-curves, no transmitted radiation was measured for the very small radii of 6, 8 and 10 mm. Presumably, for the material here, the limit radius at which total reflection can still occur is underrun, so that all the radiation to be guided is coupled out. At curvature radii of 50 mm, a maximum of 27% transmission was measured, which corresponds to an optical attenuation of 0.57 dB/cm. This low value is probably due to high coupling out of the fiber into the glass substrate, since light cannot be guided in a fiber core. Increasing the radius to 60 mm allows transmission of up to 68% of the coupled radiation, which corresponds to an optical attenuation of 0.169 dB/cm. All measurements of the straight and curved structures were performed with a fiber-coupled single-mode laser diode of the wavelength 1064 nm. [20]

Transmission studies were also carried out for the core fibers. A measurement of the initial fiber resulted in a transmission of 98% after deduction of the Fresnel reflection. The straight deposited fibers allow a transmission of the radiation of 93%. This value is lower than expected. After a more detailed examination of the fibers, it was found that small defects are present within the waveguide, which presumably act as scattering centers and thus reduce the transmissivity value. The S-curves with a radius of 19 mm still transmit 46% of the coupled radiation. This value is already significantly better than that of the coreless fibers. Whether the still significant losses occur because the radius of curvature is too small or because small defects are still present in the fibers must be clarified in the future.

Sphere lenses: Like the waveguides, the spherical lenses were transmitted with a single-mode diode of the wavelength 1064 nm for the optical analysis (BF-A64-0180-S5F, Sheaumann Laser Inc.). The spherical lenses will function as collimating optics in this case. The spheres are mounted on a three-axis stage. A beam camera is set up behind the sphere to be measured in order to be able to analyze the beam profile behind the
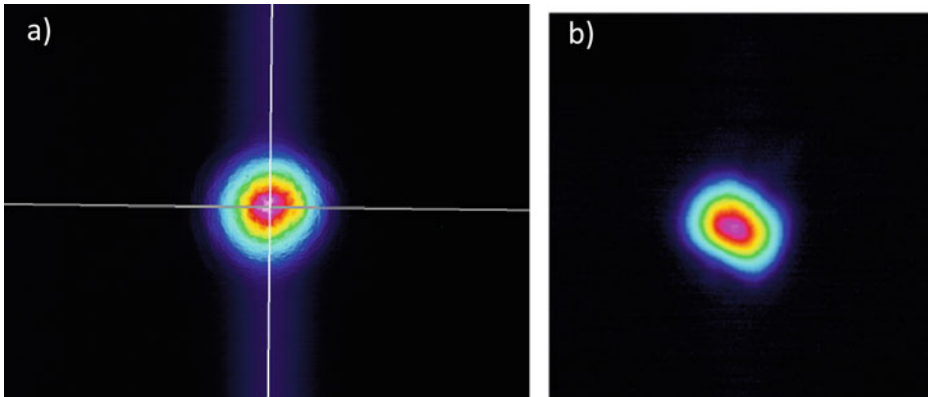
Fig. 11 Beam profile measurements detected with a beam camera. **(a)** Cross-section of the beam profile of the single-mode diode; **(b)** Cross-section of the beam profile after passing through the spherical lens of the parameter set h = 7 mm [19]

sphere. For this measurement, the spheres must be positioned precisely on defined areas of the substrate. For a calculation of the focal lengths of the spheres, the beam camera is positioned at several positions with different distances to the sphere and the profile is measured. It can be clearly seen in the images that the spherical lenses have an optical effect, but that imaging aberrations still occur (Fig. 11). The Gaussian intensity distribution remains, but the almost ideally round beam cross-section of the single-mode diode is no longer present. Behind the spherical lens, the beam cross section exhibits an elliptical shape. [19]

This effect can be explained with regard to the reproducibility of the sphere. All manufactured spheres have a slightly elliptical shape, which is caused by the manufacturing process and could not yet be completely eliminated. The shape of a spherical lens has a significant influence on the optical quality. If the shape is not ideally round, the transmitted radiation will also not have a round beam cross-section. Thus, for further improvements in the manufacturing of glass spherical lenses, a way must be found to reduce this elliptical preferred direction. [19]

Volume parts: For the volume components, a fundamental investigation was carried out to determine whether it is possible to manufacture components without visible boundary layers in order to realize a transparency for the human eye in a first step. For this purpose, a wall structure consisting of 80 layers was created in an endless process. The process parameters used were selected as follows: Laser power of 163 W, axis speed of 90 mm/min, fiber feed speed of 180 mm/min and fixed layer height of 0.15 mm. These chosen parameters are based on the experiments described in Sect. 3.4. This fabrication of a multi-layered wall is intended to investigate the fabrication quality over the part height with constant parameters. [21]
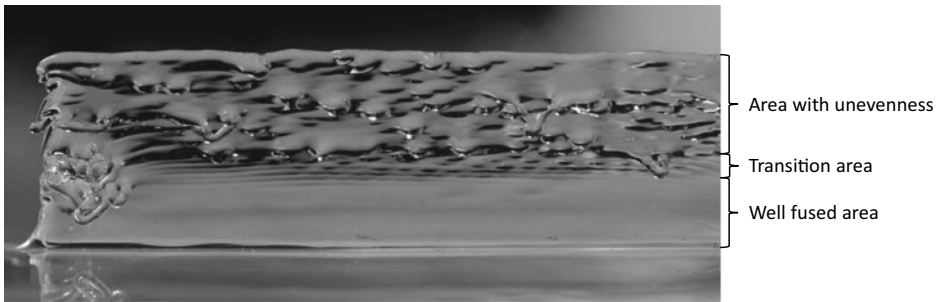
Fig. 12 Result of the endless wall printing process of 80 layers with the named quality ranges [21]

It is noticeable here that different quality zones have formed within the manufactured component. Within the first estimated 30 layers, the material is completely fused, so that no boundary layers are visible. After these layers, however, a transition zone occurs in which the boundary layers become increasingly clear from layer to layer (Fig. 12). Presumably, the thermal management is no longer ideally balanced here, so that the layers fuse well together. The last zone, the upper structural region, shows very high unevenness in the deposited layers. This unevenness in particular significantly reduces the transparency of the finished wall. [21]

A possible factor for this effect is that a reduction of the process temperature occurs with the component height at constant process parameters. Due to a reduced temperature in the process zone, the glass material is no longer low viscosity enough and is pushed out of the process zone. This effect could be remedied, for example, by gradually increasing the laser power or actively controlling the laser parameters via temperature detection. [21]

5 Process Chain

The process chain for additive manufacturing of glass components can be set up in a first draft based on the test results presented here. This process chain is composed of three essential steps: Process preparation, process run and post-processing of the manufactured samples. Based on VDI 3405 [23], a subdivision is made into pre-process, in-process and post-process.

No special process or sample preparation was carried out for the tests performed here. Only surface impurities were removed from the glass substrates. Depending on the function and shape of the components to be manufactured, different requirements for the substrate surfaces emerged in the course of the parameter studies. For the waveguides, the substrate must be cleaned and as free as possible from irregularities. The substrate edges must be straight and may not have any curves or phases, as otherwise the fiber end can only be deposited in a downward position.

For the manufacturing of the spherical lenses, slight unevenness, as in the case of a glass substrate polished with a gas flame, is not a major limitation. However, during observation of the process cycle, it was noticed that the viscous glass sphere does not adhere reliably to the substrate surface and can thus be deposited. This is presumably caused by the fact that the viscous sphere at the end of the fiber causes the substrate surface underneath to lie in the shadow of the laser beam and is not sufficiently heated. An upstream treatment of the substrate, e.g. by laser-based slight structuring of the surface, could improve adhesion of the spheres to be deposited. The implemented surface structure is polished out again laser-based within the current depositing process.

The manufacturing of volume components again requires a different condition of the substrate surface. This must not contain any unevenness, as there is a risk that the waviness can be continued by the layer deposition throughout the complete volume component. However, an optical quality of the substrate surfaces is not necessary. The substrates are selected and prepared according to these specifications.

The in-process is selected and carried out as described in the course of this chapter for the different components to be manufactured. The process parameters must be selected according to the component to be manufactured.

Several finishing methods are available, each of which depends on the component to be manufactured. The printing of functional waveguides always requires post-processing of the manufactured samples. No optical end faces can be created directly within the printing process in order to couple radiation into the waveguides. Using a laser-based cleave process, the end regions of the deposited fibers are cut off and the end surfaces are polished using laser technology. No such finishing process is required for the spherical lenses. Only subsequent overpolishing can be used to produce plano-convex lenses instead of spherical lenses. Other methods were not investigated for the spherical lenses. For the volume components, several post or intermediate processing steps can be used. For example, a polishing process for intermediate polishing between the individual layers, or for final polishing of the component surface. In addition, a laser-based tempering process may be necessary to remove the thermally induced stresses from the manufactured components.

Thus, it becomes clear that the type of process chain is strongly dependent on the component to be manufactured.

6   Conclusion and Outlook

In the context of this paper, it has been successfully demonstrated that the LGD process can be used for additive glass manufacturing without the use of additional bonding materials. With the help of the process strategy and process monitoring it is possible to process a brittle material like glass. Likewise, a manufacturing of optical components with an optical function has been demonstrated.

With the help of a suitable selection of the glass fiber, it is possible to adjust the properties of the waveguides to be printed. The optical properties of the fiber core are retained. With the deposition process, the glass fibers can be deposited on suitable glass substrates in curved shapes that are not possible with the starting fibers alone, without a forming process, since these fibers would otherwise break. Optical analysis of the printed waveguides has shown promising results, with core fibers deposited in a 19 mm radius of curvature still transmitting up to 46% of the coupled radiation. In further investigations, the point defects within the fibers must be avoided so that no scattering centers are created. This eliminates a major reason for the high losses. Furthermore, investigations must be carried out into the possible forms of waveguide deposition and the possibility of printing fiber-based networks.

Functional glass sphere lenses have also been produced in the project. The selectively introduced laser radiation enables viscous glass spheres to be formed only at the fiber end, which can be deposited in a defined manner on a glass substrate. By using a coreless glass fiber as the starting fiber, spherical lenses with a focusing effect can be manufactured in different diameters and thus with different focal lengths. However, a measurement of the individual sphere has shown that slight variations of up to 4% of the sphere diameter can occur within one process run. In addition, the spherical lenses manufactured to date have a slightly elliptical preferred direction. In further investigations, this preferred direction must be avoided in order to reduce the imaging errors. This can be realized, for example, by using a coaxially mounted laser process head as described in mGROTESK (see Chap. 6 "Development of System Technology for Coaxial Laser Material Deposition of Optical, Thermal and Structural Components").

Initial tests on the production of volume components from up to 80 layers have also been carried out. These have shown that a disproportionate material flow in the process zone is advantageous for production without visible boundary layers. This was successfully demonstrated for a height of 30 layers. The results have also made it clear that active control of the process and the laser power is essential in order to produce consistent results over a changed component height. This has to be integrated into the process for future experiments. Furthermore, an implementation of a laser-based polishing and annealing process is necessary to produce surfaces with an optical quality and to reduce the process-related thermal stresses within the manufactured components.

EUROPÄISCHE UNION
Europäischer Fonds für
regionale Entwicklung

References

1. Gebhardt, A.: Additive Fertigungsverfahren—Additive Manufacturing und 3D-Drucken Für Prototyping—Tooling—Produktion, Vol. 5. Hanser Verlag GmbH Co KG, München (2016). ISBN: 978-3446444010

2. Lachmayer, R., Lippert, R. B. (eds.): Additive Manufacturing Quantifiziert: Visionäre Anwendungen und Stand der Technik. Springer Verlag, Berlin (2017). ISBN: 978-3-662-54112-8

3. Petzoldt, J.: Spezialgläser und glaskeramische Materialien für neue Produktanwendungen, Mat.-wiss. u. Werkstofftech., vol. 19, pp. 258–261. VHC Verlagsgesellschaft mbH, Weinheim (1988). https://doi.org/10.1002/mawe.19880190803

4. Ehrt, D., Seeber, W.: Glass for high performance optics and laser technology. J. Non Cristall Solids **129**(1–3), 19–30 (1991). https://doi.org/10.1016/0022-3093(91)90076-I

5. Teschner, R.: Glasfasern, vol. 2. Springer Vieweg Verlag, Berlin (2019). ISBN: 978-3-662-58370-8

6. Scholze, H.: Glas – Natur, Struktur und Eigenschaften, vol. 3. Springer-Verlag, Berlin Heidelberg GmbH (1988). ISBN: 978-3-662-07496-1

7. https://www.heraeus.com/de/hca/fused_silica_quartz_knowledge_base_1/properties_1/properties_hca.html#tabs-608478-3. Date of last access 04 Nov 2021

8. Kotz, F., Quick, A. S., Rischm P., Martin, T., Hoose, T., Thiel, M., Helmer, D., Rapp, B. E.: Two-Photon Polymerization of Nanocomposites for the Fabrication of Transparent Fused Silica Glass Microstructures. Advanced Materials 2021, vol. 33, Issue 9, Article 2006341 (2021). doi: https://doi.org/10.1002/adma.202006341

9. Cai, P., Guo, L., Wang, H., Li, J., Qiu, Y., Zhang, Q., Lue, Q.: Effects of slurry mixing methods and solid loading on 3D printed silica glass parts based on DLP stereolithography, Ceramics International, vol. 46, Issue 10, Part B, pp. 16833–16841 (2020). https://doi.org/10.1016/j.ceramint.2020.03.260

10. https://www.chemistryworld.com/news/new-injection-moulding-technique-allows-glass-to-be-cast-in-any-shape/4013491.article, Date of last access 04 Nov 2021

11. https://www.brecorder.com/news/462681. Date of last access 04 Nov 2021

12. Datsiou, K.C., Saleh, E., Spirrett, F., Goodridge, R., Ashcroft, I., Eustice, D.: Additive manufacturing of glass with laser powder be fusion. J. Am. Ceram. Soc **102**, 4410–4414 (2019). https://doi.org/10.1111/jace.16440

13. Klein, J., Stern, M., Franchin, G., Kayser, M., Inamura, C., Dave, S., Weaver, J. C., Houk, P., Colombo, P., Yang, M., Oxman, N.: Additive manufacturing of optically transparent glass. 3D Print Additive Manufact. **2**(3). https://doi.org/10.1089/3dp.2015.0021

14. Von Witzendorff, P., Pohl, L., Suttmann, O., Heinrich, P., Heinrich, A., Zander, J., Bragard, H., Kaierle, S.: Additive manufacturing of glass: CO_2-Laser glass deposition printing. 10th CIRP Conference on Photonic Technologies, vol. 74, pp. 272–275 (2018). https://doi.org/10.1016/j.procir.2018.08.109

15. Curtis, B., Peters, D., Hostetler, J., Landers, R., Bristow, D., Kinzel, E. C.: Printing free-form free-standing glass structures. In: Proceedings of ASME. Additive Manufacturing, Ausgabe 1, MSEC2018-6677 (2018). https://doi.org/10.1115/MSEC2018-6677

16. Pohl, L., von Witzendorff, P., Chatzizyrli, E., Suttmann, O., Overmeyer, L.: CO_2 laser welding of glass: numerical simulation and experimental study. Int J Adv Manufact Technol **90**, 397–403 (2017). https://doi.org/10.1007/s00170-016-9314-9

17. Rettschlag, K., Kranert, F., Hohnholz, A., Wienke, A., Suttmann, O., Neumann, J., Kracht, D., Lachmayer, R.: Laser deposition of fused silica coreless fibers to generate functional waveguides. In: Proceeding of Laser in Manufacturing Conference. Munich (2019)

18. Rettschlag, K., Hohnholz, A., Jäschke, P., Kracht, D., Kaierle, S., Lachmayer, R.: Laser glass deposition of spheres for printing micro lenses. In: 11th CIRP Conference on Photonic Technologies, Procedia CIRP, vol. 94, pp. 276–280 (2020). doi: https://doi.org/10.1016/j.procir.2020.09.052

19. Rettschlag, K., Ley, P.-P., Kranert, F., Hinkelmann, M., Kaierle, S., Lachmayer, R.: Additive gefertigte Glaskugellinsen für die Anwendung, In: Lachmayer, R., Rettschlag, K., Kaierle, S. (eds) Konstruktion für die Additive Fertigung 2020, Springer Vieweg Verlag, Berlin, pp. 143–163 (2021). ISBN: 978-3-662-63029-7

20. Kranert, F., Rettschlag, K., Wienke, A., Hohnholz, A., Neumann, J., Jäschke, P., Kracht, D., Lachmayer, R.: Generation of functional curved waveguides by CO_2-laser based deposition of coreless fused silica fibers. In: Proceedings SPIE, vol. 11349, 3D Printed Optics and Additive Photonic Manufacturing II, Article 1134909 (2020). https://doi.org/10.1117/12.2554516

21. Rettschlag, K., Stieß, S., Jäschke, P., Kaierle, S., Lachmayer, R.: Manufacturing of fused silica parts by means of laser glass deposition. In: Proceeding of Laser in manufacturing Conference (2021)

22. Luo, J., Gilbert, L. J., Bristow, D. A., Landers, R. G., Goldstein, J. T., Urbas, A. M., Kinzel, E. C.: Additive manufacturing of glass for optical applications. In: Proceeding SPIE, Laser 3D Manufacturing III, Article 97380Y, vol. 9738 (2016). doi:https://doi.org/10.1117/12.2218137

23. VDI Gesellschaft Produktion und Logistik – VDI 3405 Blatt 5.1: Additive manufacturing—Legal aspects of the process chain, VDI Handbuch Beuth, Berlin (2020)

Additively Manufactured Polymer Optomechanics and Their Application in Laser Systems

Fabian Kranert, Jana Budde, Moritz Hinkelmann, Roland Lachmayer, Jörg Neumann, and Dietmar Kracht

1 Introduction

In the past decade, additive manufacturing (AM) has established itself as an innovative production process in many areas of industry and research [1]. Thereby, AM can be used to create individualized parts and function-integrated systems in a single manufacturing step, which meets the requirements of new industrial demands summarized under the term "Industry 4.0" [2, 3]. Among the various polymer-based 3D printing techniques, Fused Filament Fabrication (FFF) is most prevalent, since different materials as well as printers for this process are available at low cost. It is particularly interesting for in-house fabrication, enabling components to be available at short notice [4]. Many different areas of application are now being addressed, from rapid prototyping and the manufacturing of individualized components to applications in the field of research and education. As with most AM processes, users benefit from the additional degrees of freedom in design that result from the layer-by-layer production. In addition, the use of polymers in combination with infill structures leads to lightweight components, even if the design itself was not developed with weight optimization in mind. The FFF process, in particular, also allows multi-material printing, as well as the imprinting of additional components into a structural part, which further scales the functionality [5].

F. Kranert (✉) · J. Budde · M. Hinkelmann · R. Lachmayer · J. Neumann · D. Kracht
Laser Zentrum Hannover e.V. (LZH), Hollerithallee 8, 30419 Hannover, Germany
e-mail: f.kranert@lzh.de

R. Lachmayer
Institute for Product Development, Leibniz University Hannover, An der Universität 1, 30827 Garbsen, Germany

In the following chapter, we investigate the advantages of AM based on FFF to demonstrate potentials and limitations in terms of structural and thermal functionality for the production of optomechanical parts. First, the stress-free imprinting of conventional optical elements in polymer structures is presented, leading to a higher degree of integration in optomechanical systems and, at the same time, to a reduction–of complexity, since additional screws or clamping elements for holding optics become redundant. Subsequently, the application potential of these simple optomechanics will be exploited by integrating the imprinted optics into additively manufactured, adjustable optomechanics and quantifying their functionality. In addition, we present manufacturing of heat sinks for mounting active optical components, such as laser crystals. Here, the imprinting of optical elements as well as sensor elements is used to advance functional integration, too. These three aspects will be combined in the end to demonstrate the applicability in a rather sophisticated optomechanic for a low-power solid-state laser system, which will be characterized in detail.

2   State of the Art

2.1   Fused Filament Fabrication

Like in most AM processes, the starting point for 3D printing a part via the FFF process is a CAD-file defining the geometric dimensions. This is converted into the STL file format, which was originally developed for stereolithography. It describes the surfaces of a solid as triangular facets and can be read by a so-called slicer, a software creating the machine code (G-code) for the printer. Therefore, the software slices the three-dimensional volume into single layers and those into the individual lines. Here, the pre-defined parameters like layer height or infill degree are considered. A more detailed explanation of these parameters follows in this section.

FFF is the most common temperature-driven extrusion method for the additive manufacturing based on polymers [6]. A schematic representation of the process is given in Fig. 1. The process is also known under the trade name Fused Deposition Modeling (FDM®) by the inventor company and by the term Fused Layer Modeling (FLM) [7]. As with any extrusion-based process, material is forced from a feedstock through a heated nozzle. In case of FFF the thermoplastic material is delivered as a filament, which is melted by electrical heating in the print head and fills a material reservoir from which the viscous polymer is extruded. The continuous, constant pressure of the subsequently fed filament forms a strand with a constant diameter and rate. By placing the strand on a building tray, i.e. a glass plate, on the building platform (x–y-plane), lines are formed, which, placed next to each other, produce two-dimensional surfaces. After completion of a layer, the build platform moves downwards and printing of the next layer is started. The stacking of several layers generates a three-dimensional structure. An important parameter
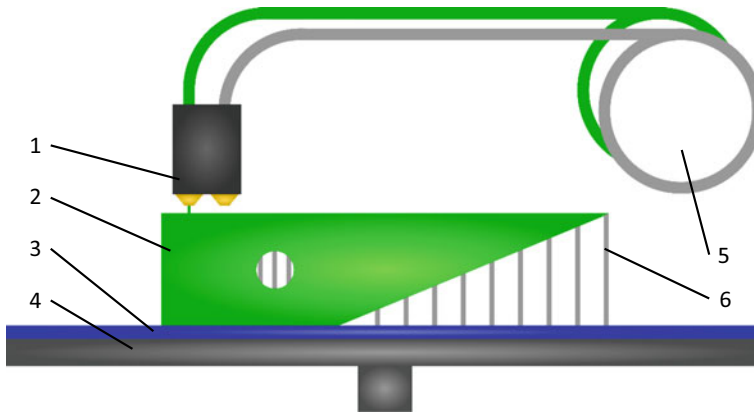
Fig. 1 Schematic illustration of the FFF process. 1: Print head with heated nozzle. 2: Generated part. 3: Build tray. 4: Build platform with retractable table. 5: Coiled filament as material stock. 6: Support structure

is the processing temperature of the material, as the polymer must be sufficiently viscous during extrusion but needs to cool quickly afterwards, to maintain the shape of the 3D printed structure [6, 8]. At the same time, the material must be warm enough when it meets the previous layer to enable a sufficient interfacial healing and achieve a solid bond between the layers. However, thermal degradation of the material must be prevented.

The nozzle in the print head defines the diameter of the extruded material strand and thus the resolution of the printing process. Consequently, it is not possible to print a feature smaller than the nozzle diameter. Thereby, a large nozzle diameter allows a higher material deposition rate, but reduces the shape fidelity compared to the digital model. The distance between nozzle and build platform or previous layer respectively, i.e. the layer height, defines the shape of the extruded strand (Fig. 2 a). Typically, this is less than or equal to half the nozzle diameter, creating an oval cross section while reducing the void space between individual lines [9, 10]. To reduce the void between the single lines further and, thus, increase the mechanical strength, they can be printed with an overlap. Same as for the nozzle diameter, a smaller layer height leads to a higher printing resolution, but a longer printing time. Usually, bodies 3D printed using FFF are not massive volumes. For sufficient structural stability, the walls, floor and ceiling are printed several layers thick, while the interior is filled with a so-called infill structure (Fig. 2b). This can be realized by different geometric patterns, for example a triangular, cubic or honeycomb structure. This infill structure as well as the infill percentage together with the shell thickness influence, among other, the mechanical stability of the 3D printed part [10]. A detailed overview of the publications that have investigated the change of different mechanical properties under variation of various parameters is presented in Popescu et al. [11]. The start and stop position of a line is always the same point. This results in a slight overlap at this
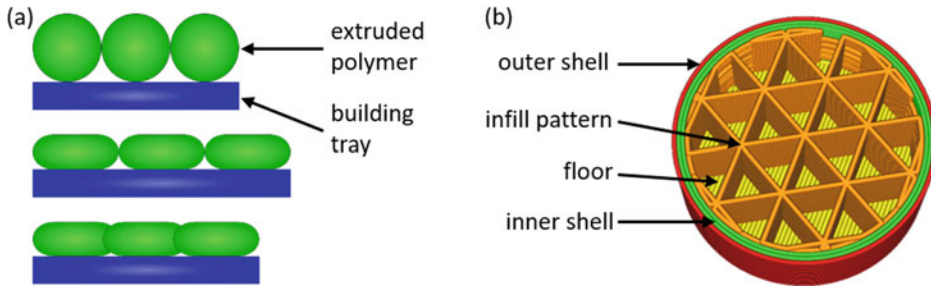
Fig. 2 **a** Illustration of the change in line cross section when the distance between the nozzle and the build platform is changed. Top: Distance equals nozzle diameter. Middle: Distance smaller than nozzle diameter. Bottom: Distance smaller than nozzle diameter with simultaneous line overlap. **b** Cross section through 3D printed cylinder. Red and green lines build the walls and represent the outer and inner shell respectively, orange lines build a triangular infill pattern and the yellow lines are the floor

point, which is visible in the case of outer lines. If the start and stop points of each layer are in the same place, a seam is formed along the z-axis. This results in a shape deviation from the CAD model along this vertical line. Either this is removed after printing, which requires a corresponding post-processing step, or a random distribution over the outer shell is created in the slicer software to minimize the influence of these points. Another factor influencing the shape fidelity is the round nozzle geometry, which generates rounded edges on outer corners [9]. The shape of the 3D printed component is also influenced by the interaction between material flow rate and axes velocity. If these are not matched, too much or too little material will be deposited in a certain area: when the print head moves at a fixed speed parallel to the x-direction and is then required to describe a right angle by transitioning the movement into the perpendicular y-direction, it will have an instantaneous speed of zero at the corner. If the extrusion volume is not zero here, excess material will be deposited.

Although the AM in general allows creating parts with a much higher design freedom than that using conventional subtractive manufacturing, limitations specific for the AM technique regarding printable structures are still given. Keeping in mind the layer-wise build-up in the FFF process it is obvious that every line needs an underlying one. Thereby, specific geometries like protruding or freestanding parts cannot be realized or only with reduced quality, since the layer will sink into the empty space underneath [6]. To avoid this, support structures are used (Fig. 1), which can be removed in a post-processing step. They can be created using either a different material than that for the actual part or the same one. In the case of a different material water-solvable polymers are often used. The benefit of these materials is evident: they can be removed easily by immerging the part into a water bath. When using the same material for part and support structure, the latter is generated to be broken off. Most slicers can generate support structures automatically.

Nevertheless, the usage of support structures always makes post-processing necessary. The exact overhang, at which the use of support structures is helpful or necessary, depends not only on the angle but also on the length of the projecting component and ranges between 45° and 75° [12–14]. At the same time, it must also be taken into account which target value is more decisive: shape accuracy or short production time with acceptance of lower surface quality and shape fidelity.

As already described, thermoplastic polymers are processed in the FFF printing. Many different polymer materials with a wide range of mechanical properties are available [11, 15]. First, FFF 3D printers were based on acrylonitrile butadiene styrene (ABS) [6, 9]. In the meantime, polylactic acid (PLA) has become a material of particular interest because, unlike many others, it can be produced from renewable raw materials and is biodegradable, non-toxic and biocompatible [16–19]. Nowadays, composite materials with added metal, stone, wood, and other particles are also commercially available and expand the application possibilities of FFF printing [16, 20–22].

Besides the above-mentioned benefits of the FFF process, two additional features are given, which are of special interest using FFF to manufacture highly integrated components. The first one is the so-called print-pause-print (PpP) scheme [5, 23]. Hereby, the printing process is paused at a specific height and an additional component, e.g. a sensor, an optical element or a previously 3D printed component is placed in a designated cutout. Afterwards, the printing process continues imprinting the component into the overall structure. This not only increases integration and functionality, but sensors also enable monitoring from within the part. The second one is the possibility to easily generate multi-material parts using a dual extrusion print head (cf. Fig. 1) and addressing different tasks of the part by tailored materials [24]. It should be noted that the use of different materials has an influence on the tensile strength of the components [25].

2.2   Printing of Optomechanical Components

AM is already present in many different areas of industry and research for a wide variety of applications. In the field of photonics, two areas have to be distinguished from each other. One is the printing of transparent and reflective optical elements for light manipulation and the other is the production of optomechanical components for mounting and adjusting optics. For the printing of optical elements, please, refer to Chap. 1 "Additive Manufacturing of Glass Materials for the Production of Optical, Thermal and Structural Components" and the relevant literature [26, 27]. The motivation for 3D printing optomechanics is driven by the cost efficiency and short-term availability, which is especially beneficial for the use in research and education. Some research groups demonstrated single optomechanics or toolboxes presenting a wide variety of components for different purposes like for example mounting or adjusting optical elements [25, 28–30].

In addition, laboratory setups for interferometry, spectroscopy or microscopy are also fabricated from such individualized toolboxes [31–35]. Next to the development of systems consisting of discrete optomechanical elements, integrated systems for a specially defined application are also demonstrated. These are systems for microscopy applications [36, 37], different kinds of spectrometry [38–41], fluorescence lifetime measurement [42], and optical scattering instrumentation [43]. For individual optomechanics, such as mirror or lens holders, commercial components are simply reprinted. In more complex systems, often only structural and, in particular, housing elements are manufactured additively. However, a higher function integration is barely addressed despite the huge potential offered by the AM approach in comparison to conventional subtractive manufacturing methods. Nevertheless, initial approaches are demonstrated to produce compact, more integrated systems. The PpP scheme is used to integrate as many of an optical system's elements as possible directly into the optomechanics, thus reducing the effort required for subsequent assembly and at the same time consistently implementing the idea of cost reduction by rendering as many commercial mechanics as possible redundant. This increase in the degree of integration of optomechanical systems through additive manufacturing is the core goal of the sGROTESK project and is demonstrated on a laser and laser amplifier system based on polymer-based additive manufacturing [44, 45]. In addition to the imprinting of optics, the embedding of additional thermal sensors for component-integrated temperature monitoring is also successfully tested here. Besides the AM based on polymers, initial preliminary work is presented to use metal-based AM processes for optomechanics [46–48]. The focus here is primarily on exploiting the several orders of magnitude higher thermal conductivity of metallic materials compared to polymers, which should enable more efficient cooling of e.g. laser crystals. The aim is also to create and take advantage of a direct bond between the optics and metal with a high heat transfer coefficient. Moreover, the higher mechanical stability of metallic materials compared to polymers is also a benefit. Although these techniques still have outstanding challenges, such as dealing with the high process temperatures required for additive processing of metallic materials, they are promising for the use in optical systems with high heat load like high-power lasers. More detailed explanations of this research can be found in Chap. 4 "Molybdenum Copper MMC for Additive Manufacturing of Thermal and Structural Components" and Chap. 5 "Additive Manufacturing of Optical, Thermal and Structural Components by Laser Metal Deposition".

3   Experiments

3.1   Printing of Single Optomechanical Components

In the following section, various 3D printed optomechanical components are presented and their functionality is quantified. Unless otherwise stated, they are printed from PLA.

Furthermore, the same commercial 3D printer (Ultimaker 3, Ultimaker) is used for all components.

3.1.1 Imprinting of optics

For the proper use of an optical element in an optical system, it must be fixed in its defined position and secured against misalignment. Usually, optics are fixed with a side-engaging screw, a retainer ring applied to the optical surface, or by other clamping mechanisms [49]. To avoid additional components such as screws and to keep the stresses introduced into the optics low, the PpP scheme, as described above, can be used for fixing the optics. Hence, the optical elements are secured directly in their respective positions in the optomechanical system. In the following, it will be examined how this imprinting affects the optical elements compared to other mounting options. For this purpose, a lens and mirror in a 3D printed holder are compared to a conventional holder from a laboratory setup in terms of induced mechanical stress and how stable the optic is seated. When designing an optomechanic, an appropriate recess for imprinting an optic needs to be considered (Fig. 3a). In addition, the described deviations between the 3D printed component and the digital model depending on the printing parameters used must be taken into account. Accordingly, the recess must be designed larger than the optical element in the lateral direction. Furthermore, the seam generated by the start and end point of the outer line of the cutout must be considered, as otherwise the insertion of the optics is more difficult and undesirable stress-generating contact points are created as described later on the basis of the measurement results shown in Fig. 5. To prevent this, an additional triangular feature is added to the round cutout (Fig. 3) where the seam is formed along the outer tip of the triangle and, thus, does not interfere further. The transition from the triangle to the circle must be rounded, to avoid the above-explained bead formation due to the inconstant print head movement in combination with the material extrusion. Since the nozzle moves close over already printed structures during the printing process, care must be taken that the components do not protrude too far to prevent a collision. This leads to problems with
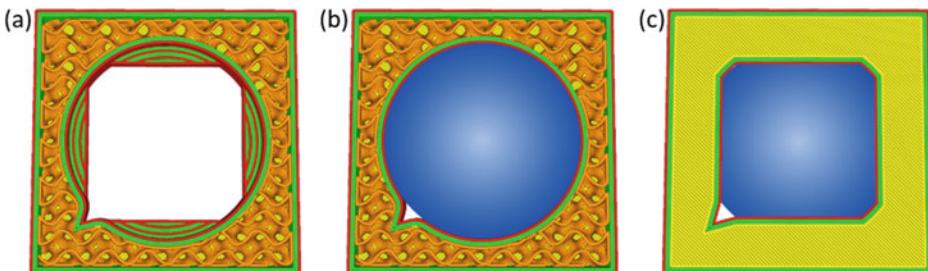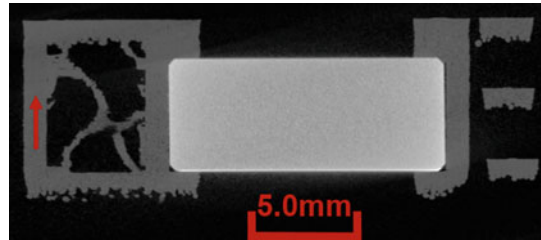

Fig. 3 Print-pause-Print scheme for the embedding of optics directly into the polymeric optomechanic. **a** The optomechanic is printed up to a defined height and the printing process is paused. **b** The optical element is inserted manually. **c** The print is continued and the optic is fixed in its position

5.0mm

non-planar optics, for example the convex side of a lens. Accordingly, the design should consider the flat surface for imprinting. If this is not possible, adapters must be used. The cutout must also not be higher than the optical component, otherwise it will not be firmly secured. It was shown that protrusion of the optic by one layer height or less gives proper results for a stable and secure imprint.

As the printing material does not adhere to glass or metal surfaces, the optomechanic must be designed in a way that the printing process does not start on the inserted component but on the surrounding polymer to ensure a stable layer connection. Taking these aspects into account, form-fit imprinting of the optics is possible. To evaluate the seating of an embedded optic, tomographic images (nanotom S, GE Sensing and Inspection Technologies GmbH) of such an element were taken with a resolution of 20 µm. Figure 4 shows a cross section through a 3D printed holder with the associated 5 mm thick ½ in. fused silica mirror as an example. The polymer lines up precisely with the glass surface and no inclusions or voids are visible. Even the cavity created by the chamfer at the edge of the optic, visible on the bottom side of the optic, is closed during the imprinting process by the viscous polymer.

In addition to the X-ray image, it is also investigated whether and to what extent the imprinting of the optics introduces mechanical stress into optical elements mounted this way. Figure 5 shows the results for a stress measurement in a N-BK7 lens with a diameter of 1 in. using a polarimeter (StrainMatic M4/140, Ilis). Four different mounting cases of the lens are investigated: (a) unmounted state, (b) in a commercial mount using a retainer ring, (c) imprinted with a simple round cutout and (d) with optimized cutout (Fig. 3). Both, the commercial retainer and the plain imprinting without design optimization, result in an increased mechanical stress in the lens. Calculating the mean value of all measuring points yields a value of 0.11 MPa for the lens in the commercial holder and 0.06 MPa for the simple 3D printed holder (Fig. 5c). For the unmounted optics and the use of the improved printing design (Fig. 5d) the values are 0.04 MPa and 0.05 MPa, respectively. The same measurement is performed for a ½ in. fused silica mirror. The mirror is examined again in the unmounted state as well as after imprinting in the already optimized design. In addition, the mechanical stress is measured for the mirror being mounted in a commercial mirror holder, in which a screw clamps it laterally. In Fig. 6, the commercial holder
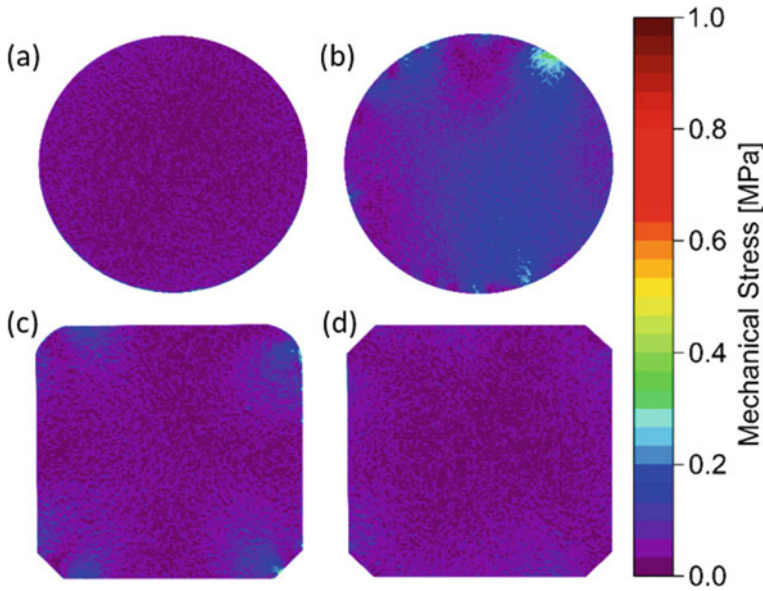
Fig. 5 Mechanical stress in a N-BK7 lens. The false color scale on the right side is valid for all graphs. **a** Unmounted. **b** Commercial holder with a retainer ring. **c** Imprinted with a simple round recess. **d** Imprinted with optimized recess, meaning the seam formation is considered

introduces stress into the optics at the points where the screw engages as well as at the two contact points of the optic in the metallic frame.

The mean stress values in the mirror are 0.04 MPa, 1.09 MPa and 0.08 MPa for being unmounted, mounted in commercial and 3D printed optomechanic, respectively. The measurements with both optics show that imprinting can reduce the mechanical stress generated compared to commercial solutions, which rely on mechanical clamping. However, even for the mirror held with the screw, the measured maximum value of 5.60 MPa is almost two orders of magnitude away from the destruction threshold for compressive loading given in the literature. Nevertheless, it must be taken into account that stress-induced birefringence in the optics already occurs at lower loads [49]. Therefore, a mounting that introduces a lower mechanical load is to be preferred.

To ensure that the optics are not less tightly fixed due to imprinting, a force is applied to the optical elements along the optical axis and at the same time it is measured whether its position changed. For the mirror fixed in the commercial holder by a screw, a force of 41 N caused the optics to slip, while the imprinted optics and the lens hold by the retainer ring did not move even at the maximum force of 50 N.
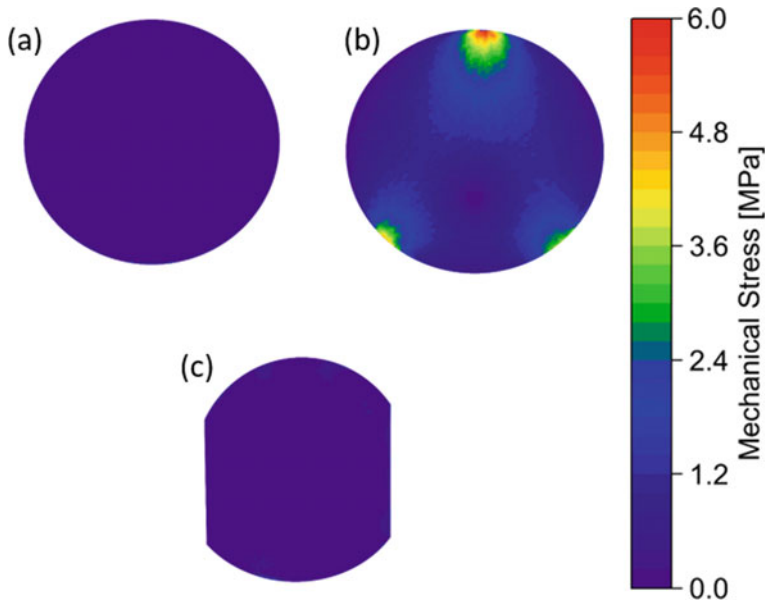
Fig. 6 Mechanical stress in fused silica mirror. The false color scale on the right side is valid for all graphs. **a** Unmounted optic. **b** Optic mounted in conventional holder. **c** Optic imprinted into PLA [28]

3.1.2 Adjustable Optomechanics

The upper sections show that an imprinting of optical elements is not only possible, but with focus on stability and induced mechanical stress beneficial. The functionality of the optomechanic is scaled by realizing adjustability, in addition to the mounting of an optical element. The use of adjustable optomechanics is crucial to enable beam alignment in an optical system. For this reason, an additively manufactured adjustable mirror mount is examined below and compared with a commercial holder. The mechanical stress was investigated for the same holder (see Fig. 6). The mechanical design in Fig. 7 consists of two individually 3D printed parts. The first, referred to below as part 1 (Fig. 7a), contains the embedded mirror, spring system and ball joint. Part 1 is printed separately from the cage system to enable the removal of the support structure, which is necessary for printing the spring system. For the part itself and the support structures the same material is used. The second part is the frame shown in Fig. 7b, referred to below as part 2. Part 1 is imprinted into part 2. The bushings for the fine thread screws are heated and inserted into the recesses provided by a proper design. The frame can also be part of a more complex optomechanic with several components imprinted. Figure 7c shows the operating principle of the kinematic holder: When the screw is turned, it moves forward and slides along the inclined surface changing the angular position of the mirror held by the spring element and ball joint. This allows the ratio of deflection angle to screw travel to be defined in the
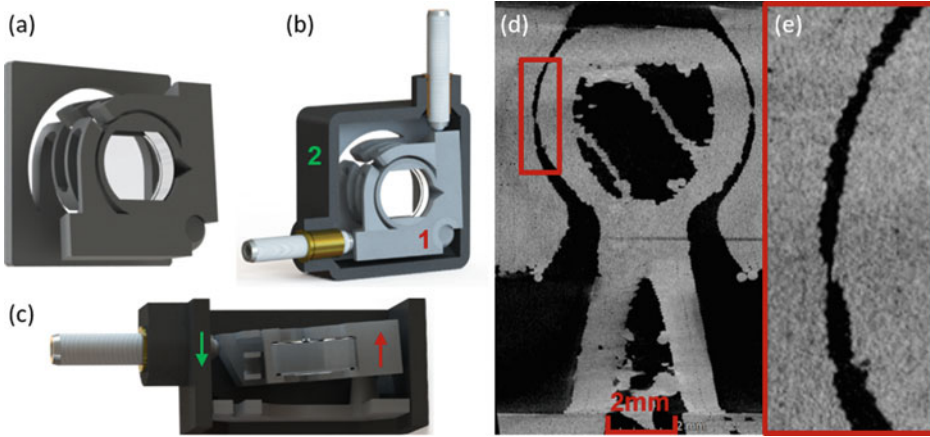
Fig. 7 **a** CAD model of mirror mount with imprinted mirror (part 1). **b** Mirror mount imprinted in frame (part 2) with fine adjuster screws and bushing. **c** Cross section of combined part with printing direction indicated. **d** Cross section through the printed ball joint. **e** Magnification by a factor of four of the area marked in red

design and adapted to different requirements. To evaluate the appearance of the printed ball joint, additional tomographic images of the holders were taken. Figure 7d shows a cross section of the 3D printed holder. An air gap between the ball and its socket is clearly visible, which is necessary to prevent the ball from sticking to its socket during printing. In the enlarged excerpt of the X-ray image, not only the step pattern from the layer-wise fabrication, but also bulges on the outer surface can be seen. Those appear, as explained, at the start and end of the outermost line of a layer. The bulges may also be contaminations from the printing process. Tests have shown that a distance of 0.25 mm between the ball and the socket in the design part reliably results in a freely movable ball joint.

The dynamic adjustment range of the 3D printed mirror mount is measured. This range is defined as the angular movement which can be realized without degeneration of performance. The initial angle is given by the design of part 1. The maximum deflection angle is defined as the angle at which the mirror returns directly to its initial position after the screw is removed. An angular range of $\pm 4°$ was aimed for, which corresponds to commercially available metal mounts. Consequently, part 1 is designed for an initial angle of $-4°$, resulting in a real initial angle of about $-3.5°$ when the fine-thread screws are in contact. With an increment of half turns, one screw is adjusted until the limits of elastic deformation are reached. During the measurement, the screw of the second axis is in contact with the holder, but its position is not changed. The maximum deflection angle is measured with $4.1°$, followed by the onset of a hysteresis, i.e. the holder did not return to its initial position immediately, but with a time delay. In another experiment, the reproducibility of the positioning as well as the crosstalk between the axes is determined. Therefore,
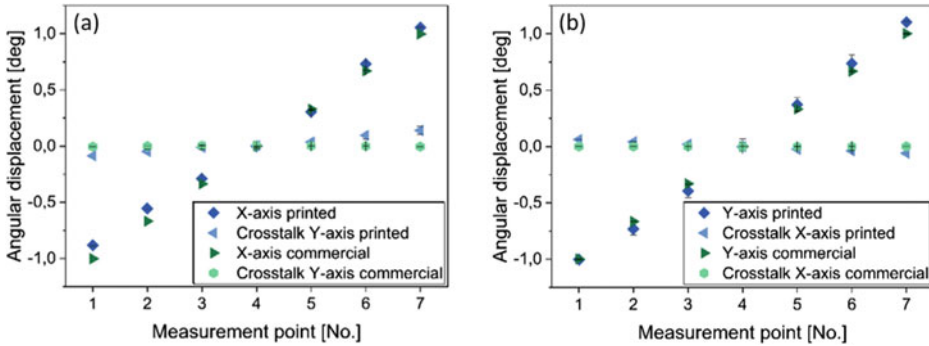
Fig. 8 Reproducibility of angular movement and crosstalk between the axes of the PLA mount compared to a commercial reference holder. **a** Displacement of the X-axis. **b** Displacement of the Y-axis [28]

the beam from a laser diode (BF-A64-0180-S5F, Sheaumann Laser, Inc.) is collimated and deflected via the mirrors onto a beam profiling camera (WinCamD-UCD12, Dataray Inc.), which returns the beam position on the camera chip. Using a 3D printed and a commercial holder (KM100, Thorlabs, Inc.), seven uniformly distributed measurement points within the range of $\pm 1°$ are approached. The measurement is performed six times with each holder. The results with the corresponding error bars are shown in Fig. 8. The first thing to note is that, like the commercial holder, the 3D printed one also shows a linear progression over the entire angular range for both axes. If the size of the error bars is considered, this gives information about the repeatability. The smaller they are, the higher the repeatability. For the metal holder and the X-axis of the 3D printed holder, these are so small that the measuring points themselves superimpose them. Quantified, the deviation for the commercial holder is less than 70 µrad for both axes and for the X-axis of the 3D printed one less than 230 µrad. However, the Y-axis of the 3D printed holder shows a significantly larger deviation of up to 1.3 mrad. An explanation for the error can be the step profile of the ball and socket described above as well as the impurities visible in Fig. 7d, which inhibit smooth gliding in the joint. The same applies to the contact surface between screw and mount. Compared to the commercial holder, a slight crosstalk of the axes can be observed, which is more pronounced for the X- than that for the Y-axis.

The long-term stability of the mirror mounts, 3D printed and commercial, is investigated by capturing the position of a deflected laser beam by the camera over 24 h with an interval of 30 s. The temperature uncertainty over a measurement period was ± 0.5 K. The angular drift for the X- and Y-axis of the commercial reference and the additively manufactured mount is depicted in Fig. 9a and b, respectively.

The metallic reference holder shows only a slight, steady drift of less than 5 µrad, which is identical for both axes. The axes of the 3D printed holder show a more pronounced shift of several 10 µrad. The measurement with this mount is performed multiple
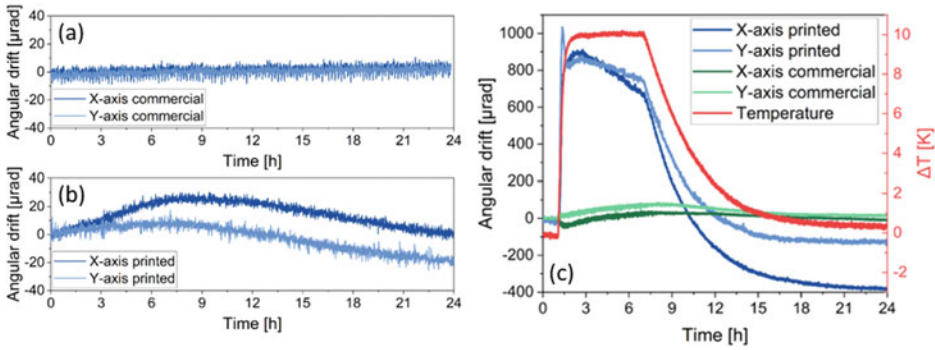
Fig. 9 Angular drift of the mount's axes over 24 h. **a** Commercial reference mount. **b** PLA mount. **c** Angular drift of the PLA and reference mount's axes under the influence of temperature change [28]

times, leading always to a drift of $\leq 100\ \mu$rad, whereas the specific profile of the drifting changes between the measurements. To ensure that the observed drift behavior is actually caused by the mirror holders, the collimated laser beam is imaged directly onto the camera chip in a further measurement. The resulting angular drift is negligibly small. The stronger drifting of the polymeric mount can be explained by the different material properties of metals and polymers. The viscoelastic properties of polymers lead to significantly stronger time-dependent effects from external influences [50].

To quantify the effect of temperature changes on the position stability of the two mounts under test, they are placed in a thermally insulated chamber, which is subjected to a temperature increase of 10 K. After a stable temperature is reached, the setup is cooled down to the initial temperature again. During the whole time the beam displacement is again captured by the beam profile camera. The test is carried out several times, leading to arbitrarily differing results, which could not be combined into a uniform scheme. Figure 9c shows a measurement in which at least the typical responses of the additive mount and the metallic reference holder to the temperature change is visible. Common to both mounts was the sudden displacement of the axes triggered by the increase in temperature. This offset reduces again with decreasing temperature. The amplitude of the displacement and the remaining offset to the initial state are varying between the different measurements. In general, the temperature increase has a significantly stronger effect on the 3D printed holder than on the commercial one. The drift of the axes is several 100 μrad up to 2 mrad for the polymer holder. In contrast, it is in the order of $\leq 100\ \mu$rad for the reference holder. Figure 9c illustrates the deflection of the 3D printed holder relative to the initial value, which is several 100 μrad. For the metallic holder, the deflection is an order of magnitude smaller. At a constant elevated temperature, a stronger drift in the axes is observed than that in the measurement at room temperature. One reason for the higher sensitivity of the polymer holder to temperature changes could be the increased influence

of temperature on material properties. For example, the coefficient of thermal expansion of the used PLA material is, compared to the aluminum-based commercial holder, about a factor of three higher.

3.1.3 Heat Sink

While optomechanics for passive optical components have been discussed so far, the following subsection will deal with active optical elements. Here, active means that there is a direct interaction with the incident light. A typical example is a laser crystal, which is excited by the absorption of pump light and emits light itself. In contrast to a passive element such as a lens, the laser crystal must not only be mounted, but generated heat must be dissipated efficiently. The main heat source in a laser crystal during the lasing process is the quantum effect, i.e. the energy difference between absorbed and emitted photons. For more detailed explanations of solid-state laser systems, and in particular of the heat generation in laser crystals and the mechanisms involved, please refer to the detailed descriptions in the relevant technical literature [51–53]. The challenge in dealing with heat generation in laser crystals, with regard to polymeric components, is that it takes place in a limited volume of often less than half a cubic centimeter, and at the same time, depending on the pump power, heating of several tens to hundreds of Kelvin can occur. At the same time, the components used are made of materials with comparably low glass transition temperatures to enable thermoplastic softening when processed by the FFF technique. For this reason, the first approach was to use a polymer, which is printable but also thermally stable. A special polyethylene terephthalate filament (PET, 3dkTOP, 3dk.berlin) is chosen, since it can be tempered after printing and is then, according to the manufacturer, mechanically stable up to 230 °C. Using this material, a holder for a laser crystal was manufactured [44]. However, it became apparent that the load limits are quickly reached here. Using a Nd:YVO$_4$ crystals with a dimension of $3 \times 3 \times 11$ mm^3 and an Nd doping of 0.27 at.% the temperature in the holder next to the crystal reaches up to 190 °C when pumped with a fiber-coupled laser diode (WSLX-808-008-M-H2, Wavespectrum Laser Group Limited) at a wavelength of 808 nm and an absorbed power of 2.5 W. Rapid functional degradation is to be expected when the polymer is subjected to a thermal load close or above the material´s glass transition temperature. For this reason, the approach of simply holding the crystal was discarded and a design was developed that allows for active cooling of the crystal [25]. The developed and investigated heat sink design implemented a water flow around the crystal (see Fig. 10). Here, the cooling channel is mainly designed with the requirements of the printing process in mind. Therefore, support structures should not be required, since they cannot be removed from the cooling channel afterwards. In-depth simulations how different parameters affect the interactions between the heat sink and the laser crystal can be found in Chap. 3 "Simulation of Additive Manufactured Optomechatronic Systems". The material thickness between crystal and cooling channel is 0.8 mm. The cooling water connection is made via the M5 thread printed along with the holder. In addition, resistance temperature detectors
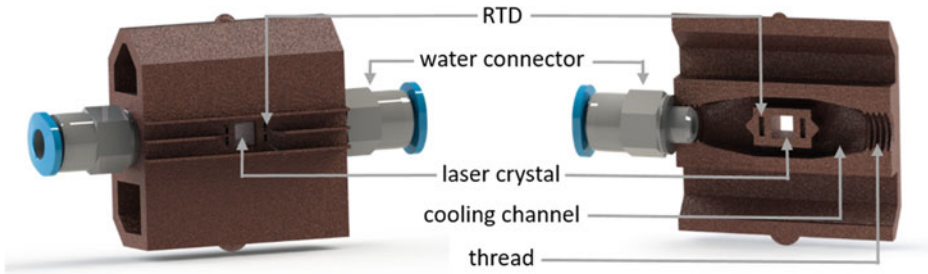
Fig. 10 CAD model of the 3D printed heat sink shown as a solid (left) and as a cross section (right). In the latter, the internal structural features are visible

(RTDs) are imprinted near the crystal at a distance of 0.8 mm, so that the temperature in the holder can be monitored. Besides the already mentioned materials PLA and PET, a third one, a copper-PLA mixture (Cu-PLA; MetalFil—Classic Copper, FormFutura) with a copper particle volume fraction of approximately 35%, is investigated for the heat sink. It is shown that the Cu-PLA material leads to the most efficient cooling, which is the reason that in the following only heat sinks 3D printed from this material are discussed [25]. Parallel to the 3D printed one, a subtractive manufactured two-part copper heat sink was tested. It is also water-cooled and serves as a reference to the printed heat sinks. An RTD is bonded to the surface of the holder to allow temperature measurement here as well. In the copper holder, the crystal is wrapped with indium foil of thickness 100 μm to optimize the contact area when clamping the crystal and thus the heat flow with the heat sink. In the case of the crystal mounted in the 3D printed heat sink, wrapping the crystal in indium foil did not show any improved heat transfer.

The interaction between the cooling water and the polymer material is investigated. For this purpose, the water absorption was determined based on the corresponding norm [54]. It is found that the water content as a mass fraction in the Cu-PLA material is only 0.2% after a storage in water for 384 h. In addition, it is tested whether the 3D printed holder remains leakage-free even when water flows through it for a longer period. After more than 210 days, no water leakage is observed. In order to evaluate the suitability of the 3D printed heat sinks in a laser system, the above described Nd:YVO$_4$ crystal is imprinted in the heat sink and excited with the fiber-coupled laser diode at the same wavelength and power. The temperature of the cooling water is set to 18.0 °C. The heat generation is measured via the imprinted RTD during optical pumping over 1 h and recorded at the crystal surface by a thermal imaging camera (E53, FLIR, accuracy $\pm$ 2 °C). The emissivity of the Nd:YVO$_4$ crystals is assumed to be 0.74 [55]. A great improvement compared to the crystal holder without water-cooling is achieved, since the temperature inside the mount drops from 190 °C to 30 °C. However, as stated in Table 1, even the Cu-PLA does not cool as efficiently as it is possible with a conventional crystal heat sink based on copper. This is to be expected since the thermal conductivity of the polymer is several orders of

Table 1 Temperature in the crystal holder and on the crystal surface

Heat sink material	Temperature holder/°C	Temperature crystal/°C
Cu-PLA	29.7 ± 0.2	40.8
Copper	18.2 ± 0.1	22.6

The temperature in the holder is averaged over one hour. The temperature at the crystal surface is measured with the thermal imaging camera. Values adopted from [25]

magnitude lower than that of copper. The literature gives a thermal conductivity of about 0.25 W/ m·K for copper-filled PLA and between 240–380 W/ m·K for copper, depending on the exact composition of the copper material [56, 57].

Comparing the temperature measured with the imprinted RTD and the one measured with the thermal camera for the Cu-PLA heat sink in Table 1, it can be seen that at the location of the RTD the temperature has already dropped noticeably compared to the crystal surface. This can be explained on the one hand by the temperature gradient between the crystal and the cooling water and on the other hand by the fact that the polymer acts as an insulator due to its low thermal conductivity. For the holder made of Cu-PLA, another measurement is carried out in which the crystal is pumped over a period of 24 h. It is found that even with this significantly longer period of use of the crystal holder, there is no reduction in the cooling power over the measurement period. In addition, no deformation could be observed on the crystal holder due to the influence of temperature. This is also not to be expected, since the glass transition temperature for this material is specified as over 60 °C. An even higher operating temperature as in the case of higher pump power seems appropriate.

3.2 Integrated Optomechanical Systems

In this section, we demonstrate the integration of stand-alone optomechanical components in a rather sophisticated and complex solid-state laser system. The corresponding optical system design is shown in Fig. 11.

It consists of a tube (blue) in which the corresponding optics for shaping the pump light and the holder for the fiber of the pump diode are imprinted. In addition, two adjustable mirror mounts for the optical resonator are embedded in the tube. The holders themselves must be printed separately, as described above, due to the spring system. The tube is designed so that the heat sinks with the laser crystal, characterized above, can be inserted. This allows examining them in the additively manufactured optomechanic (AddSys) as well as in a reference setup (RefSys) based on commercial optomechanical components for a comparative characterization. To ensure this comparability, the optics as well as their distances to each other are the same in both systems. Table 2 lists the weight of the optomechanical components 3D printed for this purpose as well as the printing time.
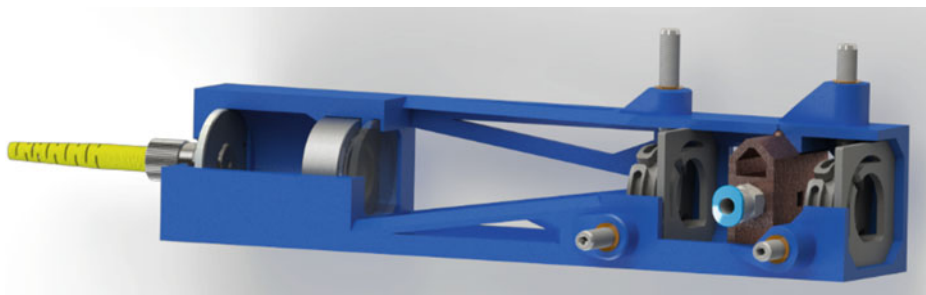
Fig. 11 CAD model of the additively manufactured optomechanic for a laser system

Table 2 List of printed optomechanics, each with material used, printing time and weight

	Material	Weight	Printing time
Tube	PLA	57 g	5 h 48 min
Mirror mount	PLA	7 g	0 h 40 min
Heat sink	Cu-PLA	21 g	2 h 36 min
Combined	–	85 g	9 h 04 min

It is worth mentioning that the laser system is not designed to reach the maximum possible optical-to-optical efficiency, since the focus is on investigating the possibilities and limitations of AM for 3D printing a laser optomechanic. In the following, three different configurations are investigated. At first, the copper heat sink is tested in the reference system, followed by the 3D printed heat sink made out of Cu-PLA. The third configuration is the 3D printed heat sink in the additively manufactured system. The laser's optical output power in the different configurations as a function of the absorbed pump power are shown in Fig. 12. In contrast to the experiments with the heat sinks in Sect. 3.1, the pump power is scaled further up the maximum output power of the pump diode of close to 9 W. The fiber of the pump diode has a core diameter of 105 µm, whereas the pump beam is collimated and focused into the laser crystal with a calculated spot size diameter of 340 µm. The cooling water for the heat sinks is set to 18.0 °C. The first resonator mirror is coated with an antireflective coating for the pump wavelength at 808 nm and a high reflective coating for the generated laser wavelength at 1064 nm. The second one, the output coupler, has a partially reflective coating for the laser wavelength with a reflectance of 91%.

The reference system has a 4% higher output power at maximum pump power when using the copper heat sink compared to using the Cu-PLA heat sink. The difference between using the additively manufactured heat sink in the reference system and the 3D printed optomechanics is marginal. For a detailed comparison, measured values for output power and optical-to-optical efficiency at maximum pump power, as well as slope
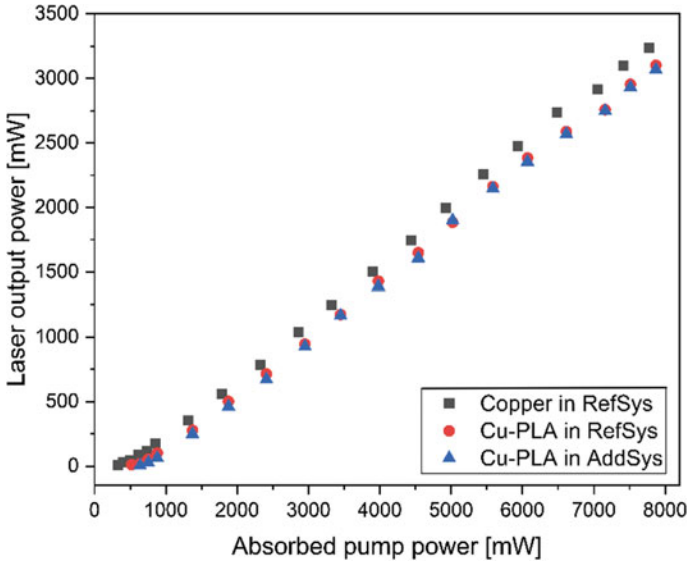
Fig. 12 Laser output power in dependence of the absorbed pump power for the copper heat sink tested in the reference system and the Cu-PLA heat sink test in both, reference and additively manufactured laser optomechanic

efficiency are listed in Table 3. In addition, the respective M^2-value is shown using a pump power of about 7 W measuring the beam diameter at five points each inside and outside the double Rayleigh length [58]. The beam pointing of the systems is determined over a period of 2 h. The value given in Table 3 describes the root mean square (rms) of all measurement points.

As described above, the differences in using the polymer heat sink in the reference system and in the additively manufactured system are negligible. This shows that the

Table 3 Overview of the parameters of the compared laser systems

System configuration	Output power / mW	Efficiency / %	Slope efficiency / %	M^2	Pointing (rms) / μrad
Copper in RefSys	3238	41.6	44.4 ± 0.3	1.36	4.53
Cu-PLA in RefSys	3101	39.4	43.0 ± 0.3	1.68	4.32
Cu-PLA in AddSys	3067	39.3	43.3 ± 0.4	1.68	5.21

The optical-to-optical efficiency is calculated at the maximum output power. The accuracy of the power values is 3.0% according to the specification of the power meter

performance of the 3D printed system, at least on short time scales, is comparable to a system based on conventional optomechanics. The slightly better performance of the laser system with the crystal in the copper heat sink can be attributed to different reasons. On the one hand, the temperature of the laser crystal has an influence on the emission cross section and, thus, on the efficiency of the laser process [59]. Furthermore, although the crystals in both holders are the same, it is not known whether they were coated in the same batch and deviations are given by the tolerance of the optical coating. In addition, the systems are adjusted manually and are therefore always subject to an individual error. In further tests, the behavior of the systems on larger time scales is investigated. The optical output power and the temperature at the heat sink are measured over a period of 10 h using a pump power of about 7 W. The results are shown in Fig. 13. Once again, the slightly higher output power of the metallic heat sink compared to the additively manufactured one is observed.

While the graphs of the output power of the Cu-PLA heat sink are almost congruent in both systems, the temperature is significantly higher when using additively manufactured optomechanics. This phenomenon will be discussed in more detail at the end of this section. In addition, the behavior of the different configurations is investigated during several on and off switching processes. For this purpose, the output power and the temperature at the heat sink are examined over 10 such cycles. Figure 14 shows for the measurements in the reference system that the output temperature remains constant over the cycles and that both temperature and output power stabilize quickly after switching on. When using the Cu-PLA heat sink in the additively manufactured system, it can be
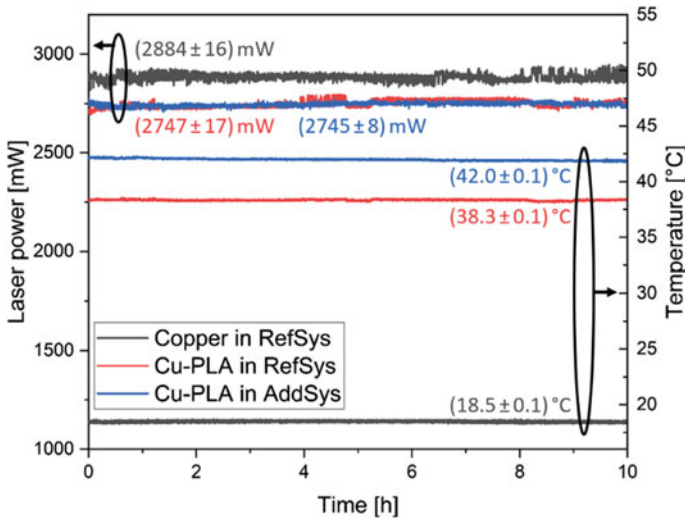
Fig. 13 Temperature measured at the heat sink and output power measured over a period of 10 h. The value in the parenthesis indicates the mean value with the associated standard deviation
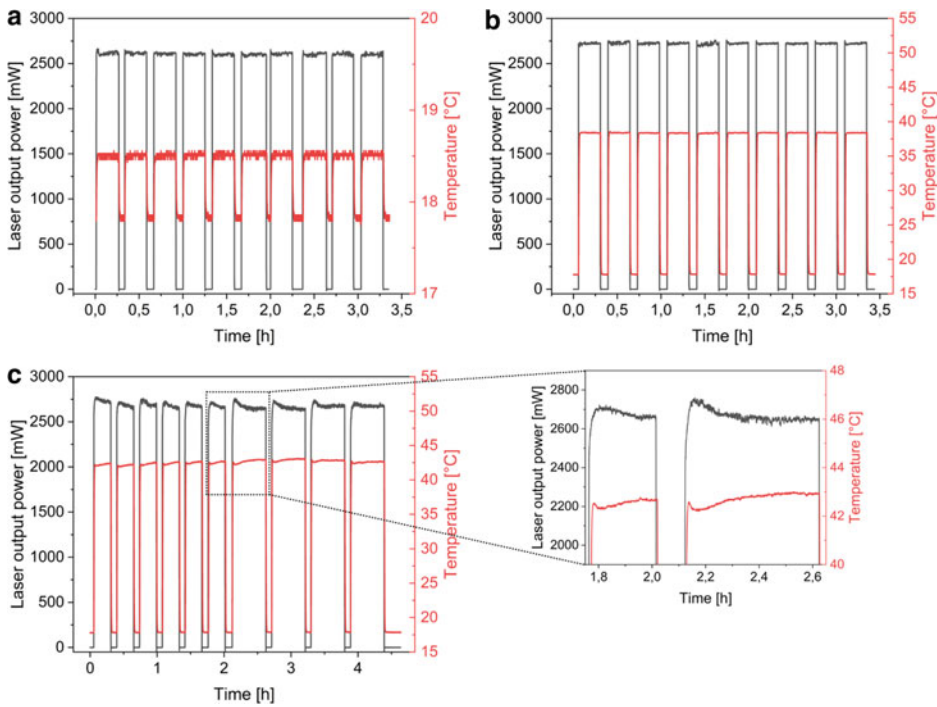
Fig. 14 Measurement of temperature and output power of the systems for 10 switching cycles. **a** Copper heat sink in reference setup. **b** Cu-PLA heat sink in reference setup. **c** Cu-PLA heat sink in additive setup

observed that longer time scales are necessary until a stable power and temperature level is reached, which is why the duration of the measurement cycles was extended. Not only the higher temperature is clearly visible again, but also the slower equilibration of the temperature accompanied by a decreasing output power.

To find a reason for the higher temperature in the additively manufactured system, a thermal imaging camera is used to take a picture of the 3D printed laser system in operation. A corresponding image is shown in Fig. 15 together with a cross section of the system's model. Thus, it can be determined at which points the system heats up (brighter areas in Fig. 15). The largest heat generation is on the right side, where the connection for the pump diode is located. The second place with a particularly high temperature development is between the first resonator mirror and the holder for the laser crystal. There seems to be a kind of heat accumulation, which leads to the stronger heating of the heat sink itself. This also explains the longer duration until a state of equilibrium is reached, since the temperature in the tube must stabilize in addition to the heat sink. However, it must also be said that the maximum temperature reached for the tube is 33 °C and thereby far from a critical thermal load for the PLA material.
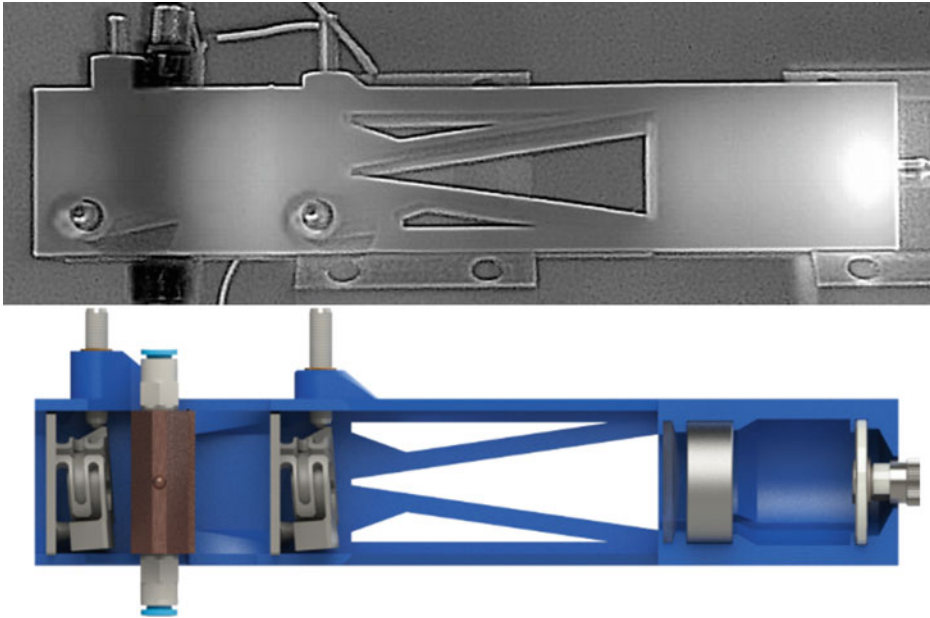
Fig. 15 Top: False color picture of the heat distribution in the laser system´s tube during operation. Brighter color corresponds to higher temperature. Bottom: Cross section of the system´s CAD model

4   Conclusion and Outlook

It has been shown that additive manufacturing based on the FFF process offers the potential for producing integrated optomechanical systems. It was thus demonstrated that optical elements can be imprinted directly into a polymer matrix, ensuring secure fixation with reduced introduction of mechanical stress. Based on this, the next innovative step to increase the level of function integration is performed by printing an adjustable optomechanic with spring system and ball joint in a single step, reducing the assembly time to a minimum. Furthermore, the possibility to manufacture water-cooled heat sinks is shown. The performance of the components is quantified by series of measurements to determine for example the stability over time or the influence of temperature changes in order to define potentials and limitations. Comparisons are also drawn with commercial and conventional components. Thereby, it was shown for the 3D printed, adjustable optomechanics that they are less stable over time and stronger influenced by temperature as the metallic one. It is quantified that polymer-based cooling performance could not be achieved to the same level as if metals were used. These points are balanced by the fact that 3D printed components can be quickly adapted to new requirements and manufactured on site, hence reducing lead-time. The elements are not only investigated

individually, but were transferred into a complex and sophisticated optomechanical system. The resulting diode-pumped solid-state laser system is compared with a conventional laboratory setup. It is shown that for low-power applications the performance of both systems is almost the same. At the same time, the 3D printed laser system benefits from a significantly reduced number of optomechanical components, as most posts and clamps become redundant. Derived from these results, the following fields of application can be defined. Since the optomechanics are highly sensitive to temperature fluctuations, it is advisable to use them in an air-conditioned environment such as a laboratory. With regard to the adjustable mirror mounts, it should be ensured that short beam paths are used in order to minimize the effect of beam drifting, which becomes particularly evident in the alignment-sensitive optical resonator. In summary, the printing of optomechanics provides the basis for cost-effective and easy-to-manufacture optomechanics. This makes such systems especially interesting for applications in the field of education or research and development, where financial resources are limited or the possibilities for manufacturing elaborately subtractive produced components are lacking. Based on the components and results presented here, a large number of other optomechanical systems can be derived and numerous applications can be addressed.

Looking at further developments, it can be said that the potential for integration has not yet been fully exploited. In order to reduce the number of single print jobs required, the next step will be to develop a system in which the heat sink for the crystal holder is also integrated with the tube for the other optics (Fig. 16).

The heat sink for the laser crystal in particular has to be redesigned, since the printing direction is different from the previous design and the cooling channel still has to be kept free of support structures. The potential of the FFF process for multi-material printing will be exploited. Furthermore, it is to be expected that the continuous progress in the field of AM, in terms of process and material development, will continuously lead to further improvements.
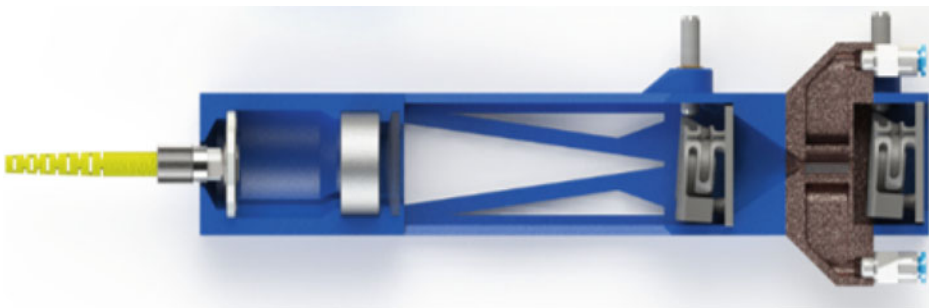

Fig. 16 Cross section of the model for an advanced additively manufactured optomechanic to scale the function integration by means of multi-material 3D printing

EUROPÄISCHE UNION
Europäischer Fonds für
regionale Entwicklung

References

1. Haleem A., Javaid, M.: Additive manufacturing applications in industry 4.0: a review. J. Ind. Integr. Manage. **4**(4), 1930001 (2019). https://doi.org/10.1142/s2424862219300011
2. Dilberoglu, U. M., Gharehpapagh, B., Yaman, U., Dolen, M.: The role of additive manufacturing in the era of industry 4.0. Procedia Manufact **11**, 545–554 (2017). https://doi.org/10.1016/j.promfg.2017.07.148
3. Zawadzki, P., Żywicki, K.: Smart product design and production control for effective mass customization in the industry 4.0 concept. Manage Prod. Eng. Rev **7**(3), 105–112 (2016). https://doi.org/10.1515/mper-2016-0030
4. Sculpteo: The State of 3D Printing 2021 (2021)
5. Li, F., Macdonald, N.P., Guijt, R.M., Breadmore, M.C.: Increasing the functionalities of 3D printed microchemical devices by single material, multimaterial, and print-pause-print 3D printing. Lab Chip **19**(1), 35–49 (2019). https://doi.org/10.1039/c8lc00826d
6. Gibson, I., Rosen, D., Stucker, B.: Additive manufacturing technologies-rapid prototyping to direct digital manufacturing. Springer, New York (2010). ISBN: 978-1-4419-1119-3
7. VDI Gesellschaft Produktion und Logistik—VDI 3405—Additive manufacturing processes, rapid manufacturing—Basics, definitions, processes. VDI Handbuch Beuth, Berlin (2014)
8. Lepoivre, A., Boyard, N., Levy, A., Sobotka, V.: Heat transfer and adhesion study for the FFF additive manufacturing process. Procedia Manufact **47**, 948–955 (2020). https://doi.org/10.1016/j.promfg.2020.04.291
9. Gebhardt, A.: Additive Fertigungsverfahren—Additive Manufacturing und 3D-Drucken für Prototyping—Tooling—Produktion, vol. 5. Hanser Verlag GmbH + Co KG, München. ISBN: 978-3-446-44401-0
10. Akhoundi, B., Behravesh, A.H.: Effect of filling pattern on the tensile and flexural mechanical properties of FDM 3D printed products. Exp. Mech. **59**(6), 883–897 (2019). https://doi.org/10.1007/s11340-018-00467-y
11. Popescu, D., Zapciu, A., Amza, C., Baciu, F., Marinescu, R.: FDM process parameters influence over the mechanical properties of polymer specimens: a review. Polym. Testing **69**, 157–166 (2018). https://doi.org/10.1016/j.polymertesting.2018.05.020

12. Bintara, R. D., Aminnudin, A., Ida, Z., Arbianto, F., Prasetiyo, D.: The characterisitc of over-hang object to material usage on FDM 3D printing technology. J. Mech. Eng. Sci. Technol. **3**(1), 35–41 (2019). https://doi.org/10.17977/um016v3i12019p035

13. Brackett, D., Ashcroft, I, Hague, R.: Topology optimization for additive manufacturing. In: 2011 International Solid Freeform Fabrication Symposium, pp. 348–362 (2011). https://doi.org/10.26153/TSW/15300

14. Mirzendehdel, A.M., Suresh, K.: Support structure constrained topology optimization for additive manufacturing. Comput. Aid. Des. **81**, 1–13 (2016). https://doi.org/10.1016/j.cad.2016.08.006

15. Roj, R., Theiß, R., Dültgen, P.: Mechanical properties of 16 different FDM-plastic types. Mater. Test. **61**(10), 999–1006 (2019). https://doi.org/10.3139/120.111413

16. Fafenrot, S., Grimmelsmann, N., Wortmann, M., Ehrmann, A.: Three-dimensional (3D) printing of polymer-metal hybrid materials by fused deposition modeling, materials **10**(10), 1199 (2017). https://doi.org/10.3390/ma10101199

17. Kuznetsov, V., Solonin, A., Urzhumtsev, O., Schilling, R., Tavitov, A.: Strength of PLA components fabricated with fused deposition technology using a desktop 3D printer as a function of geometrical parameters of the process. Polymers **10**(3), 313 (2018). https://doi.org/10.3390/polym10030313

18. Palacio, J., Orozco, V.H., López, B.L.: Effect of the molecular weight on the physicochemical properties of poly(lactic acid) nanoparticles and on the amount of ovalbumin adsorption. J. Braz. Chem. Soc. **22**(12), 2304–2311 (2011). https://doi.org/10.1590/s0103-50532011001200010

19. Afrose, F., Masood, S., Iovenitti, P., Nikzad, M., Sbarski, I.: Effects of part build orientations on fatigue behaviour of FDM-processed PLA material. Progr. Additive Manufact **1**, 21–28 (2015). https://doi.org/10.1007/s40964-015-0002-3

20. Lebedev, S.M., Gefle, O.S., Amitov, E.T., Zhuravlev, D.V., Berchuk, D.Y., Mikutskiy, E.A.: Mechanical properties of PLA-based composites for fused deposition modelling technology. Int. J. Adv. Manufact. Technol. **97**, 511–518 (2018). https://doi.org/10.1007/s00170-018-1953-6

21. Duigou, A.L., Castro, M., Bevan, R., Martin, N.: 3D printing of wood fibre biocomposites: from mechanical to actuation functionality. Mater. Des. **96**, 106–114 (2016). https://doi.org/10.1016/j.matdes.2016.02.018

22. Butt, J., Oxford, P., Sadeghi-Esfahlani, S., Ghorabian, M., Shirvani, H.: Hybrid manufacturing and mechanical characterization of Cu/PLA composites. Arab. J. Sci. Eng. **45**, 9339–9356 (2020). https://doi.org/10.1007/s13369-020-04778-y

23. Pinger, C.W., Heller, A.A., Spence, D.M.: A printed equilibrium dialysis device with integrated membranes for improved binding affinity measurements. Anal. Chem. **89**(14), 7302–7306 (2017). https://doi.org/10.1021/acs.analchem.7b01848

24. Espalin, D., Ramirez, J.A., Medina, F., Wicker, R.: Multi-material, multi-technology FDM: exploring build process variations. Rapid Prototyping J **20**(20), 236–244 (2014). https://doi.org/10.1108/rpj-12-2012-0112

25. Kranert, F., Budde, J., Hinkelmann, M., Neumann, J., Kracht, D., Lachmayer, R.: Thermische und strukturelle Analyse von Polymermaterialen in generativ gefertigten Optomechaniken für den Einsatz in der Laserentwicklung, Tagungsband 4. Niedersächsisches Symposium Materialtechnik: 25. bis 26. Februar 2021, Clausthal-Zellerfeld, virtuel (2021). https://doi.org/10.21268/20210518-5

26. Heinrich, A.: 3D-printing of optical components. Springer, Cham (2021). ISBN: 978-3-030-58959-2

27. Kloppenburg, G., Knöchelmann, M., Wolf, A.: Additive fertigung transparenter Optiken. In: Lachmayer, R., Lippert, R. B. (eds.) Additive Manufacturing Quantifiziert. Springer Vieweg Verlag, Berlin, pp. 163–174 (2017). ISBN: 978–3–662–54112–8

28. Kranert, F., Budde, J., Hinkelmann, M., Neumann, J., Kracht, D., Lachmayer, R.: 3D fabrication and characterization of polymer-imprinted optics for function-integrated, lightweight optomechanical systems. J. Laser Appl. **33**(4), 042010 (2021). https://doi.org/10.2351/7.000 0492

29. Zhang, C., Anzalone, N. C., Faria, R. P., Pearce, J. M.: Open-source 3D-printable optics equipment. PLoS One **8**(3), e59840 (2013). https://doi.org/10.1371/journal.pone.0059840

30. Salazar-Serrano, L. J., Torres, J., Valencia, A.: A 3D printed toolbox for opto-mechanical components. PLoS One **12**(1), e0169832 2017, https://doi.org/10.1371/journal.pone.0169832

31. Winter, B., Shepler, D.: 3D printable optomechanical cage system with enclosure. HardwareX **3**, 62–81 (2018). https://doi.org/10.1016/j.ohx.2017.12.001

32. Gunderson, J.E., Mitchell, D.W., Bullis, R.G., Steward, J.Q., Gunderson, W.A.: Design and implementation of three-dimensional printable optomechanical components. J. Chem. Educ. **97**(10), 3673–3682 (2020). https://doi.org/10.1021/acs.jchemed.0c00631

33. Davis, E.J., Jones, M., Thiel, D.A., Pauls, S.: Using open-source, 3D printable optical hardware to enhance student learning in the instrumental analysis laboratory. J. Chem. Educ. **95**(4), 672–677 (2018). https://doi.org/10.1021/acs.jchemed.7b00480

34. Delmans, M., Haseloff, J.: µCube: a framework for 3D printable optomechanics. J. Open Hardw. **2**(1), 2 (2018). https://doi.org/10.5334/joh.8

35. Diederich, B., Lachmann, R., Carlstedt, S., Marsikova, B., Wang, H., Uwurukundo, X., Mosig, A. S., Heintzmann, R.: A versatile and customizable low-cost 3D-printed open standard for microscopic imaging. Nat. Commun. **11**, 5979 (2020). https://doi.org/10.1038/s41467-020-194 47-9

36. Maia Chagas, A., Prieto-Godino, L.L., Arrenberg, A.B., Baden, T.: The €100 lab: A 3D-printable open-source platform for fluorescence microscopy, optogenetics, and accurate temperature control during behaviour of zebrafish drosophila, and caenorhabditis elegans. PLoS Biol. **15**(7), 1–21 (2017). https://doi.org/10.1371/journal.pbio.2002702

37. Nuñez, I., Matute, T., Herrera, R., Keymer, J., Marzullo, T.;, Rudge, T., Federici, F.: Low cost and open source multi-fluorescence imaging system for teaching and research in biology and bioengineering. PLoS One **12**(11), e0187163 (2017). https://doi.org/10.1371/journal.pone.018 7163

38. Aydogan, O., Tasal, E.: Designing and building a 3D printed low cost modular Raman spectrometer. CERN Idea Square J. Exp. Innovation, **2**(2), 3–14 (2018). https://doi.org/10.23726/CIJ.201 7.799

39. Pereira, V. R., Hosker, B. S.: Low-cost (<5€), open-source, potential alternative to commercial spectrophotometers. PLOS Biol., **17**(6), e3000321 (2019). https://doi.org/10.1371/journal.pbio. 3000321

40. Porter, L. A., Chapman, C. A., Alaniz, J.A.: Simple and Iinexpensive 3D printed filter fluorometer designs: user-friendly instrument models for laboratory learning and outreach activities. J. Chem. Educ., **94**(1), 105–111 (2016). https://doi.org/10.1021/acs.jchemed.6b00495

41. Porter, L.A., Washer, B.M., Hakim, M.H., Dallinger, R.F.: User-Friendly 3D printed colorimeter models for student exploration of instrument design and performance. J. Chem. Educ. **93**(7), 1305–1309 (2016). https://doi.org/10.1021/acs.jchemed.6b00041

42. Zou, L., Mahmoud, M., Fahs, M., Liu, R., Lo, J. F.: 3D printed miniaturized spectral system for tissue fluorescence lifetime measurements. In: Proceedings SPIE, vol. 9711. Imaging, manipulation, and analysis of biomolecules, cells, and tissues IX, Article 97111S. San Francisco. https:// doi.org/10.1021/acs.jchemed.6b00041

43. Nadal-Serrano, J. M., Nadal-Serrano, A., Lopez-Vallejo, M.: Democratizing science with the aid of parametric design and additive manufacturing: design and fabrication of a versatile and

low-cost optical instrument for scattering measurement. PLoS One 12(1), pp. e0187219 (2017). https://doi.org/10.1371/journal.pone.0187219

44. Kranert, F., Budde, J., Neef, P., Bernhard, R., Lammers, M., Rettschlag, K., Grabe, T., Wienke, A., Neumann, J., Wiche, H., Weslin, V., Ahlers, H., Lachmayer, R., Kracht, D.: 3D-printed, low-cost, lightweight optomechanics for a compact, low-power solid state amplifier system. In: Proceedings SPIE, vol. 11261. Components and Packaging for Laser Systems VI, Article 1126105. San Francisco, 202010.1117/12.2544268

45. Kranert, F., Budde, J., Hinkelmann, M., Wienke, A., Neumann, J., Kracht, D., Lachmayer, R.: Quasi-monolithic laser system based on 3D-printed optomechanics. In: Proceedings SPIE, vol. 11667. Components and Packaging for Laser Systems VII, Article 116670L (2021). https://doi.org/10.1117/12.2577457

46. Grabe, T., Budde, J., Kranert, F., Wienke, A., Neumann, J., Kracht, D., Lachmayer, R.: Kühlkörper-Designansatz für einen in AlSi10Mg eingebetteten YAG-Laserkristall. In: Lachmayer, R., Rettschlag, K., Kaierle, S. (eds) Konstruktion für die Additive Fertigung 2019, Springer Vieweg Verlag, Berlin, pp. 159–175 (2020). ISBN: 978-3-662-621148-7

47. Neef, P., Bernhard, R., Wiche, H., Wesling, V.: Verwendung von Kupfer-Molybdän-Pseudolegierungen für die laserbasierte additive Fertigung von Multimaterial-Verbindungen, Tagungsband 4. Niedersächsisches Symposium Materialtechnik: 25. bis 26. Februar 2021, Clausthal-Zellerfeld, virtuel, 2021, https://doi.org/10.21268/20210519-1

48. Bernhard, R., Neef, P., Wiche, H., Wesling, V., Hoff, C., Hermsdorf, J., Kaierle, S.: Additive manufacturing of copper-molybdenum pseudoalloys. In: Proceedings SPIE, vol. 11349, 3D printed optics and additive photonic Mmanufacturing II, Article 113490C. San Fransisco (2020). https://doi.org/10.1117/12.2555708

49. Yoder, P.: Mounting Optics in Optical Instruments. SPIE, Bellingham (2008). ISBN: 978-0-8194-7129-1

50. Brostow, W.: Mechanical properties. In: Mark, J. E.: Physical properties of polymers Hhandbook. Springer Science+Business Media LLC, New York, pp. 423–446 (2007). ISBN: 978-0-387-31235-4

51. Koechner, W.: Solid-State Laser Engineering. Springer Science+Business Media, New York (2006). ISBN: 978-0387-29094-2

52. Paschotta, R.: Field Guide to Lasers. SPIE, Bellingham (2008). ISBN: 978-0-8194-7826-9

53. Siegman, A.: Lasers (Revised), University Science Books, Mill Valley (1986). ISBN: 9780935702-11-8

54. DIN EN ISO 62:2008-05, Plastic. Determination of water absorption, German version

55. Newburgh, G.A., Dubinskii, M.: A high gain, composite Nd:YVO$_4$/SiC thin disk amplifier. In: Proceedings SPIE, vol. 9081, Laser Technology for Defense and Security X, Article 908110. Baltimore (2014). https://doi.org/10.1117/12.2053751

56. Elkholy, A., Rouby, M., Kempers, R.: Characterization of the anisotropic thermal conductivity of additively manufactured components by fused filament fabrication. Prog. Additive Manufactur. **4**, 497–515 (2019). https://doi.org/10.1007/s40964-019-00098-2

57. Bargel, H.-J., Schulze, G.: Werkstoffkunde. Springer, Berlin. ISBN: 978-3-540-79296-3 (2008)

58. Eichler, J., Dünkel, L., Eppich, B.: Die strahlqualität von lasern – wie bestimmt man beugungsmaßzahl und strahldurchmesser in der Praxis? Laser Tech. J. **1**(2), 63–66 (2004). https://doi.org/10.1002/latj.200790019

59. Délen, X., Balembois, F., Georges, P.: Temperature dependence of the emission cross section of the Nd:YVO$_4$ around 1064 nm and consequences on laser operation. J. Opt. Soc. Am. B **26**(5), 972–976 (2011). https://doi.org/10.1364/josab.28.000972

Additive Manufacturing of Optics and Optomechatronics: Multiphysics Simulation Environments for Process, Materials and Design Analysis

Tobias Grabe, Julian Röttger, Katharina Rettschlag, and Roland Lachmayer

1 Introduction

Today, the manufacturing and operation of highly functional and precise optical systems are based on complex multi-stage processes and labor-cost intensive adjustment. The associated high costs prevent the mass use of high-quality technologies in the life sciences, production engineering, sensor technology and daily life. The keywords "additive manufacturing" and "Industry 4.0" describe the shift toward IT-connected production and individualized manufacturing at low cost [1]. Even if additive manufacturing seems to be related to long machine operating times, considerable potential for the development and production of optomechatronic systems results from function integration, material savings, reduction of assembly effort and, in particular, function improvement [2–4]. The GROTESK project aims to explore the fundamental potentials of the additive manufacturing of optical components and systems by considering these opportunities. For this goal, simulation plays a central role in investigating thermal, optical and mechanical effects within complex systems. Thus, the implementation of simulation environments is beneficial for developing a qualified process chain [5]. Following, a typical process

T. Grabe · J. Röttger · R. Lachmayer
Institute of Product Development (IPeG), Leibniz University Hannover, Garbsen, Germany
e-mail: grabe@ipeg.uni-hannover.de

K. Rettschlag (✉) · R. Lachmayer
Laser Zentrum Hannover e.V. (LZH), Hannover, Germany
e-mail: k.rettschlag@lzh.de
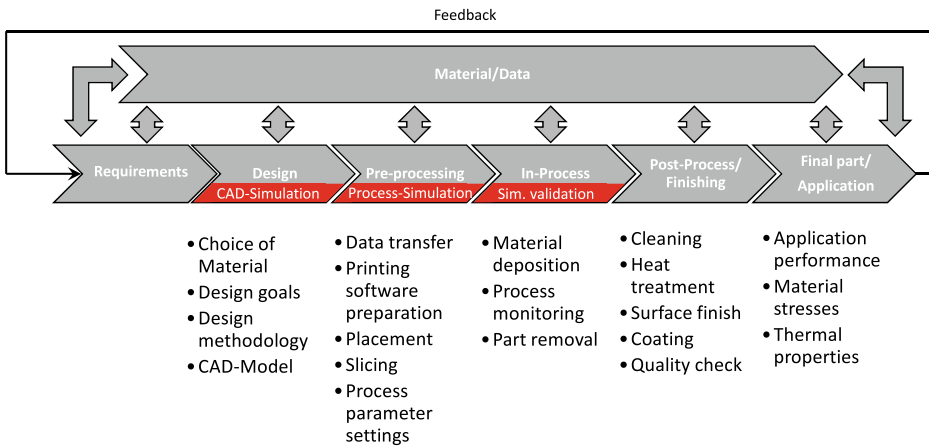
Fig. 1 Schematic representation of the process chain for developing additive manufactured components [6]

chain for additive manufacturing processes is described in Fig. 1. This chain can generally be divided into the following phases: "Requirements", "Design", "Pre-process", "In-process", "Post-process/Finishing" and the "Application" [6].

The components' requirements are defined at the outset between the players involved in the value creation process. These include the choice of material, the required technological properties, the subsequent function and application of the component. The requirements define the choice of the additive manufacturing process, the necessary steps, and measures for quality assurance. In the "Design" phase, digital three-dimensional volume models are derived. Intermediate steps such as those in conventional manufacturing, including tools, are not required for an exclusively additive manufacturing process. In addition to the design of the components, simulations and optimization of the components are carried out in the design phase in order to meet the previously set requirements and to be able to make an appropriate material selection. In the "Pre-process" the three-dimensional model is digitally divided into individual layers and necessary additional geometries, such as support structures, are generated. Following the slicing process, process and machine parameters are set, and the equipment is prepared for the printing process. The actual production of the components begins in the "In-process". Here, the operations set in the pre-processing are implemented. The manufacturing is controlled with the help of process monitoring systems. A "Post-process" is required for almost all additive manufacturing processes. The manufactured components must be separated from the build platform and the support structures, in individual cases, the materials residues must be removed [7].

Especially in the "Design" and "Pre-processing" phases, digital development environments can be utilized so that the individual process steps can be efficiently performed. Furthermore, the simulation driven development of the manufacturing technology enables

the analysis and minimization of processing errors and tolerances. Thus, these environments support the targeted reduction of the pre- and post-processing activities. As digitization and automation advance, additive series production will become increasingly important [8]. In general, process chains are application and typological and must therefore be specified individually [9]. This means, for example, that the product requirements, the manufacturing machine specifications and the thermochemical properties of the material used in production but available development tools must be taken into account when setting up additive manufacturing processes [10]. The implementation of multiphysics simulation environments within the process chain can support the process and material development at multiple steps. For example, for the evaluation of CAD models, the calculation of process data of new manufacturing processes, or the investigation of the influence of material properties on thermal, mechanical, or optical component properties. A wide range of concepts can be examined computationally to minimize the number of cost-effective physical setups.

In particular, the GROTESK project aims to explore integrative generative manufacturing to manufacture novel optical, thermal and structural multi-material components. For this purpose, multifunctional optomechanical assemblies, including optics, are being designed for the manufactured from several materials in a single process environment and characterized concerning the requirements related to the field of laser technologies. Therefore, materials combinations are to be developed and processed in a novel way into functional components, such as optical and optomechanical components [11]. Hereby, the focus relies mainly on the additive manufacturing of glass optics and novel materials for application in high-power laser systems which can be derived as follows:

Glass optics are characterized by their excellent optical properties and high thermal and chemical resistance. However, conventional manufacturing of specialized free-form optics from glass is challenging. Additive manufacturing offers a promising solution to this challenge. However, additively manufactured glass components have only been used in architecture due to their low optical quality. In addition, functional glass elements intended to guide or manipulate light cannot yet be reliably additively manufactured due to the insufficient components homogeneity and its often undefined optical properties. For this reason, the further development of the manufacturing processes, such as the Lateral (see Chap. 1) and the Coaxial Laser Glass Deposition (see Chap. 6), is of central importance.

In order to implement additive manufactured optical components into systems, the use of optomechanical elements, as shown in the GROTESK Laser demonstrator (see Chap. 2), is required. In general, these elements require a lower manufacturing accuracy compared to optical components. However, optomechanics has to meet application-specific thermal and mechanical requirements. Thus, new materials for additive manufacturing are being developed in GROTESK to meet these particular demands (see Chap. 4). However, during their development, the thermal specification necessary for the reliable operation in the optical application area are often insufficiently described. In

particular, the thermal properties of the interface between an optically and a mechanically functionalized material are not considered.

Due to these challenges, two primary goals for developing simulation environments are set to address these challenges in GROTESK. On the one hand, in Sect. 2, a simulation environment shall be developed, which allows a theoretical analysis of the glass printing process and thus potentially the development of a more stable manufacturing process. Furthermore, these simulations enable the thermal analysis and development-driven comparison of the Lateral and Coaxial Laser Glass Deposition (LGD) approach. On the other hand, different materials used for the additive manufacturing of optomechanics are to be analyzed regarding their thermomechanical behavior in the application. Based on this, in Sect. 3, requirements for the development of future materials will be derived.

2 Thermal Simulation of the Lateral and the Coaxial Laser Glass Deposition (LGD) Process Used for Optics Manufacturing

Fused silica is a promising material for achieving high component durability and good optical properties [12]. However, additive manufacturing of glass is associated with several challenges. For example, glass processing requires a material temperature of more than 2000 °C [13, 14]. These extreme process temperatures can lead to high stresses in the material and potentially to the destruction of the glass component after the layer-by-layer additive manufacturing process is completed [13, 14]. Furthermore, these stresses can affect the optical properties of the glass through refractive index variations [15]. Therefore, for the development of additive manufacturing processes for functional optical glass components, the analysis of the machine and material parameters that influence the thermal processes during the manufacturing process is of great importance.

2.1 LGD Processes in GROTESK

In the LGD Process, the fused silica fiber is fed into the processing zone and heated by the laser beam. In the LGD processing machines used in GROTESK, a CO_2 laser with a wavelength of $\lambda = 10.6$ µm is utilized to process fused silica because this wavelength is absorbed by the material to a high degree. The fused silica fiber is deposited on a fused silica substrate. The substrate is mounted on an axial table of a two-axis system (x, y) for the process. A third axis is used to move the glass print head in the z-direction. Both, coreless fibers and fibers with cores in variable diameters, can be processed with this method [14].

In GROTESK two different LGD process setups are developed: the lateral (see Chap. 1) and the coaxial Laser Glass Deposition (see Chap. 6). The two processes differ in the glass
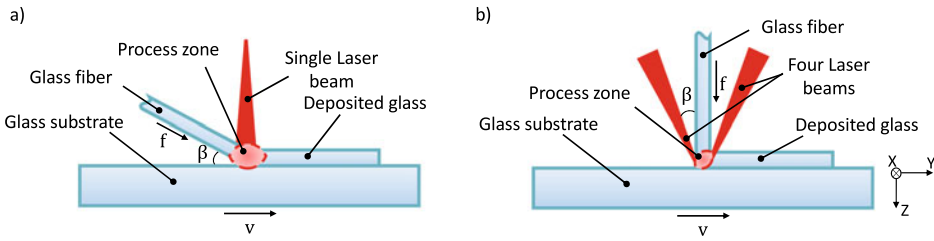
Fig. 2 Schematic diagram of the process for **a** the lateral and **b** coaxial LGD process

fiber and laser beam guidance into the process zone. In the lateral process, the fused silica fiber is guided into the process zone from the outside at an inclination angle β and heated by the incident laser beam. The heat source is a single laser beam directed perpendicular to the substrate (see Fig. 2a). The lateral process has been developed for several years and is often used for cladding glass fibers. As a result, straight, curved and rotationally symmetric geometries can be realized. The lateral wire feed leads to a considerable interference geometry of the system technology, limiting the potential for manufacturing more complicated geometries. For example, welding tracks cannot be welded to an existing component wall because the welding nozzle would collide with the structures already applied.

This problem can potentially be solved by developing a coaxial process where the fiber is fed into the process zone perpendicular to the substrate plate in the coaxial process [16]. With this principle, the laser beam, which also serves as the heat source, is split into multiple partial beams and radiates the glass fiber from four sides with an inclination angle β (see Fig. 2b). This allows the processing head and the substrate not to be rotated relative to each other to deposit glass in different directions. Thus, significantly simplified system operation and additive manufacturing of free-form objects could be potentially achieved in comparison to the lateral process. However, the coaxial LGD process is almost not experimentally investigated due to its first introduction within the GROTESK project (see Chap. 6).

As part of the GROTESK project, the lateral LGD process is further developed for the additive manufacturing of optical components made of glass (see Chap. 1). Based on its experimental investigation, the fundamentals for the control of this technology are developed and a thermal simulation model for its description is built up. This model is evaluated experimentally and then transferred to the coaxial principle. This procedure allows the numerical comparison of these two processes. Based on this comparison, optimization potentials and development targets for further development can be derived.

2.2 Simulation Approach for the Lateral LGD Process

Several approaches have already been developed for the thermal simulation of the lateral LGD process. For example, based on the mass and energy balance, the equilibrium temperature in the process zone, shown in Fig. 3, is simulated by Luo et al. [15]. The laser power P, the absorption coefficient α the supplied mass flow $\dot{m}_{in} = \dot{m}_{out} = \dot{m}$ which depends on the fiber and substrate feeding rate f and v, respectively, the specific enthalpy of fused silica Δh, the heat loss from the glass fiber into the substrate plate $\dot{q}_s$, the heat loss by thermal radiation $\dot{q}_r$, the heat flow into the filament $\dot{q}_f$, the heat loss by convection $\dot{q}_c$ are taken into account. At constant laser power and constant material feed rate, an equilibrium of the thermal energy ΔE ideally occurs in the process zone. This condition can be described by Eq. (1), assuming an isentropic model approach.

$$\Delta E = \alpha P - \left(\dot{m} \cdot \Delta h + \dot{q}_s + \dot{q}_f + \dot{q}_c + \dot{q}_r \right) = 0 \tag{1}$$

This approach demonstrates the material and machine parameters that have to be taken into consideration to analyze the thermal equilibrium temperature in the process zone. However, it does not enable the analysis of the temperatures and heat fluxes occurring in the glass fiber cross-section, inside the substrate plate and the fiber-substrate interface. For this reason, a 3D approach is an alternative for the numerical representation of local effects. For this approach, simulations describing the LGD process have already been performed by Pohl et al. [17]. Nevertheless, for the proposed simulation, computation costs are very high. Furthermore, the glass fiber diameter, its geometry and mass, and the feed angle between the glass fiber and the substrate plate are not considered, which also does not allow the analysis of the glass fiber cross-section. Therefore, a 2D approach is adopted in this work, which takes these geometrical parameters into account to enable the cross-section analysis of the fiber for the first time. For this, a geometrical and material
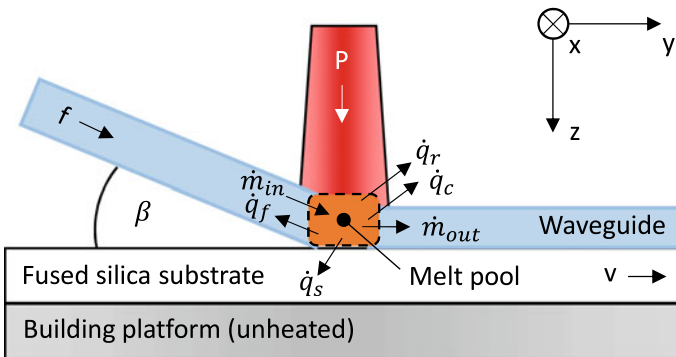
Fig. 3 Mass and energy balance in the process zone exemplarily shown for the lateral LGD process derived from Luo et al. [15]
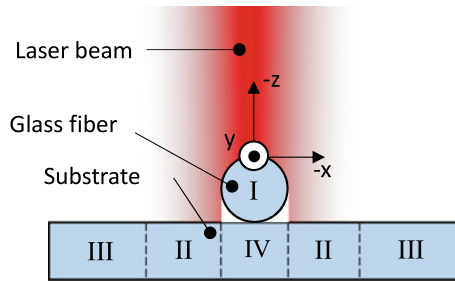
Fig. 4 Cross-section through glass fiber and substrate plate. The division into four sub-areas: I: Direct laser irradiation into glass fiber, II. direct laser irradiation onto substrate plate, III. no laser irradiation, IV. substrate plate in the shadow of the glass fiber

model is defined, which represents the fiber and substrate geometry. Further, the process paremeters are considered by defining appropriate boundary conditions.

In the geometric model, the glass fiber and substrate plate are considered as cross-sections and are divided into four areas. These are illustrated for the lateral process in Fig. 4. The optical fiber, which is directly affected by the laser power, is considered in area I. Area II includes the segment of the substrate plate that is also directly irradiated by the laser. Area III describes the region of the substrate plate that lies outside the laser radius. Finally, area IV is the part of the substrate plate that lies in the shadow of the optical fiber. The laser radius, fiber diameter, and substrate plate thickness are specified as geometric input parameters in this simulation environment.

For the thermal model, the Lambert–Beer law describes the laser energy in fused silica as a function of the absorption depth, the energy incident on the material surface and the material temperature. According to Abitan et al. [18], neglecting stimulated and spontaneous emission, it is assumed that the laser energy absorbed in the material is fully converted into heat. Based on this, the energy converted into heat is calculated in an arbitrary absorption depth interval at a defined material temperature. The energy converted into heat $\Delta Q(z,T)$ in an arbitrary absorption depth interval from z_1 to z_2 at a defined material temperature is calculated according to Eq. (2) [19], where $\alpha(T)$ denotes the temperature-dependent absorption.

$$\Delta Q(z, T) = \int_{z1}^{z2} E_0 \cdot \alpha(T) e^{-\alpha(T) \cdot z} d(z) \tag{2}$$

For the implementation of this law and the simulation of the thermal material's behavior, the influence of the temperature-dependent absorption [20], effective thermal conductivity coefficient [21], specific heat capacity [20] and density [22] of fused silica are considered in the simulation. Since the glass is typically molten within the process zone, high temperatures of more than 2000 °C occur. Thus, it should be noted that according to

Luo et al. [15] and Hildebrand et al. [23], the temperature-dependent thermal conductivity coefficient is formed from a material value for thermal conduction and a transmission value of infrared radiation at high temperatures (> 750 °C). Therefore, material deformations due to surface tensions which are expected to occur for temperatures above the melting temperature are neglected for the thermal analysis.

For considering the opto-thermal boundary conditions, an ideal Gaussian laser with the Gaussian radius ω and total power P is assumed. The laser intensity $I(x,z,T)$ at absorption depth z at time t of maximum energy input for areas I and II are calculated according to Eq. (3) and for area III according to Eq. (4). According to Eq. (2), most laser energy is absorbed near the fiber optic surface. Consequently, for area IV, refraction in the glass is neglected. Based on these assumptions, the laser intensity under the glass fiber with diameter d can be approximated according to Eq. (5) [19].

$$I(x, z, T)_{1,2} = \frac{2\alpha(T)P}{\pi\omega^2} e^{-2\frac{x^2}{\omega^2} - \alpha(T)(z - z_0)} \tag{3}$$

$$I(x, z, T)_3 = 0 \tag{4}$$

$$I(x, z, T)_4 = \frac{2\alpha(T)P}{\pi\omega^2} e^{-2\frac{x^2}{\omega^2} - \alpha(T)\left(2\sqrt{\frac{D_f^2}{4} - x^2} + z - D_f\right)} \tag{5}$$

Furthermore, Fresnel reflections, which reduce the energy input into the glass, are taken into account [24, 25]. Fresnel reflections occur due to reflections on the surface of the glass fiber and the substrate plate. These reflections are calculated based on the feed angle and the filament geometry [26]. The underside of the substrate plate rests on the aluminum traversing table and is thermally connected to it. Therefore, at the glass fiber surface and the surface of the substrate plate, thermal power is emitted to the environment by convection and thermal radiation [27, 28].

For taking the third spatial dimension into account, it is assumed that the cross-section traverses the process zone along the y-axis at the feed rate f as a function of simulation time. By this assumption, the influences of Gaussian radius, angle of glass fiber feed and filament feed rate can be analyzed [29]. After the contact between the glass fiber and the substrate plate, the fiber rests on the substrate. Thus, in this case β = 0 is applied. The time coefficient τ(t) introduced for this purpose is calculated by Eq. (6) and multiplied by Eqs. (3)–(5) for each time step t. Here, the parameter a denotes the threshold where τ(t) ≥ 0 applies.

$$\tau(t) = e^{-2\frac{\left(f \cdot t \cos(\beta) - \frac{\sqrt{-0.5 \cdot \log(a) \cdot \omega^2}}{\cos(40° - \beta)}\right)^2}{\omega^2}} \quad \text{mit } \beta = 0° \text{ for } t > \frac{\sqrt{-0.5 \cdot \log(a) \cdot \omega^2}}{\cos(40°)} \tag{6}$$

2.3   Simulation of the Lateral LGD Process

The simulation is performed with the parameters listed in Table 1 based on a 2D finite element mesh with 22,335 Elements in COMSOL-Multiphysics 5.5. These parameters are derived from experiments where the lateral LGD process is sufficiently performed in experiment, meaning no cracks and interlayer defects occur in the glass after its deposition (compare [13]).

From the technological point of view of glass production and processing, Teschner et al. [30] set reference points for fused silica related to the temperature which characterize the glass melt. The technological fixed points, starting with the highest viscosity, are as follows: The "Transformation point" (T_1 = 1171 °C) that is also referred to as freezing temperature, "Softening Point" (T_2 = 1676 °C) that is the lowest temperature at which the glass deformation can be observed, "Flow Point" (T_3 = 2116 °C) where a relatively strong glass deformation is occurrent and "Working Point" (T_4 = 2359 °C) which is also referred to as the sinking temperature. Above this temperature, the glass can be processed well and the glass has sufficient forming ability.

Following, the simulation results for the time-dependent temperatures of the fiber surface, the bottom of the optical fiber, and under the surface of the substrate plate are compared to these reference points and shown in Fig. 5. In the simulation, inhomogeneous heating is calculated over the cross-sectional area of the glass fiber. Consequently, a temperature gradient is formed across the fiber. The top surface of the glass fiber reaches a maximum in the simulation, while the opposite point on the underside reaches a lower temperature. Significantly lower temperatures are calculated below the glass fiber on the substrate plate.

In the contact area between the glass fiber and the substrate plate, rapid convergence of temperatures occurs due to the fusion of the two components. Subsequently, the glass cools down steadily at all measuring points. Here, the temperature gradient in the cooling of the substrate plate is lower than that in the glass fiber. From the comparison with the reference points, it can be seen that the bottom side of the glass fiber reaches the

Table 1 Process parameters and materials of the lateral LGD process

Parameter	Symbol	Value	Unit
Laser power (cw)	P	67.5	W
Beam waist diameter (Gaussian)	ω	2.1	mm
Fiber feed velocity	f	1.5	mm/s
Substrate feed velocity	v	1.5	mm/s
Incident laser angle on fiber	β	40	°
Fiber diameter	d	0.4	mm
Initial substrate temperature	T_s	20	°C
Environmental temperature	T_∞	20	°C
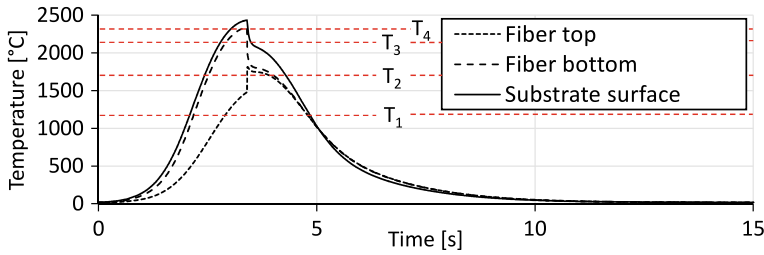
Fig. 5 Simulated temperatures in the glass fiber and on the surface of the substrate plate within the lateral LGD process

working point (T_4) before contact with the substrate plate. This enables the successful deposition of the glass fiber. Furthermore, after contact, the interface cools very quickly to a temperature below the transformation point (T_2) so that further deformation of the glass can not occur for the subsequent cooldown process.

2.4   Evaluation of the Simulation Results for the Lateral LGD Process

For evaluating the simulation results, a temperature measurement is carried out in the lateral LGD process (see Chap. 1) with a pyrometer. With this pyrometer, the average temperature can be recorded in a measuring range of 1.5 mm diameter on the substrate plate. The center of the measuring range is located in the maximum laser intensity in the process zone. In contrast to the simulation, this measurement measures the mean temperature in the measurement area rather than the temperature at a cross-section of the optical fiber passing through the process zone. Thus, it is expected that the measured temperatures may be affected by the emission and transmission properties of the glass and by its evaporation.

In order to compare the simulation results with the measured data of the pyrometer, the average temperature is defined. First, the temperatures of the FEM nodes are read at seven analysis points located in the pyrometer measurement range at the glass surface to calculate the average temperature. Then the arithmetic mean is formed. On this basis, the influence of process parameters on the average temperature can be evaluated. The values of pyrometer measurement and mean temperature are shown in a range of values from $1.3 \frac{mm}{s} \leq f \leq 2.0 \frac{mm}{s}$ and $56.3 \ W \leq P \leq 78.8 \ W$ in Fig. 6. With increasing laser power, the simulated average temperature in the process zone increases. This temperature development is nonlinear since the heat losses due to thermal radiation increase exponentially. Thus, at $P = 53.3 \ W$ laser power and $f = 1.5 \ mm/s$, the mean temperature is $T_{M,S} = 1746 \ °C$ and at $P = 78.8 \ W \ T_{M,S} = 2078$. Furthermore, the temperature increasaes with decreasing feed rate.
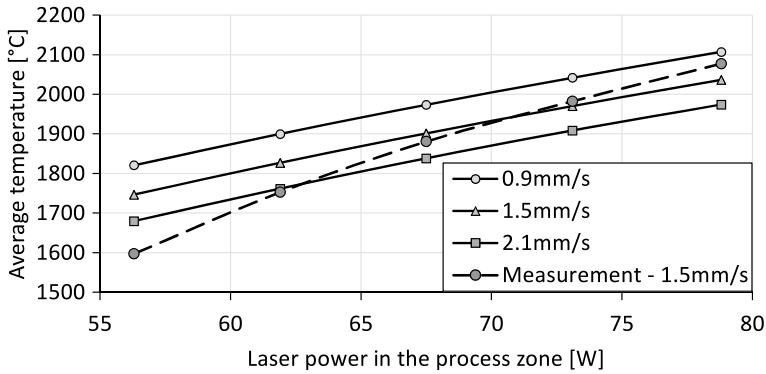
Fig. 6 Simulated mean temperatures for different laser powers in the process zone and feed speeds compared to the measurement results

Compared to the measured data, a deviation from the simulation data to the measured data is noticeable. This can be caused on the one hand by the boundary conditions or on the other hand by the physical model of the simulation. Furthermore, factors such as the measurement accuracy of the pyrometer or deviating process environments lead to this deviation. The impact of these factors on the result is discussed in Sect. 2.9. The discrepancies and similarities found here have to be further analyzed in future work.

2.5   Transfer of the Model to Simulate the Coaxial LGD Process

As part of the GROTESK project, a multi-material process option is being developed to process the material designed for the deposition welding of glass and metal powder (see Chap. 6). Therefore, based on the simulation model for the lateral LGD process, the simulation of the coaxial process for the additive manufacturing of glass is implemented. For this, the thermal model of fused silica and the 2D geometric model are transferred, for the new process simulation. This requires, significant changes are made in the thermo-optical boundary conditions.

In a first step, the fiber is now fed into the process zone perpendicular to the substrate plate and is guided out horizontally after welding. Here, the glass fiber is irradiated by four beam bundles focused onto the process zone. Accordingly, the boundary conditions for the heat input into the glass fiber and onto the substrate plate must be adapted. For this reason, areas II and IV shown in Fig. 4 are combined in the geometric model and calculated according to Eq. (8). Next, the optical fiber is assigned to area I analogous to the lateral model and the coaxial irradiation is determined with Eq. (7). Note that the angle β is the incident laser angle on the fiber. The coefficients f(t) and g(t) denotes the energy incident into the fiber and substrate, respectively, as a function of time.

$$I(x, z, T)_1 = \frac{2 \cdot \alpha(T)P}{\pi \omega^2 \cdot \sin(\beta)} e^{-2\frac{x^2}{\omega^2} - \alpha(T)(z-z_0)} \cdot f(t) \tag{7}$$

$$I(x, z, T)_2 = \frac{2 \cdot \alpha(T)P}{\pi \omega^2 \cdot \sin(\beta)} e^{-2\frac{x^2}{\omega^2} - \alpha(T)(z-z_0)} \cdot g(t) \tag{8}$$

$$f(t) = \begin{cases} e^{\frac{-2(v_F \cdot t)^2}{\left(\frac{\omega}{\sin(\beta)}\right)^2}} & for \ t < \frac{1.7[\text{mm}]}{f} \\ 0 & for \ t \geq \frac{1.7[\text{mm}]}{f} \end{cases} \tag{9}$$

$$g(t) = \begin{cases} 0 & for \ t < \frac{1.7[\text{mm}]}{v_F} \\ e^{\frac{-2(v_S \cdot t - 1.8[\text{mm}])^2}{\left(\frac{\omega}{\sin(\beta)}\right)^2}} & for \ \frac{1.7[\text{mm}]}{v} \leq t < \frac{3.4[\text{mm}]}{v} \\ 0 & for \ t \geq \frac{1.7[\text{mm}]}{v} \end{cases} \tag{10}$$

The time coefficients f(t) and g(t) are calculated using Eqs. (8) and (9). Then, f(t) and g(t) are considered for each time step Δt. In these equations, the factors for the distance are related to the laser beam guiding and laser spot size.

2.6 Simulation of the Coaxial LGD Process

The simulation is conducted based on a 2D finite element mesh with 40,587 elements and is carried out with the parameters listed in Table 2. These parameters are derived from experiments where the coaxial LGD process is successfully performed, meaning no cracks and interlayer defects occur in the glass after its deposition (compare [16]).

The result for the time-dependent temperature on the top, the middle, the bottom of the glass fiber and under the surface of the substrate plate is shown in Fig. 7. In the simulation, the top of the glass fiber reaches a maximum temperature of 2585 °C. Further, the fiber's middle and bottom reach maximum temperatures of 2500 and 2474 °C,

Table 2 Process parameters and materials of the coaxial LGD process

Parameter	Symbol	Value	Unit
Laser power (cw)	P	67.5	W
Beam waist diameter	ω	1.12	mm
Fiber feed velocity	f	600	mm/min
Substrate feed velocity	v	100	mm/min
Incident laser angle on fiber	β	16.81	°
Fiber diameter	d	0.4	mm
Initial substrate temperature	T_s	20	°C
Environmental temperature	T_∞	20	°C
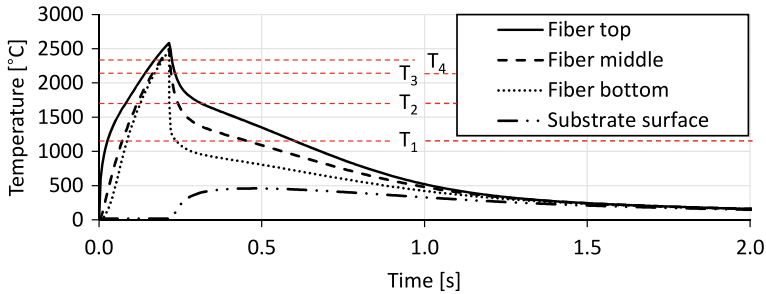
Fig. 7 Simulated temperatures in the glass fiber and on the surface of the substrate plate within the coaxial LGD process

respectively. Under the surface of the substrate plate positioned below the glass fiber, significantly lower temperatures with a maximum value of 462 °C are estimated. The simulation shows that along the contact surface between the glass fiber and the substrate plate, the melting of the fiber causes a rapid convergence of the temperatures before all measuring points approach the environmental temperature. Based on the simulation, it can be derived that almost homogeneous heating of the glass fiber is achieved by using the coaxial process principle [16].

From the comparison with the reference points of glass (compare Sect. 2.4), it can be seen that the entire glass fiber reaches the working point (T4) before contact with the substrate plate and even exceeds it significantly. This presumably leads to the glass's melting and thus enables successful deposition welding of the glass fiber. After contact, the glass of the fiber cools very quickly to a temperature below the transformation point (T2) so that further glass deformation can no longer occur.

2.7 Comparison of the Lateral and the Coaxial LGD Process

Considering the temperature development shown in Fig. 7, most of the incident laser beam energy is introduced into the fiber using the coaxial LGD process. This characteristic is achieved by the coaxial beam guidance and several individual beams surrounding the fiber. The laser power focus on the fiber leads to less heat generation in the substrate than the lateral process and consequently to a significant temperature difference between the fiber and the substrate, shown in Fig. 8. This difference can lead to stress-induced cracks within the material during the coaxial glass deposition process [16].

Compared to the lateral LGD process, the energy input into the fiber is more homogeneous due to the coaxial beam guidance. Thus, a more uniform melting and focused heat induction can be achieved, enabling up to six times higher fiber feed velocity at constant laser power [16]. Based on these results, it can be concluded that separate temperature control of the substrate, such as hot air heating and a thermal-controlled
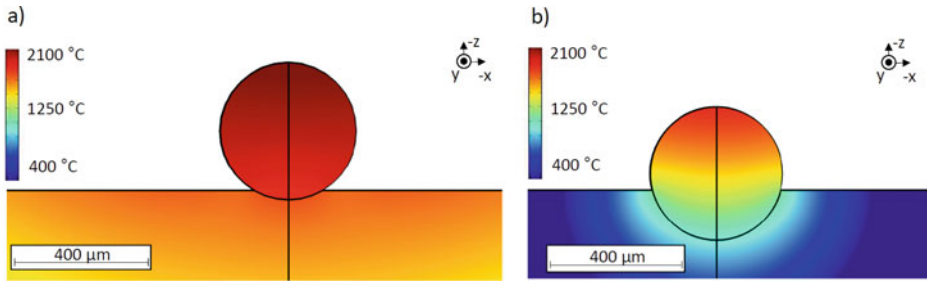
Fig. 8 Comparison of the temperature distribution in the fiber and substrate 0.1 s after contact between them within **a** the lateral process and **b** the coaxial process for the process parameters shown in Tables 1 and 2

mounting work platform, can be considered for future process development. These measures might increase the process's stability and robustness and can be advantageous when manufacturing multi-layer structures.

2.8   Evaporation of Glass

In the lateral and coaxial LGD experiment presented (see Chaps. 1 and 6), glass evaporation can be observed [13, 14]. Since the impact of the evaporation on the process stability is unknown, an estimation of its rate is performed. According to Yang et al., fused silica's evaporation can be considered to be significant above at 2526.85 K [31] since visible evaporation starts to occur after the temperature surpasses the boiling point. Thus, the heat loss due to evaporation cannot be neglected. According to the measurements of Elhadj et al. [32], the evaporation rate of fused silica can be expressed as a function of temperature. Therefore, the heat loss due to evaporation can be derived, where $h_l = 425$ kJ/mol is the latent heat of evaporation for fused silica [21]. Here, the mass losses of the fiber and substrate due to evaporation are determined with 5.01×10^{-7} kg/m for the lateral and with 6.8910×10^{-6} kg/m for the coaxial process, respectively. Thus, it is estimated that the coaxial approach leads to increased evaporation of fiber material compared to the lateral one. The evaporated glass might condensate on the manufactured components and the machine parts and absorb the radiation of the process laser. Thus, in future works, the impact of glass evaporation on the process stability has to be analyzed.

2.9   Simulation Methodology Discussion

The simulation environment presented here is based on a 2D approach and allows the analysis of the spatially and temporally resolved temperatures during the lateral and the

coaxial LGD process, which are both developed within the GROTESK project. In the simulation, it is assumed for simplicity that the glass fiber is already melted at the time of contact with the substrate plate and thus, high-speed heat exchange between glass fiber and substrate takes place after contact. Furthermore, the shape of the fiber cross-sectional area and its contact angle to the substrate plate are strongly dependent on the temperature in the process zone, as these strongly influence the surface tension and viscosity of the glass [33, 34]. However, this influence is not considered in the simulation.

Further, the convection coefficient for the heat transfer from the glass fiber surface to the ambient air is also estimated within the simulation environment. In practice, this factor is determined using a process gas flow and the component and installation space geometry and is subject to significant uncertainty. With the presented simulation, the geometrically multidimensional consideration of the process zone in the LGD process is calculated. In this work, the thermal behavior of the glass material within the process zone is numerically resolved. This approach enables a simulation-based process development, and particularly a local thermal process analysis. Extending the approach of Luo et al. [15], Pohl et al. [17], a comparison is made with a series of temperature measurements of the process zone. Furthermore, the simulation is also applied to the coaxial LGD process. These measurements qualitatively confirm the local temperature distributions in the process zone calculated in this work. The accuracy of the simulation must be analyzed in further work.

In a further development step of the simulation, the simulative representation of the temperature distribution can be used to infer the spatially resolved formation of stresses in the substrate and waveguide by implementing a thermo-mechanical calculation. These stresses are crucial for the success of the additive manufacturing process and they influence the light propagation within the waveguides. Especially for manufacturing multi-layer structures and volume components, the thermal influence of the substrate plate and the heat flow can be quantitatively considered for optimization of the In-process phase in the additive manufacturing process chain of glass optics (compare Fig. 1) by extending the simulation. These considerations are significant for the future development of the pre-process phase of LGD manufactured optics which includes the design, slicing and machine settings before starting the In-process.

3   Thermomechanical Simulation of an Additively Manufactured Laser Heat Sink Used as Optomechanical Component

The additive manufacturing of optomechanical components like mounts for lenses and mirrors offers increased freedom in their geometric design compared to conventional manufacturing processes. In conventional manufacturing, manufacturing costs generally rise significantly with increasing component complexity until the fabrication cannot be further realized. In contrast, additive manufacturing enables a high degree of design freedom,

with no significant increase in manufacturing costs, especially for complex geometries. As a result, additive manufacturing processes can be used for complicated component geometries, such as integrated channels, in a technically and economically viable solution [35]. This advantage is addressed in GROTESK to develop components that integrate several functions into a single component. For example, it is demonstrated that low-cost and lightweight components can be manufactured using the Fused Filament Fabrication (FFF) [36]. Mounts are used for holding and stabilize optical components such as lenses or crystals. During the operation of optical systems, the components are affected by optical, thermal and mechanical effects, such as ray heating and thermal lensing. Therefore, domain-specific effects and their interactions are required to be considered for designing, evaluating, and optimizing additively manufactured mounts. Due to the significant number of potential solutions for the material selection and mount geometry designs, an experimental analysis of critical parameters, such as temperature development, mechanical forces, or light propagation, is cost-inefficient. However, numerical simulation of additively manufactured components can be used to investigate these parameters and take them into account for further development. Thus, within the scope of GROTESK, multiple materials used for the additive manufacturing of optomechanics are numerically analyzed regarding their thermomechanical behavior in the exemplary application in a laser heat sink. Furthermore, the integrated design of internal channels, enabled by the additive manufacturing process, is numerically investigated for guiding a cooling fluid.

3.1 Additively Manufactured Optomechanics for a Solid-State Amplifier System

The heat sink is part of a laser system assembled from conventional and additively manufactured components (Fig. 9). The components which are additively manufactured include
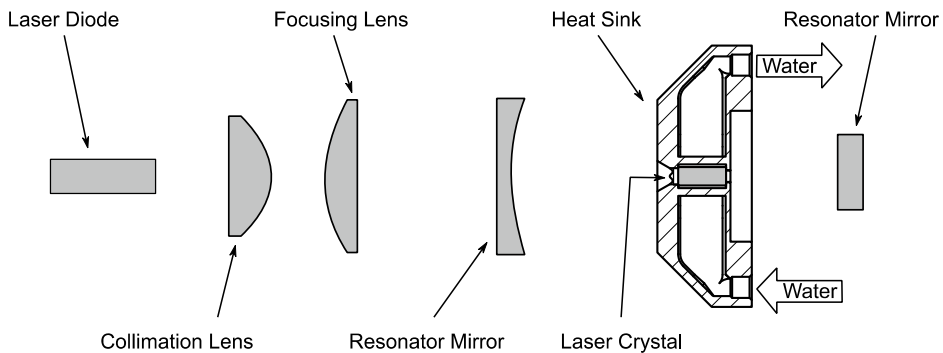
Fig. 9 Schematic representation of laser system demonstrator developed in GROTESK

a system housing and the laser crystal heat sink (see Chap. 2). Conventional components are a laser diode, lenses, resonator mirrors and a laser crystal. The solid-state laser is excited via a laser diode with an optical output power of 8 W and a central wavelength of 808 nm. The light is collimated via a first lens and focused via a second lens onto an Nd:YVO$_4$ laser crystal with a doping concentration of 0.27 at.%. In the crystal, the quantum defect causes a wavelength shift of the incident pump light. During this transformation, part of the input energy is converted into heat. Heat is conducted through the material of the heat sink to the cooling medium (here water), which flows through the integrated channel. The optical slope efficiency of a laser crystal is influenced by its temperature [22]. Therefore, an efficient cooling concept is required to minimize the heating of the crystal and thus energy losses within the optical system.

3.2 Heat Generation in Laser Crystals

When the laser crystal is excited by a pump source, a part of the energy introduced into the laser crystal is converted into heat. By pumping an Nd:YVO$_4$ crystal, the heat generation is caused by the quantum defect, the quantum efficiency, quenching and excited-state absorption. The thermal efficiency η_{th} of a Nd:YVO$_4$ crystal which is dominated by the quantum effect for doping concentration of lower than 0.5 at.% can be obtained according to Eq. (11), where λ_{Pump} denotes the wavelength of the pump source and λ_{Lasing} denotes the wavelength of the emitted laser light [37].

$$\eta_{th} = \left(1 - \frac{\lambda_{Pump}}{\lambda_{Lasing}}\right) \tag{11}$$

The total heat load Q can be derived from the output power of the laser diode P_{in} and the thermal efficiency η_{th} according to Eq. (12).

$$Q = P_{in} \cdot \eta_{th} \tag{12}$$

By assuming a radial Gaussian intensity distribution in the laser crystal and a decreasing intensity distribution in the longitudinal direction due to absorption effects, the heat energy source can be described with Eq. (13) [38].

$$q(r, z) = \frac{2Q\alpha}{\pi \omega_p^2} \left(1 - e^{-\alpha l}\right) e^{\frac{-2r^2}{\omega_p^2}} e^{-\alpha l} \; [\text{W/m}^3] \tag{13}$$

3.3   Multiphysics Simulation Approach

Individual domain-specific simulation approaches are combined into a common approach within a multiphysics simulation. For example, the simulation model of the heat sink combines optical, thermal, fluid mechanical and mechanical simulation approaches.

Based on the finite element method (FEM), the beam propagation of the pump light source through the laser system and the crystal is calculated in an optical simulation model (Fig. 10). The distribution of radiation intensity in the crystal and absorption characteristics are used as input parameters to set up the heat source model of the thermal simulation approach. Due to the temperature-dependent refractive index of the crystal, a thermal lensing effect influences the light propagation within the laser system. Furthermore, the thermal simulation applied to simulate the heat propagation from the crystal towards the cooling channel. A Computational Fluid Dynamics (CFD) model simulates the flow and thermal characteristics of the cooling fluid. Further, the heat convection from the heat sink material into the cooling fluid is considered. Finally, the temperature gradient is used as input information for a mechanical model to simulate the thermal expansion and the resulting mechanical stresses in the heat sink and the crystal [39]. In order to reduce uncertainties in the results, which may occur due to interactions between domain-specific effects, only steady-state studies are performed for the investigation of temperatures and stresses.

For each domain-specific approach, boundary conditions are identified and applied to the simulation model to represent the conditions of the actual application with the simulation (compare Chap. 2). In order to define the boundary conditions for the optical
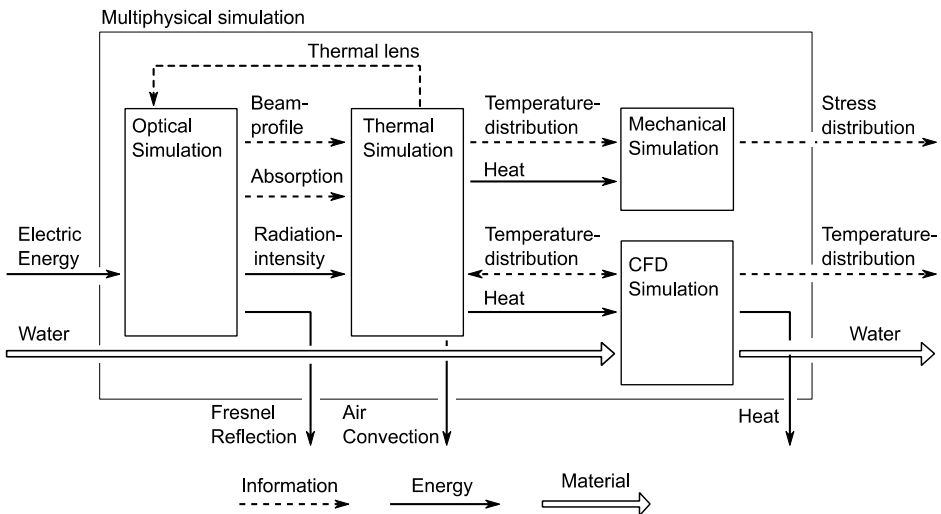
Fig. 10 Multiphysics simulation domains and boundary conditions for the analyzing the laser heat sink

simulation of the intensity distribution within the crystal, the Laser System Demonstrator Developed in GROTESK is experimentally analyzed. As a result, a Gaussian beam with a radius of $\omega_p = 182$ µm on the face surface of the crystal and a beam power P_{Pump} = 8 W are measured. The pump light source emits a center wavelength of 808 nm. The absorption coefficient of the Nd:YVO$_4$ crystal with a doping concentration of 0.27 at.% is determined with $\alpha = 3.54$ cm^{-1} [40]. For the thermal simulation model, free air convection is assumed on the surface of the heat sink and the surfaces of the crystal. Further, a room temperature of 20 °C is estimated. The cooling water flows in the heat sink at a pressure of 1 bar and has an input temperature of 18 °C. The crystal is inserted into the heat sink during the manufacturing process. For this purpose, the FFF process is paused and the crystal is inserted into a cavity provided. The process is then continued and the crystal is imprinted into the component. By printing on the upward-facing surfaces of the crystal, a form fit in the cavity can be achieved (see Chap. 2).

3.4 Investigation of Cooling Concepts for Additively Manufactured Heat Sinks

Two approaches are being pursued further to develop the thermal concept of additively manufactured heat sinks. First, the thermal energy is dissipated via a cooling channel. Due to the high degree of design freedom using additive manufacturing processes, complex cooling channel geometries can be realized. Different channel geometries and the resulting flow characteristics of the coolant will be quantified in terms of heat reduction and compared with conventionally manufactured ones. Second, the material properties of the heat sink influence the cooling efficiency of the heat sink. Due to the choice of the additive manufacturing process, limited material selections are available. Therefore, the investigation of filaments properties for the FFF process is used to quantify the cooling capabilities of the heat sink.

The additive manufacturing of the heat sink allows the design of a complex cooling channel. Three design approaches are investigated (Fig. 11) to compare the influence of the cooling channel geometry on the resulting temperature. Model A represents a heat sink with a single cooling channel manufactured with conventional manufacturing processes. In model B, the cooling channel of model A is implemented twice to guide the cooling fluid around the crystal from two sides to target a more uniform temperature distribution. Finally, in model C, the design freedom of additive manufacturing processes is exploited to minimize the wall thickness between the crystal and the cooling fluid. In addition, the radial flow around the crystal aims at a uniform distribution of the temperature. The same material model is defined to compare of the heat sink models.

The thermal simulation of the steady-state temperature distribution in the crystal shows that the highest temperatures occur in the core of the crystal for the models studied. Figure 12 shows the temperature in the core of the crystal as a function of crystal length.
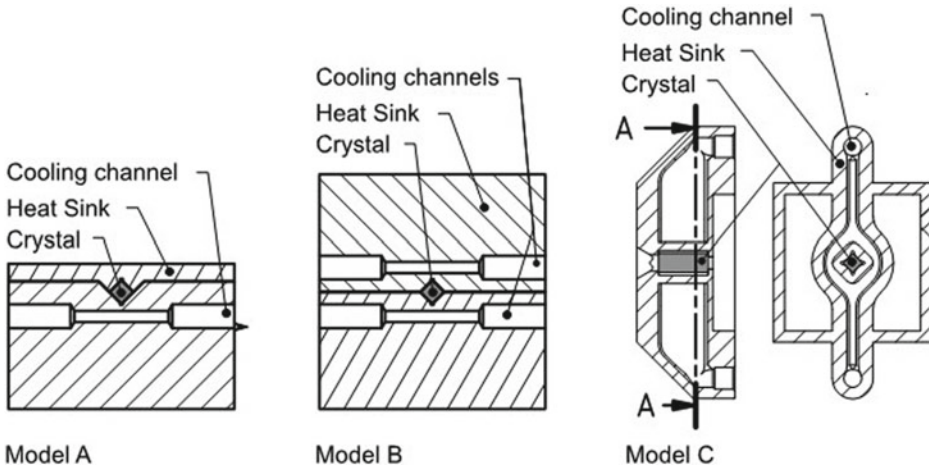
Fig. 11 Cross-sectional view of heat sink design approaches
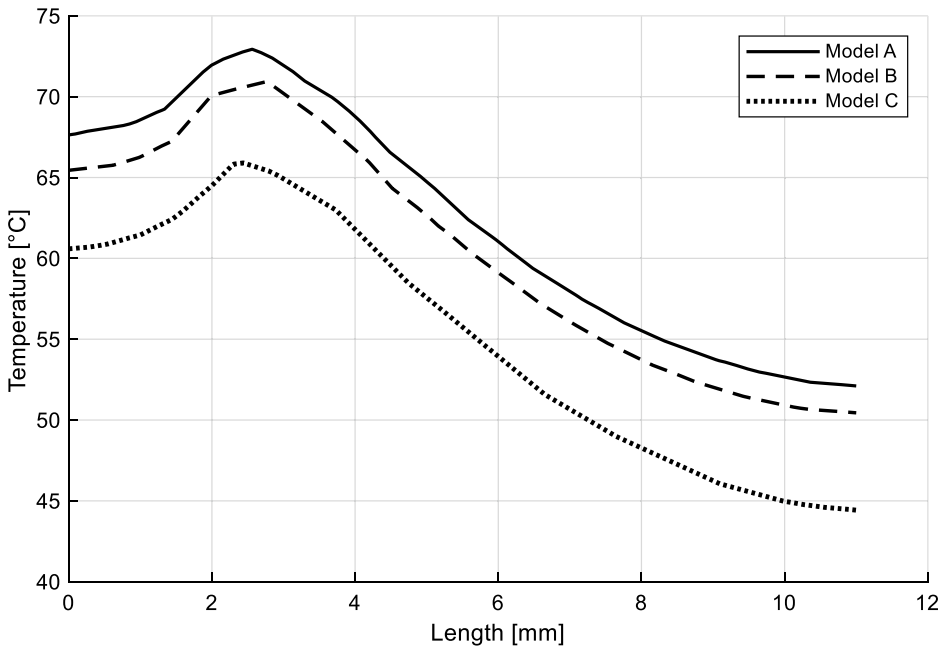
Fig. 12 Temperature gradient alongside the core of the laser crystal

Due to the undoped end cap of the crystal, the maximum temperature is not at its surface and occurs at a depth of about 2.5 mm. It can be seen that the use of two cooling channels instead of a single conventionally manufactured one has only a minor effect on the cooling efficiency of the heat sink. However, reducing the wall thickness between the cooling channel and the crystal significantly impacts the resulting temperature. As hypothesized, the freedom of design enabled by additive manufacturing can be utilized to develop a heat sink that efficiently dissipates the heat from the laser crystal.

By designing advanced cooling channel structures, developed a system that increases the cooling efficiency of the crystal heat sink by 10% compared to a conventional heat sink with the same material properties.

3.5 Heat Sink Filament Selection Criteria for a Non-destructive Laser System Operation

The cooling efficiency of the heat sink is influenced by the printing material's thermal properties and the heat sink's geometry. Thus, a lower stationary temperature results from better heat conduction between the crystal's surface and the cooling channel. In order to avoid the softening of the printing material and achieve a high optical slope efficiency of the crystal, minimum thermal requirements have to be derived. Based on this, the selection of a suitable material can be performed. Therefore, a parametric material model is integrated into the multiphysics simulation model. By iteratively changing the material properties of the heat sink, dependencies between material properties and physical state variables are obtained.

The Fused Filament Fabrication (FFF) process is chosen for its cost efficiency and lightweight construction (compare Chap. 2). Despite these advantages, some compromises must be considered. A significant one is the limited selection of available printing materials, which are often polymer-based. For example, Acrylonitrile–butadiene–styrene (ABS), Polylactic acid (PLA) and Copper-filled Polylactic acid (CoPLA) are available filament materials. However, the use of polymers as a printing material leads to the challenge that the material-dependent critical softening temperature that must not be exceeded is significantly lower than the maximum permitted temperature of the laser crystal. Furthermore,

Table 3 Material properties of filaments [41–44]

Material	Softening temperature	Heat conductivity
Acrylonitrile–butadiene–styrene (ABS)	80–95 °C	0.1 W/(m * K)
Polylactic (PLA)	49 °C	0.13 W/(m * K)
Copper-filled polylactic acid (CoPLA)	66 °C	0.25 W/(m * K)
Copper	1083 °C	240–380 W/(m * K)
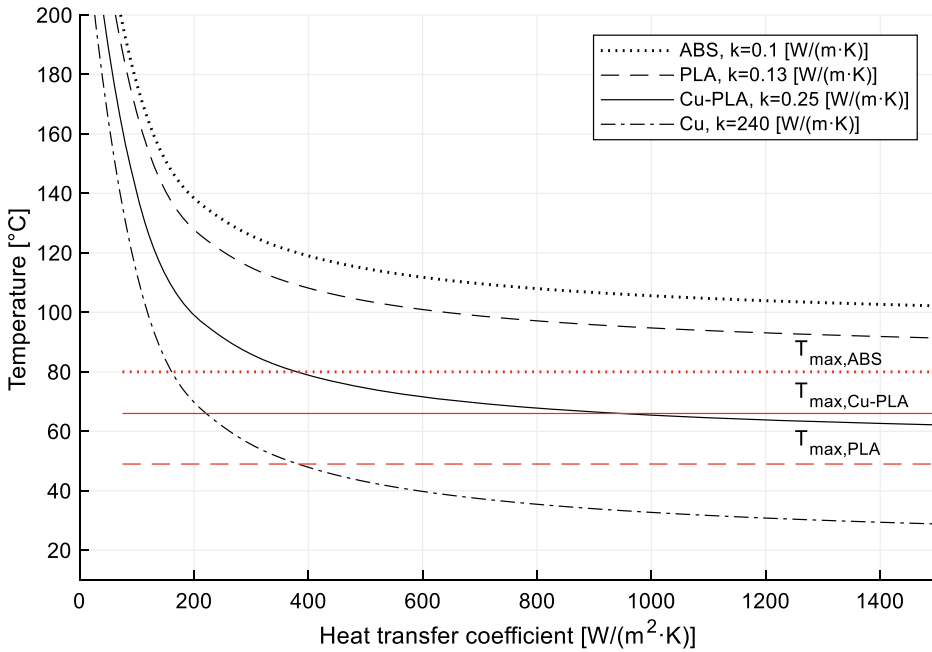
Fig. 13 Thermal study: maximum temperature depending on material properties of the filament

the thermal conductivity of polymers is much lower than conventionally used materials such as copper (compare Table 3).

The parametric material model is used to investigate two material properties: the influence of the filament's thermal conductivity and the influence of the heat transfer coefficient between the heat sink material and the laser crystal on the resulting maximum cystal temperature. Figure 13 shows the results of the temperature study for a selection of filaments. In addition, copper is listed as a reference material for conventional heat sink fabrication. The maximum temperature in the heat sink decreases exponentially with increasing heat transfer coefficient. When ABS and PLA material properties are implemented in the simulation model, the resulting temperature will not drop below the softening temperatures of the materials, even if a heat transfer coefficient of h > 1400 W/(m²*K) can be achieved (Fig. 13). Instead, the CoPLA filament descends below the critical softening temperature of 66 °C with a heat transfer coefficient of h > 1000 W/(m²*K). This study shows that polymer-based filaments are suitable for the application studied. Furthermore, due to the exponential decrease in temperature as the thermal conductivity increases, it can be concluded that a slight increase in thermal conductivity significantly affects the resulting temperature.

With the parametric material model, it is possible to define minimum requirements for the system. Based on this definition, the non-destructive operation of the laser system

could be realized. This information can be taken into account for the future choice and further development of the material in GROTESK (see Chaps. 4 and 6).

3.6   Simulation Methodology Discussion

A laser crystal heat sink is used as an example to investigate the potentials of Multiphysics simulation for supporting the development process of additively manufactured components (Fig. 1). When evaluating approaches for the design of cooling channels, the process chain step "Design" is processed and supported with the help of the simulation. By implementing different CAD geometries, state variables such as temperatures and stresses can be simulated in the system and used to select a suitable geometry. With the specification of material properties, further process steps are supported. By quantifying the influence of the material properties on the temperatures in the heat sink, the process step "material" of the additive manufacturing process chain is taken into account. In addition, new requirements for the development of the heat sink are defined concerning the thermal conductivity of the heat sink and the heat transfer between the crystal and the heat sink.

4   Summary and Outlook

In GROTESK, the Lateral Laser Glass Deposition (LGD) process is further developed for the additive manufacturing of optical components made of glass, and the multi-material coaxial LGD process is researched on this foundation. In this context, a simulation environment is developed and transferred to the coaxial principle based on the lateral process. Here, the two processes developed in GROTESK for additive manufacturing of glass are compared. Furthermore, the process-dependent temperature generation and distribution in the glass fiber cross-section are analyzed. Potentials for process optimization considering the lateral (see Chap. 1) and the coaxial LGD process are identified and considered for further development (see Chap. 6).

Further, various material combinations and design approaches for a laser heat sink are investigated concerning their influence on the cooling efficiency of the optomechanical component. In addition to the experimental analysis (see Chap. 2), requirements for the choice of materials and the operating parameters for the heat sink are developed in the virtual tests. In particular, by explicitly considering the heat transfer coefficient and its influence on the temperature development in the Nd:YVO$_4$, requirements for developing customized materials that are thermally optimally bonded to a laser crystal (see Chap. 4) are elaborated.

Future work can synthesize the information to align the design, material development and machine concept. Based on such information, additively manufactured

next-generation laser and its thermal management systems with integrated glass optics could be designed in simulation environments and matched automatically with optimized additive manufacturing process parameters.

References

1. Lippert, R.B., Lachmayer, R.: Einleitung. In: Lachmayer, R. (ed.) Additive Manufacturing Quantifiziert, pp. 1–6. Springer, Berlin Heidelberg, Berlin, Heidelberg (2017)
2. Grabe, T., Li, Y., Krauss, H. et al.: Freeform optics design for Raman spectroscopy. In: Soskind, Y., Busse, L.E. (eds.) Photonic Instrumentation Engineering VII. SPIE, p. 10 (2020–2020)
3. Kloppenburg, G., Knöchelmann, M., Wolf, A.: Additive Fertigung transparenter Optiken. In: Lachmayer, R. (ed.) Additive Manufacturing Quantifiziert, pp. 163–174. Springer, Berlin Heidelberg, Berlin, Heidelberg (2017)
4. Lachmayer, R., Bode, B., Grabe, T., et al.: Integration spezifischer Effekte in Strukturbauteilen mittels additiver Fertigungsverfahren. In: Lachmayer, R., Rettschlag, K., Kaierle, S. (eds.) Konstruktion für die Additive Fertigung 2019, pp. 1–10. Springer, Berlin Heidelberg, Berlin, Heidelberg (2020)
5. Ehlers, T., Lachmayer, R., Vajna, S. et al.: Producibility. In: Vajna, S. (ed.) Integrated Design Engineering: Interdisciplinary and Holistic Product Development, 1st edn, pp. 287–323 (Springer International Publishing; Imprint Springer, Cham, 2020)
6. VDI-Gesellschaft Produktion und Logistik: Additive manufacturing—Legal aspects of the process chain (VDI 3405 Blatt 5.1) (2020)
7. Rettschlag, K., Grabe, T., Müller, P. et al.: Additive Fertigungals Erfolgsfaktor für digitale Prozessketten. In: Lachmayer, R., Rettschlag, K., Kaierle, S. (eds.) Konstruktion für die Additive Fertigung 2020 (Springer Vieweg, Berlin, Heidelberg, pp. 1–16, 2021)
8. Lachmayer, R., Lippert, R.B.: Die Entwicklungsumgebung. In: Lachmayer, R., Lippert, R.B. (eds.) Entwicklungsmethodik für die Additive Fertigung, pp. 99–127. Springer, Berlin Heidelberg, Berlin, Heidelberg (2020)

9. Lachmayer, R., Lippert, R.B.: Grundlagen. In: Lachmayer, R., Lippert, R.B. (eds.) Entwicklungsmethodik für die Additive Fertigung, pp. 7–20. Springer, Berlin Heidelberg, Berlin, Heidelberg (2020)

10. Grabe, T., Biermann, T., Bayerl, M. et al.: Anisotropic characteristics analysis of 3D-printed optics. DGaO-Proceedings (2020). https://doi.org/10.15488/10199

11. Neef, P., Bernhard, R., Wiche, H. et al.: Generatives Fertigen optischer, thermaler und struktureller Komponenten für Lasersysteme: 14. bis 15. Februar 2019. In: Tagungsband 3. Niedersächsisches Symposium Materialtechnik, Band 7 (2019)

12. von Witzendorff, P., Pohl, L., Suttmann, O. et al.: Additive manufacturing of glass: CO_2-Laser glass deposition printing. In: Procedia CIRP 74, vol. 74, pp. 272–275

13. Kranert, F., Rettschlag, K., Wienke, A. et al.: Generation of functional curved waveguides by CO2-laser based deposition of coreless fused silica fibers. In: Proceeding of SPIE 11349, 3D Printed Optics and Additive Photonic Manufacturing II: 11 (2020). https://doi.org/10.1117/12.2554516

14. Rettschlag, K.: Laser deposition of fused silica coreless fibers to generate functional waveguides. In: Lasers in Manufacturing Conference (2019)

15. Luo, J., Gilbert, L.J., Qu, C., et al.: Additive manufacturing of transparent soda-lime glass using a filament-fed process. J. Manuf. Sci. Eng. **139**, 24 (2017)

16. Grabe, T., Lammers, M., Wang, S. et al.: Additive Manufacturing of fused silica using coaxial laser glass deposition: experiment, simulation and discussion. In: Helvajian, H., Gu, B., Chen, H. (eds.) Laser 3D Manufacturing VIII. SPIE, p. 32 (2021–2021)

17. Pohl, L., von Witzendorff, P., Chatzizyrli, E., et al.: CO_2 laser welding of glass: numerical simulation and experimental study. Int. J. Adv. Manuf. Technol. **90**, 397–403 (2017). https://doi.org/10.1007/s00170-016-9314-9

18. Abitan, H., Bohr, H., Buchhave, P.: Correction to the Beer-Lambert-Bouguer law for optical absorption. Appl. Opt. **47**, 5354–5357 (2008). https://doi.org/10.1364/ao.47.005354

19. Mixon, D.G., Roach, W.P. (ed.): A Thermal Model of Laser Absorption (2007)

20. McLachlan, A.D., Meyer, F.P.: Temperature dependence of the extinction coefficient of fused silica for CO(2) laser wavelengths. Appl. Opt. **26**, 1728–1731 (1987). https://doi.org/10.1364/AO.26.001728

21. Doualle, T., Gallais, L., Cormont, P., et al.: Thermo-mechanical simulations of CO_2 laser–fused silica interactions. J. Appl. Phys. **119**, 113106 (2016). https://doi.org/10.1063/1.4944435

22. Mazurin, O.V., Streltsina, M.V., Shvaiko-Shvaikovskaya, T.P.: Handbook of glass data silica glass and binary silicate glasses. Elsevier Science, Part A (1983)

23. Hildebrand, J., Hecht, K., Bliedtner, J., et al.: Laser beam polishing of Quartz glass surfaces. Phys. Procedia **12**, 452–461 (2011). https://doi.org/10.1016/j.phpro.2011.03.056

24. Born, M., Wolf, E.: Principles of Optics, Seventh (expanded) Anniversary Edition, 60th Anniversary Edition (Cambridge University Press, Cambridge, 2019)

25. Zolotarev, V.M.: Study of quartz glass by differential Fourier transform IR reflection spectroscopy: Bulk and surface properties. Opt. Spectrosc. **107**, 754–767 (2009). https://doi.org/10.1134/S0030400X09110113

26. Grabe, T., Rettschlag, K., Wang, X. et al. (eds.): Additive Fertigung von Glas: Simulation und Messung von Temperaturen in der Prozesszone. 4. Niedersächsisches Symposium Materialtechnik 2020. Shaker, Aachen (2021)

27. Lienhard, J.H.: A Heat Transfer Textbook, 4., Corr., Rev., and Updated ed. Dover Books on Engineering (Dover Publ, Mineola, NY, 2011)

28. Teixeira, P.R.F., de Araújo, D.B., da Cunha, L.A.B.: Study of the Gaussian distribution heat source model applied to numerical thermal simulations of TIG welding processes. Cieng **23**, 115–122 (2014). https://doi.org/10.14393/19834071.2014.26140

29. Grabe, T., Rettschlag, K., Wang, S. et al. (eds.): Modellierung und Evaluation thermischer Effekte für die laserbasierte Additive Fertigung von funktionalen Glaswellenleitern. Konstruktion für die Additive Fertigung 2020 (Springer Vieweg, Berlin, Heidelberg, 2020)
30. Teschner, R.: Glasfasern. Springer, Berlin Heidelberg, Berlin, Heidelberg (2013)
31. Yang, S.T., Matthews, M.J., Elhadj, S., et al.: Thermal transport in CO_2 laser irradiated fused silica: In situ measurements and analysis. J. Appl. Phys. **106**, 103106 (2009). https://doi.org/10.1063/1.3259419
32. Elhadj, S., Qiu, S.R., Monterrosa, A.M., et al.: Heating dynamics of CO_2—laser irradiated silica particles with evaporative shrinking: Measurements and modeling. J. Appl. Phys. **111**, 93113 (2012). https://doi.org/10.1063/1.4716016
33. Pilon, L., Zhao, G., Viskanta, R.: Three-dimensional flow and thermal structure in glass melting furnaces. Part II: effect of batch and bubbles. Glass Sci. Technol. **75**(3) (2002)
34. Luo J, Gilbert LJ, Bristow DA et al. (2016) Additive manufacturing of glass for optical applications. In: Gu B, Helvajian H, Piqué A (eds) Laser 3D Manufacturing III. SPIE, 97380Y
35. Lippert, R.B.: Restriktionsgerechtes Gestalten gewichtsoptimierter Strukturbauteile für das Selektive Laserstrahlschmelzen, Gottfried Wilhelm Leibniz Universität Hannover (2018)
36. Kranert, F., Budde, J., Neef, P. et al.: 3D-printed, low-cost, lightweight optomechanics for a compact, low-power solid-state amplifier system. In: Glebov, A.L., Leisher, P.O. (eds.) Components and Packaging for Laser Systems VI. SPIE, p. 4 (2020–2020)
37. Xiong, Z., Li, Z.G., Moore, N., et al.: Detailed investigation of thermal effects in longitudinally diode-pumped Nd:YVO/sub 4/lasers. IEEE J. Quantum Electron **39**, 979–986 (2003). https://doi.org/10.1109/JQE.2003.814371
38. Pfistner, C., Weber, R., Weber, H.P., et al.: Thermal beam distortions in end-pumped Nd:YAG, Nd:GSGG, and Nd:YLF rods. IEEE J. Quantum Electron **30**, 1605–1615 (1994). https://doi.org/10.1109/3.299492
39. Grabe, T., Budde, J., Kranert, F., et al.: Kühlkörper-Designansatz für einen in AlSi10Mg eingebetteten YAG-Laserkristall. In: Lachmayer, R., Rettschlag, K., Kaierle, S. (eds.) Konstruktion für die Additive Fertigung 2019, pp. 159–175. Springer, Berlin Heidelberg, Berlin, Heidelberg (2020)
40. Röttger, J., Grabe, T., Sundermeier, M.C. et al.: Additive manufacturing of a laser heat sink: Multiphysical simulation for thermal material requirement derivation (accepted). In: Lachmayer, R. (ed.) Innovative Product Development by Additive Manufacturing (Springer Vieweg, Hannover, 2021)
41. Kutz, M. (ed.): Handbook of Materials Selection. Wiley, New York (2002)
42. Bargel, H.-J., Schulze, G., Hilbrans, H. (eds.): Werkstoffkunde, 10, bearb Springer, Berlin (2008)
43. Formfutura: Datasheet Classic Copper MetalFil (2021). https://formfutura.sharepoint.com/sites/downloads/Shared%20Documents/Forms/AllItems.aspx?id=%2Fsites%2Fdownloads%2FShared%20Documents%2FDownloads%20Server%2FMaterials%2FFilaments&p=true
44. SD3D Technical Data Sheet of Polylactic Acid Filament. https://www.sd3d.com/wp-content/uploads/2017/06/MaterialTDS-PLA_01.pdf. Accessed 15 Oct 2021

Molybdenum Copper MMC for Additive Manufacturing of Thermal and Structural Components

Philipp Neef, Robert Bernhard, Henning Wiche, and Volker Wesling

1 Introduction

The holistic approach of an extensively additive manufactured laser system requires the research into the generation of optical parts as well as structural and thermal components. This includes mountings and heat sinks for crystalline active laser mediums, for example Nd:YAG (neodymium-doped yttrium aluminum garnet). Conventionally, these heat sinks are based on form-fitting copper mountings for heat dissipation and indium foil to overcome roughness [1, 2] and expansion with limited functionality due to the production techniques.

Additive manufacturing of metallic materials, however, allows for a variety of innovative application possibilities due to further degrees of freedom. Regarding topology optimization and functional integration, structures can be generated where conventional production techniques obtain unsuitable or restricted manufacturability correlating with extensive effort.

The potential range of materials, though, is mainly limited to several powder materials offered by the manufacturers of these laser metal deposition systems. Therefore, the processed materials represent a compromise for the envisaged application often while powder materials have significant benefits due to the targeted adjustment of their composition in fact. Thus, specific characteristic profiles can be achieved.

P. Neef (✉) · R. Bernhard · H. Wiche · V. Wesling
Clausthal Center of Materials Technology, Clausthal University of Technology,
Clausthal-Zellerfeld, Germany
e-mail: philipp.neef@tu-clausthal.de

V. Wesling
Institute of Welding and Machining, Clausthal University of Technology, Clausthal-Zellerfeld,
Germany

As a part of the joint project, wGROTESK (material development for additive manufacturing of optical, thermal and structural components) deals with the selection as well as the targeted adjustment of an application-specific material whilst ensuring and developing the processing by laser metal deposition (LMD). The additive manufacturing of mounting structures for YAG requires metallic materials combining suitable thermal conductivity, melting points and thermal expansion coefficients to avoid thermal damage resulting from thermal induced stress as well as a sufficient coupling of YAG and alloy to allow for a material closure.

The conventional mounting relies on copper since it offers a remarkable thermal conductivity. For the additive process, the melting point represents a major challenge due to the possibility of thermal damage to the YAG. Furthermore, the thermal expansion coefficient is unsuitable and the absorption for laser systems with infrared wavelengths, well established in small and medium-sized businesses, is insufficient.

The objective of the following work is the development and targeted adaption of a metallic alloy with a low melting point and a thermal expansion corresponding to that of yttrium aluminum garnet, while ensuring the bonding of the two incompatible materials through adequate chemical interaction.

In this context, the material development provides the approach to define a copper-based pseudo alloy for realization in an industrial laser process. The combination of copper and molybdenum allows for sufficient thermal expansion coefficients while a further adaption of the copper alloy presents the opportunity for an extensive adjustment of the material properties to meet the requirements of processing and implementation.

2   State of the Art and Scientific Bases

2.1   Challenge of Infrared Absorption of Copper

Laser sources with infrared wavelengths are largely disregarded for additive processing of copper. The main reasons for this are both the wavelength-dependent absorption and the thermal conductivity.

Pure copper shows an absorption of about 5% for wavelengths of around 1064 µm at room temperature (RT) (cf. Fig. 1 according to [3]). In combination with the high thermal conductivity, this means that only a small proportion of the laser power can be used for melting and the induced heat is immediately dissipated from the process zone. At the same time, the absorption abruptly increases directly before the melting point (MP) is reached, resulting in spatter formation and an unstable process.

Other wavelengths seem more suitable for processing copper in the laser-based additive process. Therefore, lasers with wavelengths in the green spectral range are often used to achieve improved process quality. However, these beam sources are considerably more
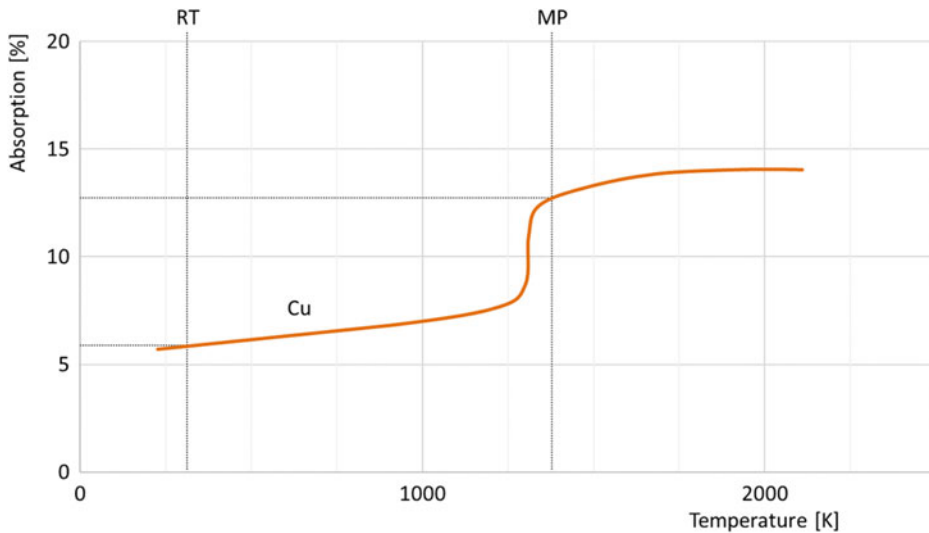
Fig. 1 Temperature dependence of the absorption for infrared wavelengths of pure copper according to [3]

expensive than IR laser sources. At the same time, IR lasers are more widespread in industry, especially among small and medium-sized companies.

Molybdenum copper pseudo alloys present a substantial benefit. The application of a powder mixture of molybdenum and copper offers the advantage of a significantly higher absorption for infrared wavelengths at room temperature (cf. Fig. 2 according to [3, 4]). This makes it possible to use reduced laser power for heat input and heat conduction to the copper in order to transfer it indirectly into the molten phase. This enables an increase in processability and thus an improved process quality.

2.2 Metal Matrix Composites and Pseudo Alloys

The term metal matrix composite generally refers to the combination of a metallic matrix with embedded ceramic particles or fibers. In addition, however, the combination of metallic matrix and high-melting metallic particles are also included.

The compound of matrix and particles primarily serves to achieve defined property profiles of the material used. This includes not only coefficients of thermal expansion for use in heat sinks, but also implementations in applications with high electrical conductivity [5, 6]. At the same time, there are also application possibilities where the ductility of metals is to be combined with the hardness of ceramics [7].

While metallic materials with low thermal expansion coefficients have been used for additive manufacturing for many years, they are primarily based on iron-nickel alloys
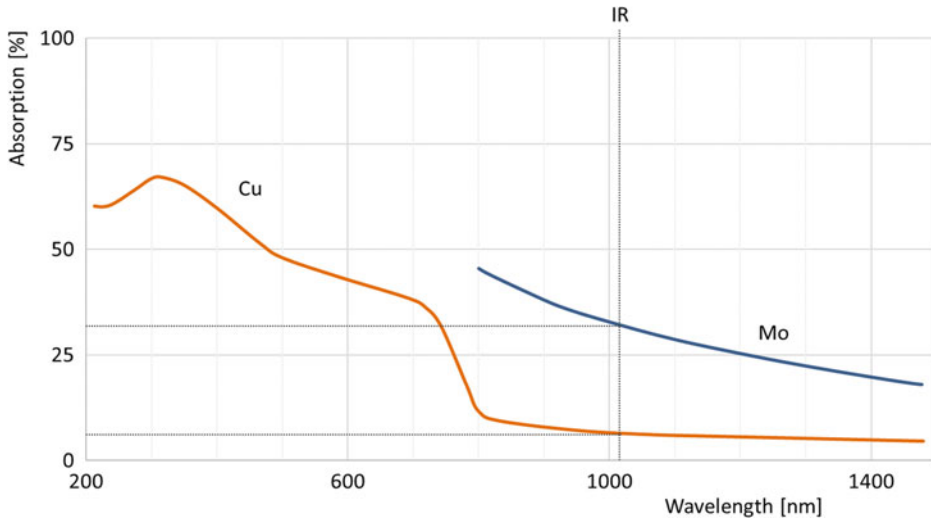
Fig. 2 Wavelength dependence of the absorption of pure copper and molybdenum according to [3, 4]

known as Invar or Kovar [8, 9]. The thermal expansion coefficient of these alloys at room temperature is between 1 and $5 \cdot 10^{-6}$ K^{-1} depending on the composition [10]. However, at temperatures above 300 °C, this increases significantly to over $12 \cdot 10^{-6}$ K^{-1} [11]. At the same time, such alloys exhibit melting temperatures above 1400 °C. Pseudo alloys offer the advantage of constant thermal expansion coefficients over a wide temperature range. In addition, only the matrix material has to be converted into the molten state.

In particular, materials combining copper and molybdenum as well as copper and tungsten also offer advantages in terms of thermal conductivity [12–14].

The production of pseudo alloys can be accomplished in different ways like layered composite materials [13], sputtered copper film with minor proportions of molybdenum [15], spark plasma sintering [16] or high pressure torsion [17]. Other approaches are based on powder metallurgy and sintering [5, 14, 18, 19]. Another conventional process route involves a two-step process in which the molybdenum grains are first sintered and subsequently the porous body is infiltrated with copper [20, 21].

The application of metal matrix composites and pseudo alloys by laser metal deposition process is a subject of research. Titanium alloys with minor proportions of Al_2O_3 nanoparticles and AlSi10Mg alloy with up to 2 vol% of tungsten carbide have been processed [22, 23].

However, additive processing of MMCs and pseudo alloys is commonly limited to material combinations with high percentage of matrix material and less bounded particles.

3 Experimental Approach

3.1 Specimen Generation at Quasi-static Ideal Thermal Conditions

In addition to the experiments for process development of the additive manufacturing process, which are carried out on a laser powder deposition system with a 680 W diode laser, the material development and adaptation is primarily performed at quasi-static thermal conditions in a furnace process. Due to the different process conditions, the influence of the divergent heating and cooling conditions can be compared and qualified. In this way, time- and temperature-dependent procedures such as diffusion processes can be represented in the different manufacturing methods.

The furnace-based generation are performed with a DataPhysics OCA drop shape analysis with a mounted furnace of the type HTFC 1800. Temperatures of up to 1800 °C can be reached under inert atmosphere with contemporaneous camera-based recording of the process zone. This enables simultaneous observation of the melt forming during the heating of the metallic powders. The experiments are carried out in an argon atmosphere at a flow rate of 200–250 l/h. The temperature is set individually above the melting temperature of the alloy applied.

This allows not only the generation of samples for microstructure analysis as well as the determination of thermal and mechanical properties but also for characterizations of the coupling of alloy and YAG. By detecting the contour of the formed melt drop, the contact angle can be automatically calculated by the definition of the substrate surface. The contact angle is directly associated with the coupling and wetting behavior. Small angles represent a proficient wetting of liquid and substrate. Thus, the objective of suitable bonding can be verified quantitatively.

Moreover, the melting temperature of the alloy can be determined by thermocouples.

Micro sections of the generated specimens are subsequently examined by means of reflected light microscopy and field emission scanning electron microscopy with regard to the formed microstructures and boundary layers.

3.2 Material Adaption

In general, the material adaptation for laser metal deposition can be differentiated according to the selected feed of the filler material. For wire-based materials, a course adjustment of the properties can be achieved by an adequate selection of the material of the wire. The usage of coatings applied with physical vapor deposition allows for a more precise adaption. Thereby, a combination of several layers is conceivable. During the manufacturing process, in situ alloying of all wire and coating components takes place. However, the application of pseudo alloys requires a complex production of cored filler wires.

In this respect, powder-based processing in the LMD process represents an improved possibility for short-term adjustments. The essential adaption is made by the suitable choice of the composition of the material. Apart from that, the admixture of additives and reactive grinding are possible as adaptations. Due to the specific adjustability of the composition, this processing offers significant advantages for achieving the defined property profiles.

Accordingly, the focus of material development is on powder-based processing with rapidly adaptable compositions. This short control loop allows a fast response to the measured properties of the material. This makes it possible to meet the objective of a targeted adaptation of the material's properties in order to realize the desired approximation to the additively manufactured laser system. The appropriate choice of the added elements can ensure the development of the alloy in terms of low melting point, suitable thermal expansion coefficients and coupling of the incompatible material groups through a sufficiently large chemical interaction.

4   Challenges in the Development of a Suitable Pseudo Alloy

4.1   Incompatibility of Material Groups

The metallic molybdenum copper pseudo alloy and the crystalline YAG represent fundamentally different material groups. With regard to the thermal expansion of the materials, the pseudo alloy is intended to overcome this discrepancy. Therefore, the near linear course of the thermal expansion coefficient of YAG must be met as well as possible.

Another challenge, however, is the coupling of YAG and metal. The material groups have a completely different structure. The objective of additive bonding of the crystalline YAG is not a form-fit connection, but explicitly a material-fit connection of the two materials. Consequently, it is inevitable that a suitable coupling of the molten metal to the YAG takes place, which also remains after cooling and solidification of the alloy. At the same time, a similar thermal expansion is required, since thermally induced stresses should be avoided as far as possible so that the risk of thermal damage is prevented.

4.2   Materials Morphology

The conventional processing of molybdenum-copper composites to date is based on the sintering of molybdenum particles with the subsequent infiltration of the sintered body with the molten copper. The resulting microstructure is formed as shown in Fig. 3a. In principle, this process can also be transferred analogously to a copper matrix.

The challenge in additive manufacturing, taking into account the thermal boundary conditions, lies in transferring the two-stage process route into a single-stage process. At
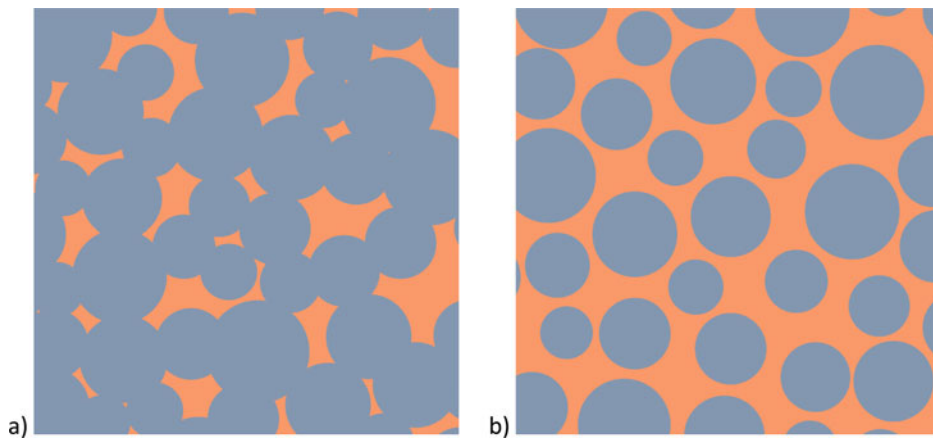
Fig. 3 Schematic microstructure of the molybdenum copper pseudo alloy **a** sintered molybdenum particles after conventional processing **b** molybdenum particles integrated in copper matrix

around 1000 °C, the process temperatures are far below the temperatures required for sintering the molybdenum particles. Consequently, only the matrix material is transferred to the molten phase in which the molybdenum particles are bonded. The formation of the microstructure is similar to that in Fig. 3b).

For the targeted adaption of the material, the specimen generation is initially focused on processing by optical contact angle goniometers. The installed furnace chamber allows for inert atmosphere combined with quasi-static thermal conditions. Figure 4 shows a molybdenum copper pseudo-alloy with a molybdenum content of about 70 wt%.

The high number of imperfections (black areas) is striking, indicating that the wetting of the copper on the molybdenum and capillary effects between the molybdenum particles are insufficient. It is therefore essential for suitable processing that the wetting is increased substantially.

5   Results

5.1   Wetting of Matrix Material on Molybdenum

Pure copper as a matrix material reveals significant imperfections during processing with regard to the microstructure. To increase mold filling, the use of copper phosphorus alloys is being investigated. Alloys of this type with about 8 wt% phosphorus are used as solders due to their capillary-active, good flow properties [24, 25]. Figure 5 shows the significant improvement of mold filling when CuP8 is applied to the molybdenum.
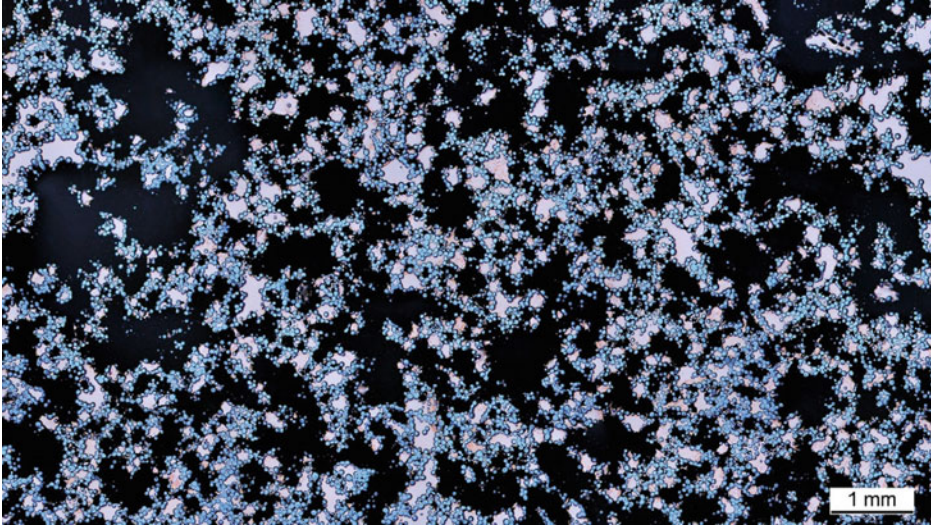
Fig. 4 Microstructure of furnace-generated pseudo alloy with 70 wt% molybdenum and copper balance
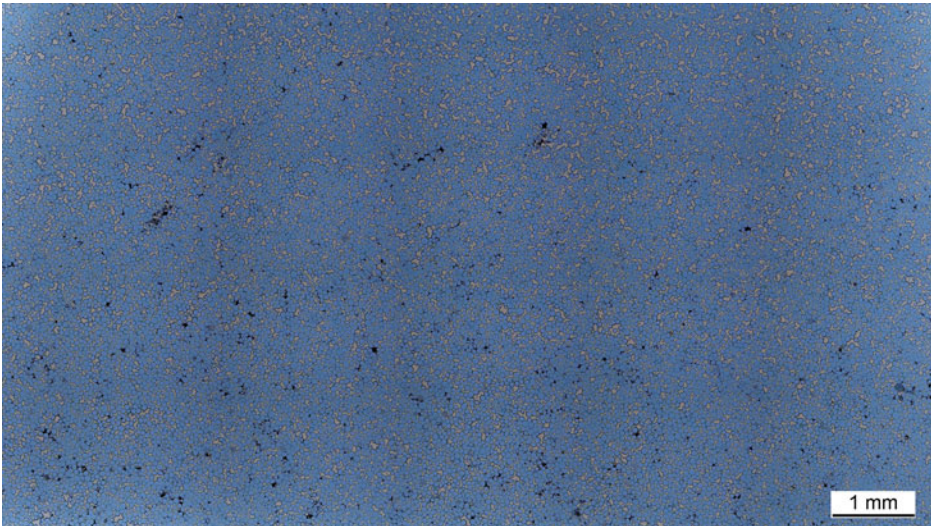
Fig. 5 Microstructure of furnace-generated pseudo alloy with 70 wt% molybdenum and CuP8 balance

The quantification of the impact of phosphorus can also be demonstrated by means of contact angle measurements. Figure 6 shows the wetting of pure copper on molybdenum with a contact angle of about 40°. Increasing the phosphorus content in the copper alloy leads to successively improved wetting on the molybdenum substrate. Figure 7 shows that already 1 wt% phosphorus in the copper leads to a significant difference while 8 wt% phosphorus results in ideal wetting.

In addition to improved wetting, the copper-phosphorus system offers the advantage of a lower melting point. At the eutectic point, this is around 714 °C and thus considerably lower than that of copper (1084 °C) [26]. Consequently, the risk of thermal damage during additive imprinting of the YAG is significantly reduced as a result of lower thermal stresses.

This provides the basis for the application of the pseudo alloy with regard to the sufficient chemical wettability of the refractory metal molybdenum and the low melting point of the matrix material.

Fig. 6 Microstructure of wetting of pure copper on molybdenum substrate
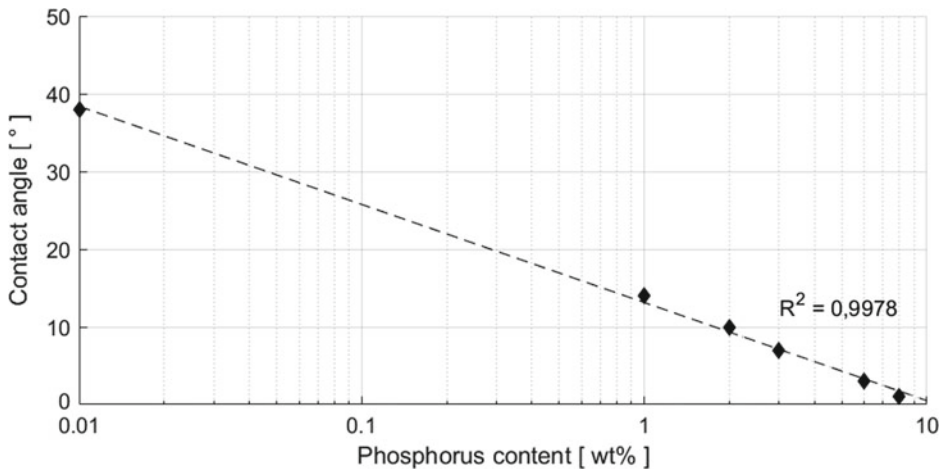
Fig. 7 Contact angle of copper alloy on molybdenum substrate depending on phosphorus content

5.2   Coupling of YAG and Alloy

While the wetting behavior of a metal–metal combination requires only limited adaptions, the combination of metal and nonmetal causes a major challenge. The realization of a sufficient coupling of these theoretically incompatible materials is implemented due to the application of suitable additives solely.

The characterization of the wettability is examined by contact angle measurements. Smaller contact angles correlate with improved wetting along with better bonding.

For the measurement of the contact angle of alloy on YAG, only the matrix material is applied. On the one hand, this is due to the high molybdenum content, which otherwise makes the measurements considerably more difficult; on the other hand, only the matrix material becomes molten and allows interaction with the crystalline YAG.

As expected, the contact angle is very high with the combination of copper and YAG as a result of which no sufficient bonding takes place. Values of about 110° are measured both with pure copper and when using the copper-phosphorus alloy. Furthermore, there is no sufficient bonding since the melt drop can be easily detached when cooled.

In previous experiments, it was demonstrated that a titanium coating of the YAG by a preceding physical vapor deposition process can lead to a significant improvement of the wetting [11].

Regarding improved processing properties, the objective is to avoid the indirect route via the coating process, reaching an increased wetting by means of a direct admixture of additives. The addition of titanium allows significantly lower contact angles, but results in pronounced oxidation on the surface of the melt droplet despite an argon atmosphere.

The wetting can also be increased by adding manganese to the copper-phosphorus matrix. Thus, the contact angle is about 80–90° (see Fig. 8a)). Although manganese, like titanium, has a high affinity for oxygen, oxidation does not occur. Since oxygen is a component of the YAG, this leads to the formation of a metallization and the associated improvement in wetting [cf. 24].
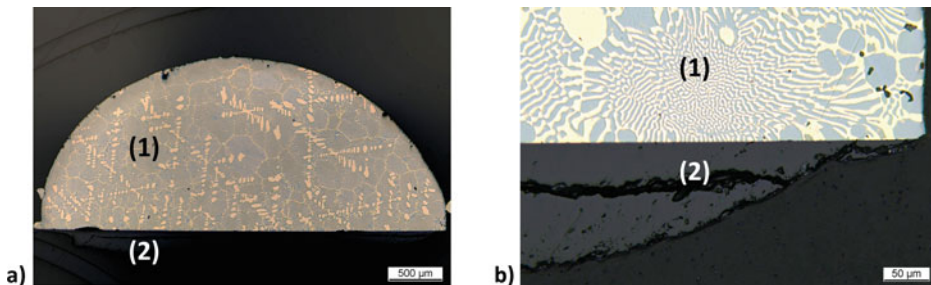
Fig. 8 Microstructure of wetting: CuPMn alloy on YAG **a** and enlarged display of detachment within YAG; explanatory note: (1) CuP alloy, (2) YAG

During cooling, the solidified metal droplet is detached from the YAG substrate. However, the microsection reveals a detachment within the YAG along with remaining adhesions of the alloy, indicating a sufficient bonding (see Fig. 8b)). Due to the unadapted thermal expansion coefficients issued from absent molybdenum admixture, high mechanical stresses are induced in the YAG and damage results.

By adding manganese, the objective of a suitable bonding of non-metallic and metallic material can be achieved much better compared to the use of titanium as an alloying element.

5.3   Thermal Expansion Coefficients

One of the main reasons for selecting the molybdenum copper pseudo alloy is the low thermal expansion coefficients that can be achieved with the conventionally processed composite. However, the innovative approach relinquishes the advantages of sintered connections to ensure low melting points. Nevertheless, the low thermal expansion coefficients of the YAG must be met.

Figure 9 shows the measured thermal expansion coefficient of YAG, copper and molybdenum as well as several compositions of the pseudo alloy generated via furnace process. The values of the pseudo alloy are marginally higher than those of the YAG. However, the curve shows a nearly parallel course. Consequently, there is a slightly higher shrinkage in
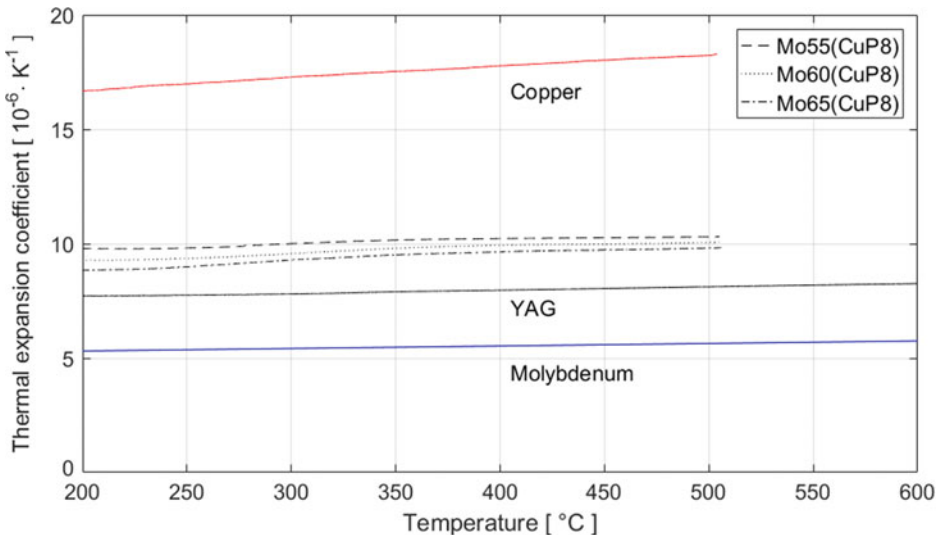
Fig. 9 Thermal expansion coefficients of pure materials and selected pseudo alloys with different contents of molybdenum

the alloy than in the crystal when cooling during the manufacturing process, with the difference showing a linear progression. As a result, low compressive stresses are expected within the YAG.

Furthermore, the graph demonstrates the relation between thermal expansion and molybdenum amount, while a higher percentage of molybdenum leads to a reduced thermal expansion coefficient.

Compared to the literature values for copper-molybdenum composites with sintered connections between the molybdenum grains, the values determined for the process route shown here are slightly higher. However, a targeted adaptation of the thermal expansion can be demonstrated via the adjustment of the composition.

5.4   Thermal Conductivity

Various aspects must be taken into account when determining the thermal conductivity of such pseudo alloys. Due to the high molybdenum content, measurement values of pure copper cannot be expected. The application of CuP8 instead of copper entails a further limitation.

Figure 10 shows the thermal conductivity of pure copper, CuP8 and MoCuP compounds with 40–60 wt% molybdenum, respectively, logarithmically plotted against the temperature. The thermal conductivity of molybdenum amounts to 140 $W \cdot m^{-1} \cdot K^{-1}$.

The difference between pure copper and CuP8 is significant. While the specimen of pure copper achieves measurement values of 250–290 $W \cdot m^{-1} \cdot K^{-1}$, the copper phosphorus alloy achieves not more than a tenth of the thermal conductivity. The measured values of the pseudo alloy amount to 35–50 $W \cdot m^{-1} \cdot K^{-1}$ depending on the content of molybdenum.

5.5   Transfer of Processing to Additive Manufacturing

Essentially, it was demonstrated that the adaptation of a molybdenum copper pseudo alloy can be successfully implemented with regard to the intended application in furnace-based sample generation. For the transfer to the additive laser metal deposition process, the absorption for infrared wavelengths is of interest to ensure process-reliable manufacturing.

Figure 11 shows measurements of various metal powders for wavelengths of 940–980 nm, which allow a qualitative classification of the absorption with respect to copper powder. Molybdenum shows more than twice the measured values than copper does, while the absorption of the copper phosphorus alloy is greater by a factor of three at least. The pseudo alloy falls in between with regard to the molybdenum content.

Consequently, the pseudo alloy allows significantly improved absorption for infrared wavelengths and is more suitable for additive processing, inevitably requiring process
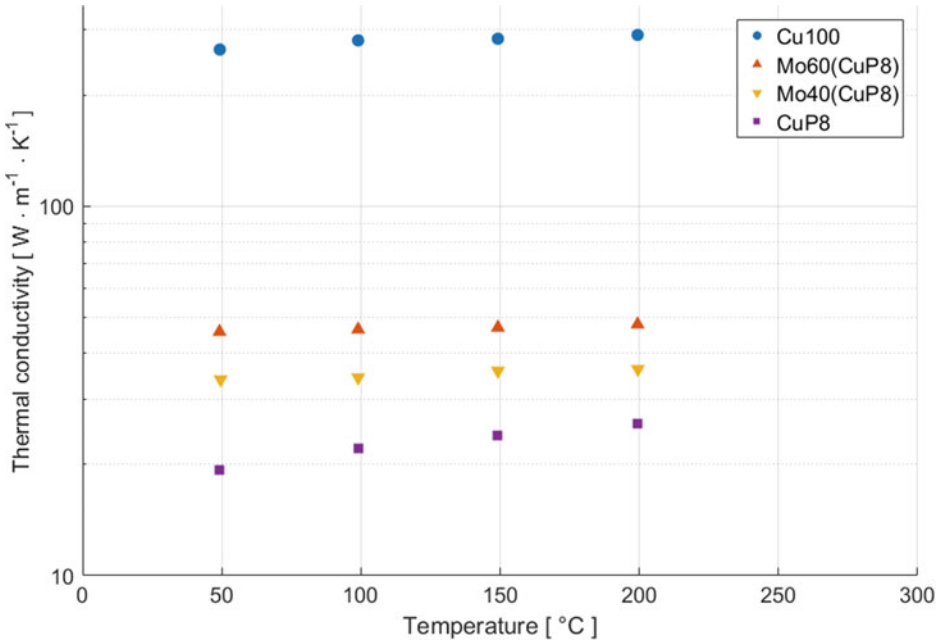
Fig. 10 Thermal conductivity of pure copper, CuP8 and MoCuP compounds as a function of temperature
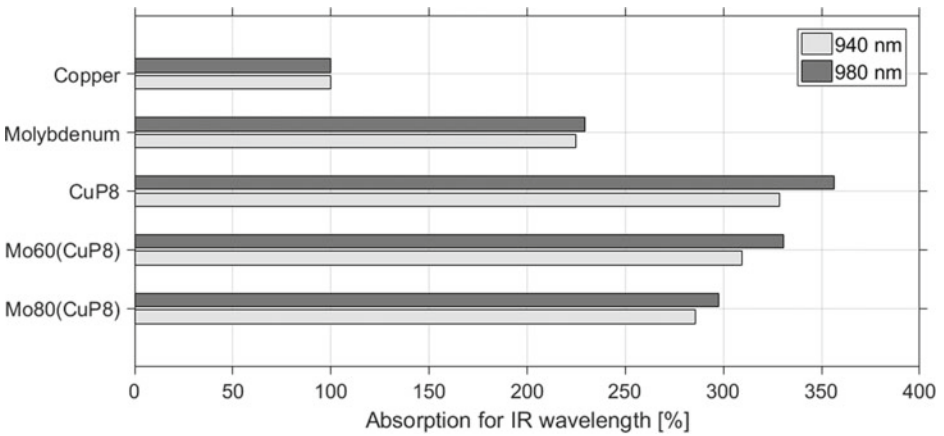
Fig. 11 Qualitative comparison of the absorption for infrared wavelengths for selected powder materials

development. During processing, it must be ensured that the temperatures are within the required range to achieve both melting of the matrix material and to prevent damage to the YAG due to excessively high temperatures. At the same time, the molybdenum particles should be distributed uniformly in the matrix in combination with a small quantity of imperfections in the structure.

In the following chapter, the development of the process strategy for laser-based additive manufacturing of this alloy will be discussed in more detail. At this point, the focus is exclusively on the fact that the pseudo-alloy can be successfully processed additively and multilayered structures with a thickness of several millimeters can be generated. Figure 12 shows the resulting microstructure with molybdenum particles bound in a copper phosphorus matrix.

While furnace-based processing has advantages with regard to the risk of damage to the YAG due to the thermal conditions, additive processing requires significant adjustments. In principle, it can be demonstrated that the processing of the pseudo alloy by laser metal deposition can be realized in a process-safe manner. For a multi material connection, on the other hand, precautions must be taken to avoid thermal damage. This requires that both the YAG is suitably prepared and the process is suitably adapted. Due to titanium coating on the YAG applied by physical vapor deposition, bonding to the pseudo alloy can be achieved much more easily while processing. By preheating the process zone, high temperature gradients and the risk of thermal shock can be eliminated. The use of
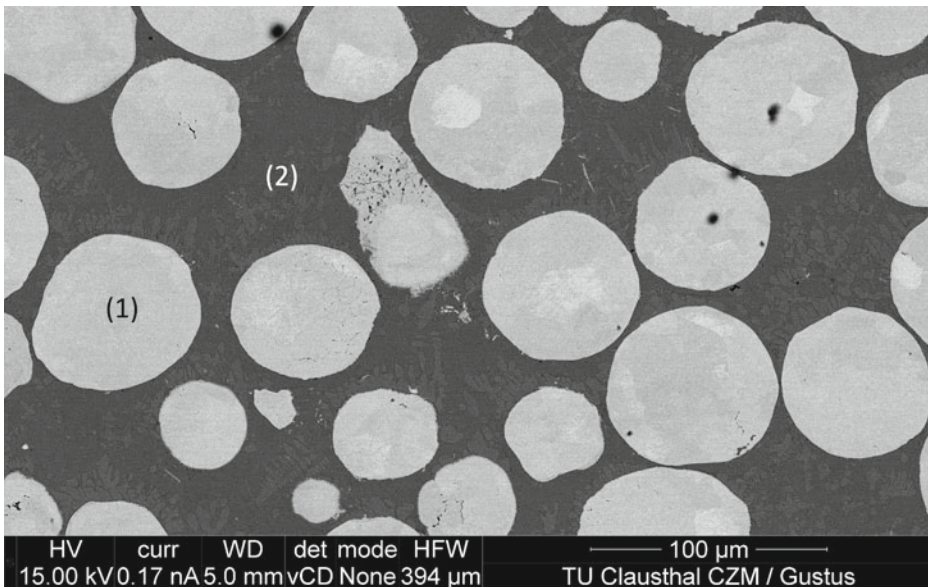
Fig. 12 FESEM picture of molybdenum copper pseudo alloy generated by additive manufacturing; explanatory note: (1) molybdenum, (2) CuP matrix

stepped seams enables uniform heat input distributed over the entire circumference. Thus a suitable additive binding and a sufficient process quality can be obtained. Initial tests on the imprinting of crystalline materials, taking into account the precautions described, achieved satisfactory results.

5.6   Formation of Microstructure

The different process conditions of furnace-based manufacturing and additive manufacturing inevitably lead to differences in microstructure formation. The quasi-static thermal conditions in the furnace allow for more extensive chemical interactions and diffusion processes in contrast to the additive process where cooling is much faster due to the high temperature gradients. This is evident by examining the microstructures of both types of specimen. The copper phosphorus matrix exhibits a structure consisting of Cu_3P and (Cu) phases.

In the furnace process, a very pronounced phosphorus-rich phase seam is formed around the molybdenum particles. At the same time, Cu_3P bypasses form between the particles (Fig. 13a)). The rest of the matrix consists largely of the low-phosphorus (Cu) phase. The thermal conditions allow for long diffusions paths.

Due to the high temperature gradients of the additive process, the lamellae consisting of Cu_3P and (Cu) form much finer (Fig. 13b)). These lamellae are also distributed throughout the matrix. At the same time, the phosphorus-rich phase seams around the molybdenum particles are much narrower.

A more detailed investigation of the interfaces of molybdenum particles and copper matrix by means of field emission scanning electron microscopy (FESEM) reveals an interaction of molybdenum and phosphorus. In the furnace-generated sample, a seam of molybdenum phosphorus phases of different composition (MoP, Mo_3P and Mo_4P_3) is detected (Fig. 14a)). In addition to the physical wetting, there is therefore also a chemical
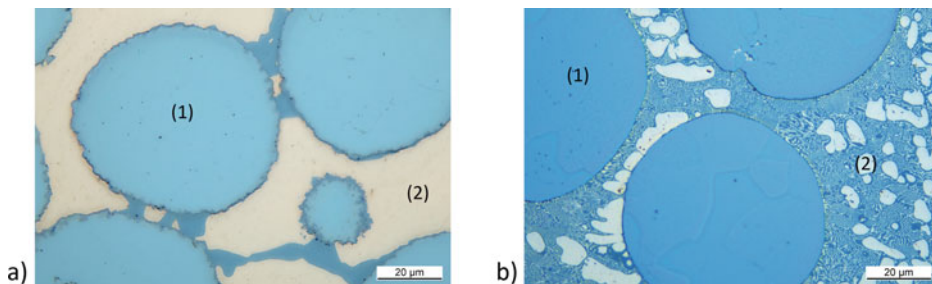
Fig. 13 Microstructure of pseudo alloy generated by furnace process **a** and additive manufacturing **b**; explanatory note: (1) molybdenum, (2) CuP matrix
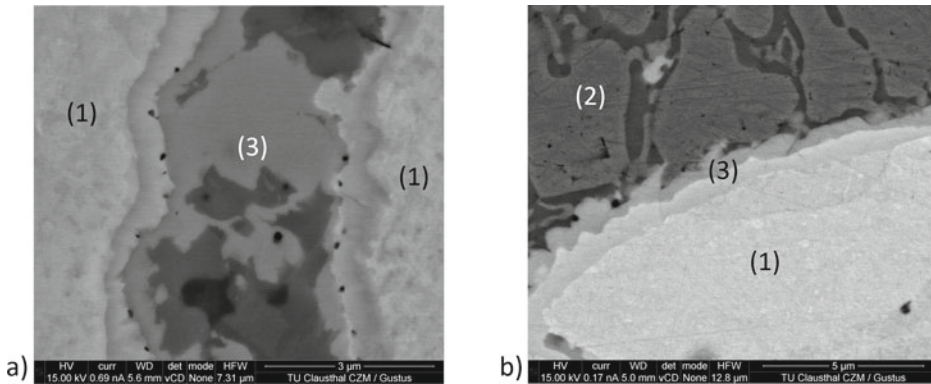
Fig. 14 FESEM picture of pseudo alloy generated by furnace process **a** and additive manufacturing **b**; explanatory note: (1) molybdenum, (2) CuP matrix, (3) Mo_XP_Y phases

interaction. Moreover, MoP bridges form between the molybdenum particles when these particles are close to each other.

Even though the high temperature gradients in additive processing significantly limit chemical interactions and diffusion processes, molybdenum phosphorus phases can also be detected. However, Fig. 14b clearly reveals that these phase seams are much smaller.

The presence of these seams therefore indicates chemical interaction between the components of the pseudo alloy. Consequently, there is inevitably a bonding of molybdenum particles and copper matrix.

6 Conclusion and Perspective

It can be shown that the transfer of molybdenum-copper composites to additive manufacturing is feasible, if the limitations of the additive process are considered. The pseudo alloy enables the properties to be adjusted according to the required profile. The combination of copper and molybdenum opens up wide-ranging possibilities for adjusting thermal expansion. The thermal expansion coefficients of the pseudo alloy show an almost parallel course compared to the YAG and can be finely adjusted by the molybdenum content.

The lack of sintered bridges is reflected in slightly higher expansion coefficients compared to conventional processing of the composites. At the same time, however, the innovative processing approach allows for the possibility of more complex structures and functional integrations that can only be implemented using additive manufacturing.

Depending on the selected process route, the microstructure differs significantly. Segregation within the copper phosphorus matrix is inevitable, but a larger seam of the phosphorus-rich phase forms around the molybdenum particles considering the furnace process. At the same time, the formation of Cu_3P bypasses between the particles occurs.

The rest of the matrix consists of low-phosphorus copper phase. Even though there are no sintered bridges between the molybdenum particles, it can be demonstrated that an interaction with the phosphorus from the matrix material takes place, since Mo_XP_Y phase bridges between the particles can also be detected. In the additive process, the segregation of (Cu) and Cu_3P is finely lamellar throughout the matrix, with much less pronounced phosphor-rich phase seams around the molybdenum particles. The background to this is the much higher cooling rates and the associated shorter diffusion paths. The bond between molybdenum and matrix material is obviously based not only on physical wetting, but also on chemical interaction.

The phosphorus, which plays a significant role in bonding, also leads to a lower melting point compared to the use of pure copper as a matrix material. This results in improved suitability for the intended application of additive mounting of the YAG. The low melting point leads to lower thermal stress and consequently a reduced risk of thermal damage to the YAG.

On the other hand, it can be seen from the thermal conductivity of the CuP alloy compared with pure copper that the CuP alloy as the matrix material of the pseudo alloy exerts a significant influence on the low thermal conductivity. Nevertheless, the pseudo alloy exhibits sufficiently high thermal conductivity for application in the additively manufactured laser system.

The bonding of matrix and YAG can be specifically improved by adding titanium or manganese. With the former, however, the oxygen affinity is particularly high, resulting in oxidation at the surface of the solidified alloy.

Since it has been shown that the additive processing of the pseudo alloy is possible, the adaptation of the material allows a use for a multi-material connection to the YAG, and first tests for additive mounting of the YAG show successful results, the upcoming final step is the process-safe generation of a laser system with mounted YAG. At the same time, a final characterization of the pseudo alloy and the multi material compound is carried out.

References

1. Sawruk, N. W., Bruns, P. M., Edwards, R. E. et al.: ICESat-2 laser Nd: YVO4 amplifier. In: Proc. SPIE 10513, components and packaging for laser systems IV, pp. 105130X (2018). https://doi.org/10.1117/12.2292256
2. Wayne, K.: Middle-infrared laser sources (2016). 10.13140/ RG.2.1.3105.2565 (DOI)
3. Hoff, C., Otero, N., Hermsdorf, J., Kaierle, S., Overmeyer, L.: Konditionierung von Kupferwerkstoffoberflächen zur Stabilisierung des Dauerstrich-Lasermikroschweißens. METALL 69. Jahrgang 11/2015, pp. 439–442
4. Grundlagen der berührungslosen Temperaturmessung. Micro Epsilon. https://www.micro-epsilon.de/download/products/dat-infrarot-grundlagen-de.pdf. Retrieved 15 Sept 2021
5. Schubert, T., Trindade, B., Weißgärber, T., Kieback, B.: Interfacial design of Cu-based composites prepared by powder metallurgy for heat sink applications. In: Materials Science and Engineering: A **475**(1–2), pp. 39–44 (2008). DOI: https://doi.org/10.1016/j.msea.2006.12.146
6. Holzer, H., Dunand, D.C.: Phase transformation and thermal expansion of Cu, ZrW2O8 metal matrix composites. J. Mater. Res. **14**(3), 780–789 (1999). https://doi.org/10.1557/JMR.1999.0104
7. Metall-Keramik-Verbundwerkstoffe mit Durchdringungsgefüge. Wissenschaftsmagazin der TU Darmstadt (2011)
8. Qiu, C., Adkins, N.J.E., Attalah, M.M.: Selective laser melting of Invar 36: Mi-crostructure and properties. Acta. Mater. **103**, 382–395 (2015). https://doi.org/10.1016/j.actamat.2015.10.020
9. Yakout, M., Cadamuro, A., Elbestawi, M.A., Veldhuis, S.C.: The selection of process parameters in additive manufacturing for aerospace alloys. Int. J. Adv. Manufactur. Technol. **92**, 2081–2098 (2017)
10. DIN 17745:2002–09: Knetlegierungen aus Nickel und Eisen. Beuth Verlag, Berlin
11. Neef, P., Bernhard, R., Wiche, H., Wesling, V.: Laser-based additive manufacturing of optical, thermal and structural components. In: da Silva, L., Martins, P., El-Zein, M. (eds) Advanced Joining Processes. Advanced Structured Materials, vol. 125. Springer, Singapore. https://doi.org/10.1007/978-981-15-2957-3_4
12. Shields, J. A.: Applications of Molybdenum Metal and its Alloys. IMOA (2013). ISBN: 978-1-907470-30
13. Seiss, M., Mrotzek, T., Dreer, N., Knippscheer, S., Knabl, W.: Molybdenum-copper-composites for the advanced thermal management of modern electronics. In: 19th Plansee Seminar (2020)

14. Yih, P., Chung, D. D. L.: Copper-matrix molybdenum particle composites made from copper coated molybdenum powder. In: JEM 24(7), 841–851 (1995). doi: https://doi.org/10.1007/BF02653333

15. Chu, J. P., Lin, T. N.: Deposition, microstructure and properties of sputtered copper films containing insoluble molybdenum. J. Appl. Phys. **85**(9), 6462–6469 (1999). https://doi.org/10.1063/1.370287

16. Kuskov, K. V., Sedegov, A. S., Novitskii, A. P., Nepapushev, A. A., Moskovskikh, D. O., Shkodich, N. F. et al.: Influence of chromium in nanocrystalline copper–chromium pseudoalloy on its structure and properties. In: Nanotechnol Russia **12**(1–2), 40–48 (2017). https://doi.org/10.1134/S1995078017010074

17. Rosalie, J. M., Guo, J., Pippan, R., Zhang, Z.: On nanostructured molybdenum-copper composites produced by high pressure torsion. J. Mater. Sci **52**(16), S9872–9883 (2017). https://doi.org/10.1007/s10853-017-1142-2

18. Sergey Gorbatyuk, S., Alexey Pashkov, A., Nikolay Chichenev, N.: Improved copper-molybdenum composite material production technology. Materials today. In: Proceedings, vol. 11, Part 1 (2019), pp. 31–35. ISSN 2214–7853. https://doi.org/10.1016/j.matpr.2018.12.102

19. Guo, S., Kang, Q., Cai, C., Qu, X.: Mechanical properties and expansion coefficient of Mo-Cu composites with different Ni contents. In: Rare Metals **31**(4), 368–371 (2012). doi: https://doi.org/10.1007/s12598-012-0522-7

20. Sun, A., Liu, Y., Wang, D., Zhou, Z.: Sintering behavior and properties of Mo-Cu composites. Adv. Mater. Sci. Eng. **2018**, Article ID 8703986. https://doi.org/10.1155/2018/8703986

21. Schubert, T., Weidmüller, H., Weißgärber, T., Kieback, B.: Kupfer-Verbundwerkstoffe für passive Kühlkörper in der Elektronik. METALL 61. Jahrgang 11/2007, pp. 752–756

22. Lanfant, B., Bär, F., Mohanta, A., Leparoux, M.: Fabrication of metal matrix composite by laser metal deposition-a new process approach by direct dry injection of nanopowders. In: Materials (Basel, Switzerland) 12(21) (2019). doi: https://doi.org/10.3390/ma12213584

23. Martin, J. H., Yahata, B. D., Clough, E. C., Mayer, J. A., Hundley, J. M., Schaedler, T. A.: Additive manufacturing of metal matrix composites via nanofunctionalization. (2018) In: *MRC* 8 (02), p. 297–302. DOI: https://doi.org/10.1557/mrc.2018.95.

24. Schnee, D.: Grundlagen des Lötens. Technical Materials BrazeTec. https://saxonia-tm.de/Brazetec/de/Downloads/Technisches%20Know-How/show_02357_BR_Brazetec_Grundlage_Loeten_MON15_low_einzel.pdf (Retrieved: 16 Dec 2020)

25. Löten von Kupfer und Kupferlegierungen. Deutsches Kupferinstitut 2015. https://www.kupferinstitut.de/wp-content/uploads/2019/08/Broschuere_Loeten.pdf. Retrieved 15 Sept 2021)

26. Perrot, P., Batista, S., Xing, X.: Cu-P binary phase diagram evaluation. MSI, Materials Science International Services GmbH. Stuttgart (2002). http://www.msi-eureka.com/full-html/20.16300.1.2/Cu-P_Binary_Phase_Diagram_Evaluation/. Retrieved: 15 Sept 2021

Additive Manufacturing of Optical, Thermal and Structural Components by Laser Metal Deposition

Robert Bernhard, Philipp Neef, Christian Hoff, Jörg Hermsdorf, Stefan Kaierle, Henning Wiche, and Volker Wesling

1 Introduction

The evolution of laser technology began with the development of the first solid-state lasers in 1960. The ability to focus coherent light with highest intensities showed great potential for material and surface processing. Lasers are considered one of the main stepping-stones for additive manufacturing. The confined heat input results in low dilution and an overall reduction of defects. Additionally, the laser beam is a very flexible tool since it can be articulated fast and precisely without any wear. Due to high initial costs and low efficiency of laser beam sources, it took over 20 years until lasers became industry-wide adopted for metal cladding [1]. True three-dimensional additive manufacturing evolved in the 2000s. Today, additive manufacturing of metals is one of the fastest growing fields in modern industry with annual growth rates of 25–35% [2, 3]. Additive manufacturing has a great potential for businesses that need individualized and function integrated metal parts [4]. These added functions can be of optical, thermal or structural nature [5]. Meanwhile, the rapid market growth increases the need of suitable materials with adapted properties. Building on this, the main goal of the wGROTESK project is to innovate materials and processes to integrate thermal, optical and structural properties into multi-material components [6]. The ambition is to demonstrate the feasibility of solid lasing mediums in combination with metals. Integrating additive manufacturing in the production of these core laser-assemblies with a direct bond between metal and lasing mediums yields an

R. Bernhard (✉) · P. Neef · H. Wiche · V. Wesling
Clausthaler Zentrum für Materialtechnik, Leibnizstraße 9, 38678 Clausthal-Zellerfeld, Germany
e-mail: r.bernhard@lzh.de

C. Hoff · J. Hermsdorf · S. Kaierle
Laser Zentrum Hannover e.V. (LZH), Hollerithallee 8, 30419 Hannover, Germany

increased thermal performance and further process automation—Pursuing the vision of 3d-printed lasers.

The investigations in this chapter focus on the development of processes that allow the bonding of yttrium aluminum garnet (YAG) lasing mediums in conjunction with materials developed in the previous chapter "Molybdenum Copper MMC for Additive Manufacturing". On a metallurgic level, metals and crystalline YAG materials are incompatible. During the research, two promising iron-nickel and copper molybdenum material systems were identified. In both cases, the investigations show that variations of the material composition allow modifications the thermal expansion coefficient [7]. Finally, the copper-molybdenum materials were selected and used to manufacture multi-material components due to their superior thermal performance.

2   State-of-the-Art

Additive manufacturing of metal alloys like aluminum and chromium-nickel stainless steels are common in modern industry [8, 9]. Typical applications are rapid prototyping, research and development up to serial production. The two most prominent powder based additive manufacturing processes are explained in the following section. Furthermore, available processes for creating state-of-the-art multi-material combinations are depicted.

2.1   Additive Manufacturing of Metals

The predominant additive metal processes are laser powder bed fusion (PBF-L/M) and laser metal deposition (LMD) [9]. Both methods use lasers as the primary energy source but they show differences regarding the material supply and beam delivery. Powder bed fusion uses a recoater blade to supply metal powder from the delivery platform to the build platform. In contrast, for laser metal deposition powder is conveyed via an inert gas stream into the process zone. This has the advantage of supplying powder only where needed. On the other hand, large amounts of powder are needed in order to build 3D objects via powder bed based machines. The principles of beam delivery are inherently different. In LMD processes, the laser beam is coaxially aligned to the powder nozzle and moves with the process head along the preprogrammed toolpath Fig. 1. In PBF-L/M, the laser can be scanned quickly over the process zone by moving mirrors reaching speeds above 10,000 mm/min.

One of the main advantages of powder-blown laser metal deposition is the alterable material composition during the process. This can accelerate process and material development for additive manufacturing, especially in the scope of building optical, thermal and structural components.
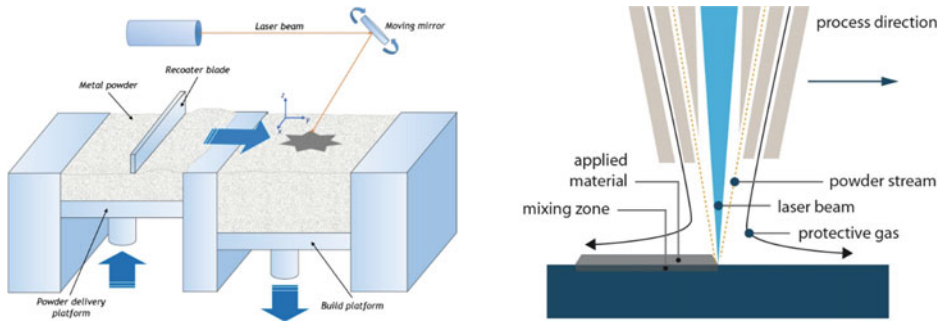
Fig. 1 Principle laser powder bed fusion (left) [10], laser metal deposition (right) [11]

At its core, laser-metal-deposition is an additive laser welding process. During this process, individual weld beads are aligned and stacked onto existing substrate material. Typical applications of this technique are reinforcements of mechanical parts or repair of worn drawing dies for metal stamping. With laser metal deposition, the properties of workpieces can be altered by adding hard and wear-resistant materials onto ductile steel [8].

Advances in process development enable increased geometric complexity and the use of special or hard-to-weld materials. Laser metal deposition is not only limited to metals; even ceramics or carbides can be dispersed into metal surfaces in order to functionalize 3D-printed parts. Leveraged through advanced process monitoring and feedback control loops, parts require minimal finishing work.

The alignment of the laser beam with the powder stream is distinctive for the process head. The systems can be designed with either an off-axis or a coaxial material supply [12]. For additive manufacturing purposes, a coaxial setup is beneficial due to the direction-independent material deposition. This setup is a requirement for sophisticated additive manufacturing. Another advantage of laser metal deposition for additive manufacturing is the maximum size of the build volume. Some build-chambers can have a size of multiple cubic meters. The possibility to add onto existing freeform surfaces allows special materials to be added on top of conventionally manufactured parts. Overall, laser metal deposition is better prepared for the intended process and material developments and consequently it is selected for the carried out experiments.

2.2 Multi-Material Metal Processes

Multi-material combinations are necessary when the physical requirements of a single material are exceeded. For example in electronics, silicon dies are attached to ceramic substrates that are thermally glued to copper heatsinks [13]. In laser applications, the
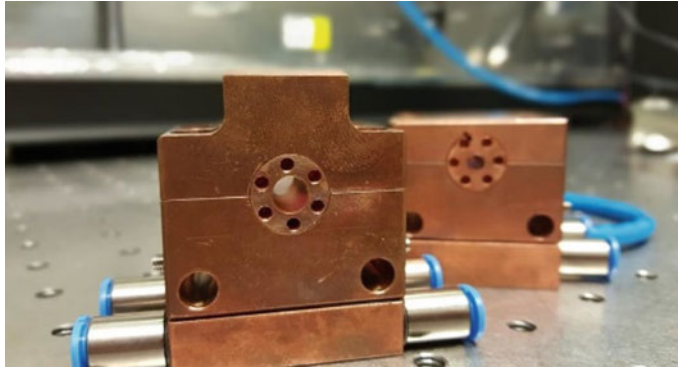
Fig. 2 Conventional copper heatsink for a solid state laser [15]

solid laser rod is connected to the copper heatsink via indium foil as an interface. Excess heat generated during operation is dissipated. Key properties in these applications are the thermal conductivity and the thermal expansion. The thermal conductivity needs to be as high as possible; any extra interface layers harm the performance significantly. The thermal expansion of the components needs to be matched across a wide temperature range to minimize thermal stresses.

State-of-the-art are diamond plates glued to disc lasers, friction fit copper heatsinks of laser rods with indium foil [14], as well as thermal paste connecting electronic packages to heatsinks (see Fig. 2). Differences in thermal expansion are overcome by slip in the contact areas. In more demanding tasks like high power electronics for e-mobility, the thermal expansions of the components are matched [13]. Available solutions use Invar (iron-nickel) alloys or sintered copper molybdenum materials.

State-of-the-art copper-molybdenum materials are created in a two-stage process. First, molybdenum powder is sintered. This skeleton is infiltrated with copper subsequently [16, 17]. Finally, molybdenum particles are embedded in a copper matrix (see Fig. 3). These industry-proven materials can only be shaped in a predefined die. For automation and function integration, the common manufacturing process lacks geometric complexity and the possibility to integrate structures.

2.3   Process-Relevant Parameters

Process parameters of laser-based additive manufacturing continue to be the subject of research. Parameter windows are strongly influenced by the material, the substrate and the geometry of the printed objects. The results of laser metal deposition and powder-based fusion are very dependent on the process parameters [9]. One of the most significant parameter sets is the laser power P (W) and the feed rate f (m/s). Their relation is
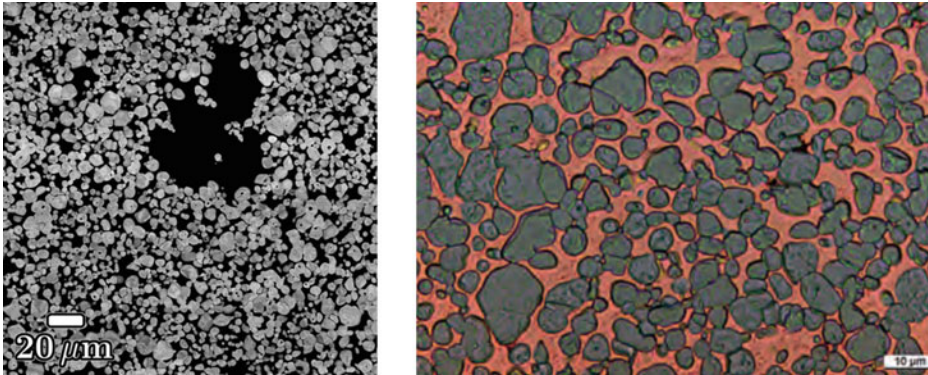
Fig. 3 Conventional copper molybdenum materials: sintered molybdenum powder that is infiltrated with copper in a secondary process step [17, 18]

described as linear energy E = P/f (J/m) and it dictates the energy input and therefore the size of the melt pool. In powder bed fusion, the layer height corresponds to the amount of powder added to the process zone during laser metal deposition. It mainly affects the resulting deposition rate and temperature of the melt-pool. The feed rate has an influence on the process time and the overall volumetric heat input regarding the size of the heat-affected zone and the dilution of the metals. Another main factor is the material used and its inherent properties. These include the melting point, weldability, surface tension of the liquid phase, thermal conductivity, and reflectivity/absorption of laser light. In situations where heat dissipation is restricted, for example at corners and sharp contour changes, once miscellaneous parameters like the flow rate of the shielding gas can become critical. The large number of parameters is a challenge for the process development. For a deeper insight into the process and in search of best parameters, the application of statistically designed experiments is indispensable.

2.4 Process Monitoring and Control

As described, additive laser processes depend on numerous process parameters and their interactions. Significant and controllable influences are laser power, laser spot size, intensity, deposition-/feedrate and the amount of filler per unit of time [8, 9]. Changes of these parameters, fluctuating ambient conditions (temperature, rel. humidity, surface finish) and effects inside the melt pool (surface tension, temperature dependent absorption and reflectivity) contribute to processes deviating from their optimal settings. As a result, defects and porosity can occur inside the workpieces (see Fig. 4).

The high demands on quality and cost of additive manufacturing are at conflict. They motivate closed loop control system and adaptive process control. At this point real-time

Fig. 4 Defects in additive
manufacturing of metals [5]
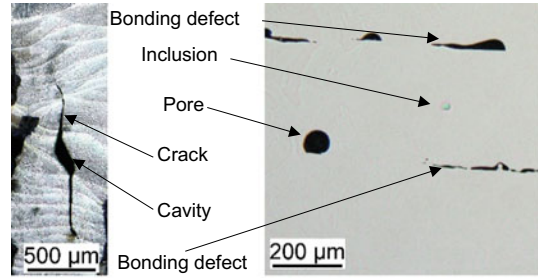
process monitoring and control are favorable over manual parameter adjustments because they guarantee high quality and advanced automation. The implementation of contactless process monitoring is valuable for laser metal deposition due to the harsh process environment. State-of-the-art in research and development are camera-based monitoring solutions that visually recognize melt pool features [19, 20] (see Fig. 5). Additionally, thermal imaging allows spatially resolved surface temperature measurements of the melt pool. Pyrometers and photo diodes can measure temperature via infrared radiation with a very high time resolution.

In additive processes, other critical defects can inherent from geometry changes. Restricted heat flux results in local overheating and irregular deposition. Commercial laser profile scanners are used to capture the height deviations.
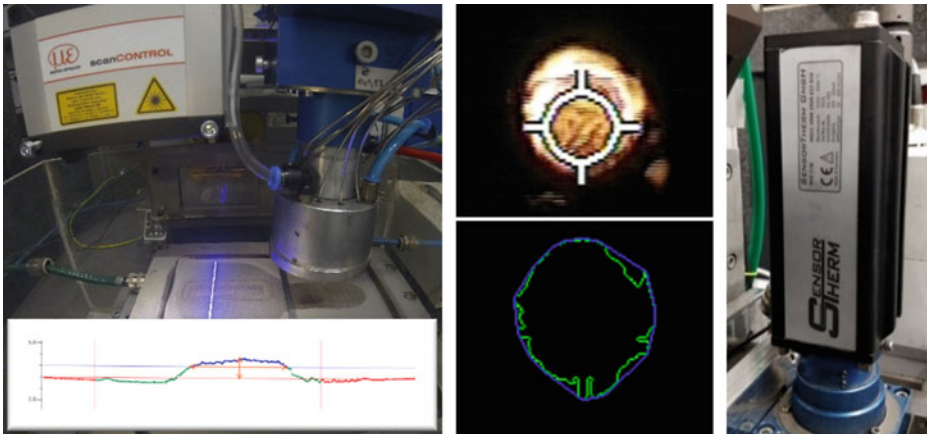
Fig. 5 Laser metal deposition process monitoring (deposition measurement, melt pool features, pyrometer)

3   Pseudoalloy Challenges

On the macroscopic scale as well as on the application level, molybdenum powder particles embedded in a copper matrix perform as a homogeneous alloy of the two metals. In contrast, on the microscopic scale the individual components still occur separately. In consequence, these special materials form a pseudoalloy. With additive manufacturing, a similarly structured material can be achieved in a single-stage process by solely melting the copper of a copper-molybdenum powder mixture. In contrast to the conventional process route, there will not be sintered bonds between the molybdenum grains. In order to achieve a pseudoalloy, a fitting additive process and a suitable copper-molybdenum powder mixture need to be developed. Based on this knowledge and the ability of combining thermomechanical properties by alloying, a new material for additive manufacturing has been developed. This material is a combination of copper and molybdenum. Both metals are commonly used for heat sinks of high power semiconductors [20]. The inherently high thermal conductivities of copper and molybdenum ($380\ Wm^{-1}\ K^{-1}$ and $139\ Wm^{-1}\ K^{-1}$) in addition with the low thermal expansion coefficient of molybdenum qualify the material for multi-material combinations with a YAG. For the intended application, the material has to be processable by laser metal deposition. Besides, its thermal expansion has to be adjusted according to the crystalline structure of the YAG. The individual thermal expansion coefficients of copper and molybdenum are shown in Fig. 6. It is obvious that the thermal expansion coefficient of copper and its increase over temperature are above the
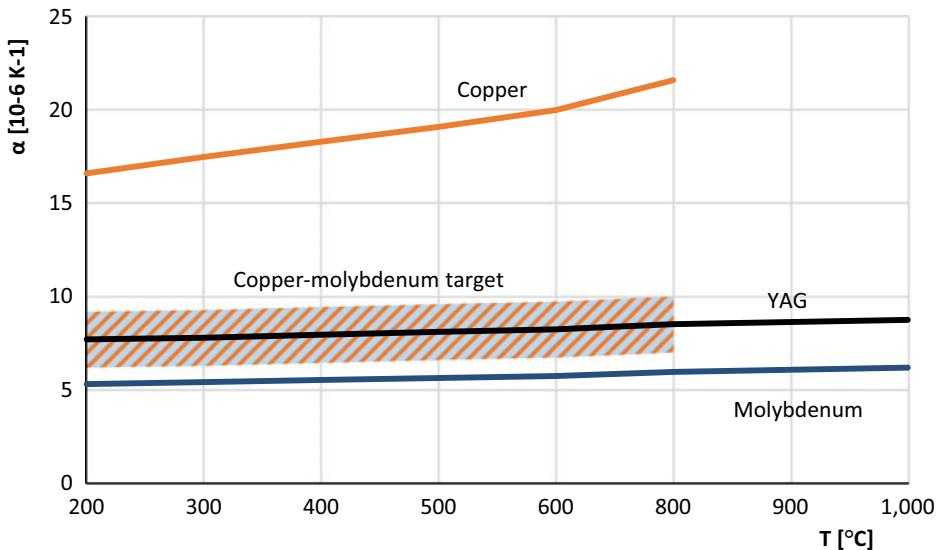
Fig. 6 Copper and molybdenum thermal expansion coefficients compared to YAG [7]
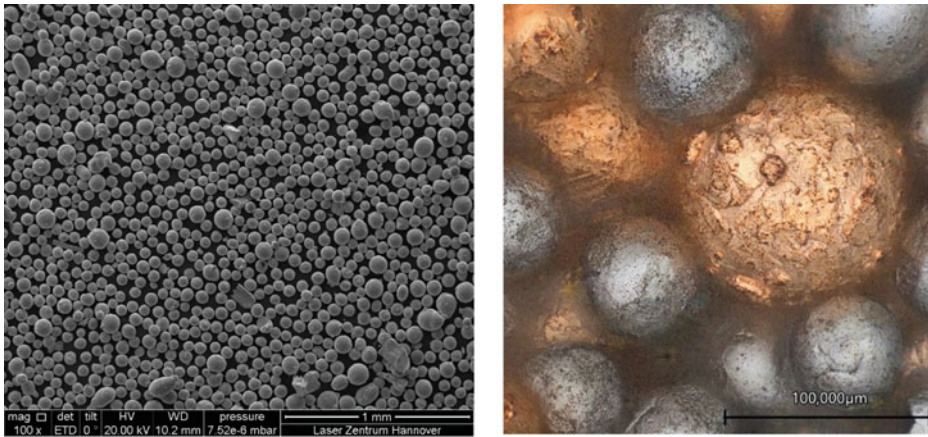
Fig. 7 Copper-molybdenum powder—SEM (left) and confocal analysis (right)

measurements of a YAG. In contrast, molybdenum has a lower thermal expansion coefficient and is almost parallel to the YAG. In order to reach the targeted zone close to the YAG a copper-molybdenum composition with 30 $_{wt}$% copper and 70 $_{wt}$% molybdenum is selected. This composition is based on industry-proven heat sink materials [13, 18]. The high copper percentage is in favor of thermal conduction and wetting behavior.

The disadvantage of a molybdenum rich alloy is the high melting point exceeding 2500 °C. This is critical for any application in contact with a YAG crystal. To benefit from the positive properties of a combination of copper and molybdenum without damaging the crystalline substrate, an inhomogeneous pseudoalloy is created. This approach leads to the investigation of an additively manufactured copper-molybdenum pseudoalloy that consists of molybdenum grains embedded in a copper matrix. An additional challenge during manufacturing is the high reflectivity of copper for near infrared laser wavelengths. The powder topology and composition is captured with a scanning electron microscope. Besides copper (ca. 30_{wt}% and molybdenum (ca. 70_{wt}%) grains, traces of non-spherical manganese ($_{>}1_{wt}$%) particles are visible. They are added for improved YAG wetting. A confocal image shows the different colors of the copper and molybdenum grains (Fig. 7).

4   Implementation

For this research project, laser metal deposition is selected for the additive manufacturing of optical thermal and structural components. As previously described, it is the preferred technology for material development and allows the deposition on freeform surfaces. A deposition process of copper molybdenum is visible in Fig. 8.
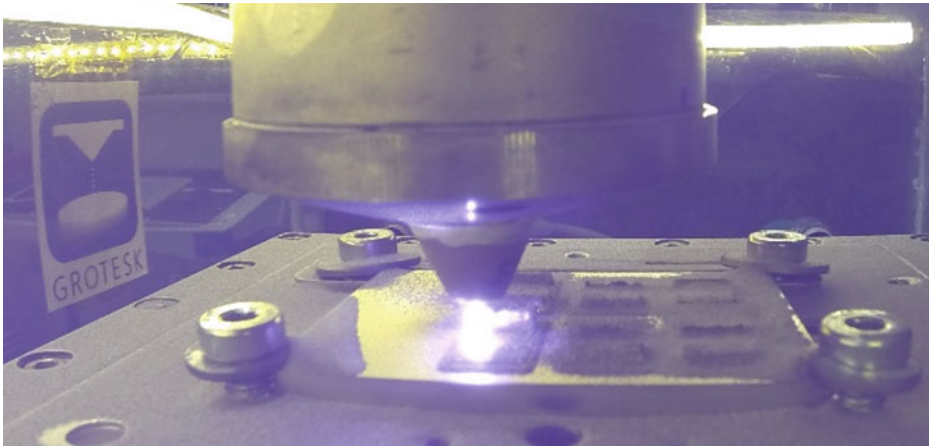
Fig. 8 GROTESK laser metal deposition process of copper-molybdenum specimens

4.1 Experimental Setup

All experiments were carried out on a custom powder-based LMD machine. Three of its six axis manipulate the processing head linearly in the X, Y and Z direction. The B and C axis tilt and rotate the workpiece. Additionally, the remaining A-axis allows for angle adjustments of the attached processing head. It consists of a nozzle, a pyrometer and optics for beam guidance. The laser beam propagates from a 680 W Laserline LDF650 diode laser source through an optical fiber to the processing head. The beam is then collimated with a converging lens. This beam is deflected with a dichroitic mirror by 90°. The mirror acts as a long-pass filter. It is reflective for the shorter 940–980 nm wavelength of the laser and transmissive for longer wavelengths. This allows the use of a SensorTherm HQ22 two-color pyrometer with its spectral range of 1.45–1.8 μm. It can sample the temperature of the melt-pool with up to 25.000 Hz between 1000 and 2500 °C. The laser exits the processing head through a nozzle. Through an annular opening, which is coaxial to the laser beam, metal powder is added to the process zone. Argon is used as conveying and shielding gas. The metal powder is injected into the gas stream with a plate feeder. Additionally, a laser profile scanner is fitted next to the nozzle. It is used for on- and offline weld seam analysis (see Fig. 9). An internet of things (IOT) sensor network gathers process data and writes is to an SQL-Database. A grafana frontend acts as a process data dashboard.
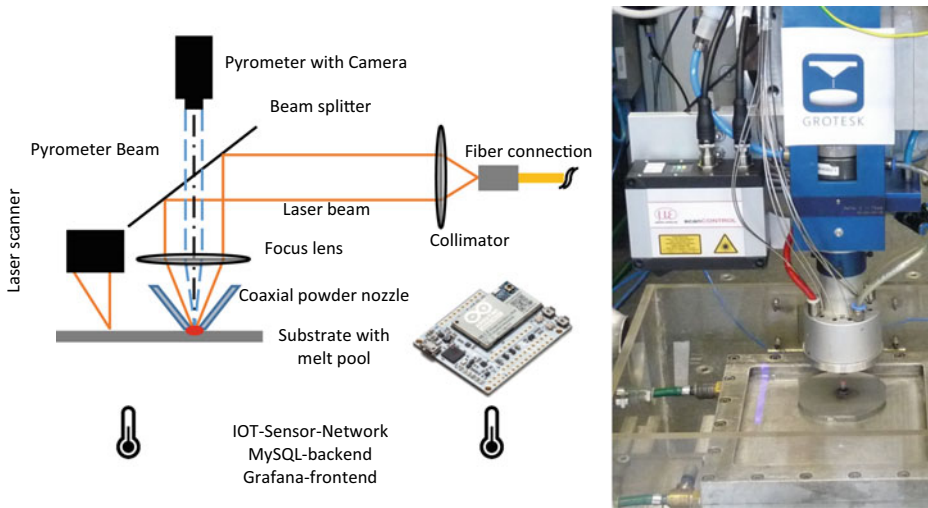
Fig. 9 Schematic setup and a picture of the GROTESK process head [7]

4.2   Design of Experiments

Due to the complexity of the laser process, structured and efficient experiment designs are indispensable. Experiments with only one parameter change at a time do not allow for conclusions about occurring effects and hide factor interactions. First, boundary process settings are developed. These act as a starting point for a parameter screening. The screening reveals the main effects and therefore the factors with the highest impact on the process results. With a custom design of experiments (DOE), main effects and interactions can be evaluated. A subsequent full factorial design tests the entire parameter combination to refine the model. Finally, the developed settings are used in consecutive experiments for confirmation and they are used for the multi-material experiments. With these subsequent multi-material experiments, more parameters are added. Therefore, an additional boundary, screening and custom design is used to gather process insights (see Fig. 10).

The specimen design includes a single weld (A), a thin wall (C), two surface clads with different seam orientation (B&D) and a multi-layer volumetric deposition (E). The experiment number is encoded bitwise in a separate field (F) (see Fig. 11). This approach allows independent as well as combined observations of process factors in the zones A to E.

For each design, the examined factors are varied in multiple levels while others are kept constant. Depending on the design type, models with emphasis on main effects or factor interactions can be realized. An overview of all designs and the factors can be seen in Table 1.
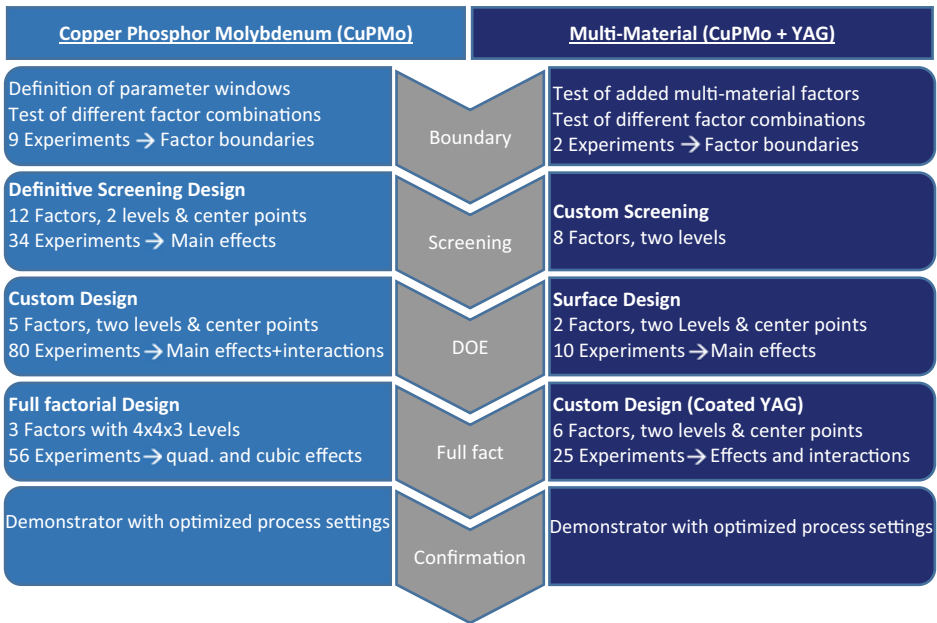
Fig. 10 DOE Implementation of copper phosphor molybdenum and multi material experiments
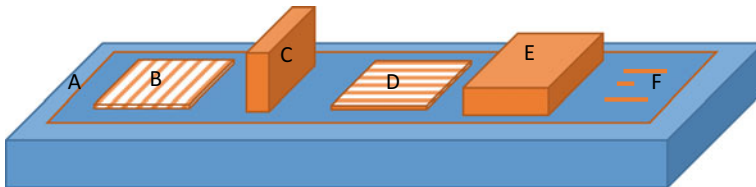
Fig. 11 DOE specimen for material analysis

The factor responses are the following for the DOE specimen.

A (Single weld):Deposition height, track width, dilution
B (vertical surface clad):Deposition height, dilution, surface roughness
C (this wall):Overall height, dilution, powder adhesion, molybdenum
D (horizontal surface clad):Deposition height, dilution, surface roughness
E (Volume):Density, imperfections, molybdenum

For the multi-material experiments, the responses include molybdenum, dilution, density, imperfections, bonding, cracks and the overall height.

Table 1 Overview of all factors and the number of factor levels during the experiments

	CuPMo				Multi-Material			
	Boundary	Definitive Screening	Custom Design	4x4x3 Factorial	YAG-Boundary	YAG-Surf	YAG-Custom	YAG-Coated
Laser power	5	3	17	5	const.	const.	2	3
Powder feedrate	5	3	17	5	const.	const.	2	3
Feedrate / speed	3	3	16	3	const.	const.	2	3
Layer height	3	3	const.	const.	const.	const.	2	3
Track distance	3	3	const.	const.	const.	const.	2	const.
Standoff distance	const.	3	const.	const.	const.	const.	const.	const.
Argon powder	const.	3	const.	const.	const.	const.	const.	const.
Argon nozzle	const.	3	const.	const.	const.	const.	const.	const.
Dwell time	const.	3	const.	const.	const.	const.	2	3
Nozzle gap	const.	2	2	const.	const.	const.	const.	const.
Molybdenum %	const.	3	3	const.	const.	const.	const.	const.
YAG Ø	n.a.	n.a.	n.a.	n.a.	const.	const.	const.	const.
Angle	n.a.	n.a.	n.a.	n.a.	2	3	2	const.
Segments	n.a.	n.a.	n.a.	n.a.	2	const.	2	2
Offset to YAG	n.a.	n.a.	n.a.	n.a.	const.	3	2	3

4.3 Process Monitoring and Feedback Control via Machine Learning

A successful three-dimensional metal deposition requires a stable process environment. The first step is to analyze the process and capture process data. Therefore, controllable and environmental parameters are logged. Using these measurements in conjunction with spatial data, irregularities and defects can be reconstructed (Fig. 12). This is implemented

Fig. 12 3D-reconstruction of temperature data mapped onto the tool path, resulting in a digital shadow [21]
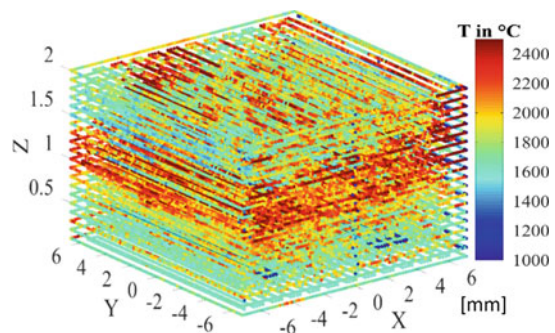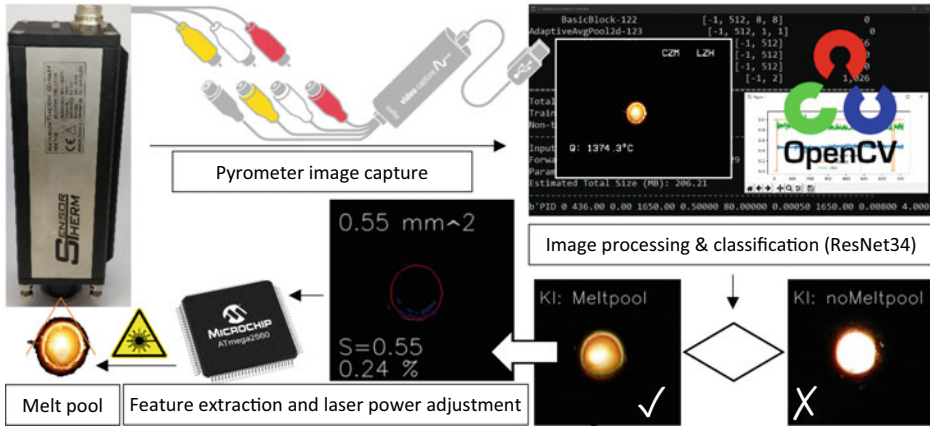
Fig. 13 Melt pool feature detection via OpenCV with ML-classification in a melt pool size control loop [22]

by a sensor network where sensor nodes communicate via message queuing telemetry transport (MQTT) to a server.

A key aspect of a successful material deposition is the melt pool. It is generated on the substrate wih the energy of the focused laser beam. The consecutive layers are deposited on top. To compensate for subsequent heat accumulation, pyrometer-based temperature control is typically used. With the development of the heterogeneous pseudoalloys, this temperature-based process control cannot be used due to the differences of laser absorption of the individual powder particles. On the contrary, the melt pool size is nearly immune against these fluctuations. In these circumstances, a process control of the melt pool size can be beneficial. In the following graphic, a control loop is visualized (see Fig. 13). Using OpenCV image processing and a machine-learning algorithm the melt pool is identified. A microcontroller handles the control of laser output power accordingly.

In detail, the integrated PID laser controller of the microprocessor is activated when a melt pool is detected. If the melt pool deviates from the setpoint, the laser power is adjusted accordingly (see Fig. 14). If no melt pool is visible, the process falls back to preset parameters that create a melt pool.

5 Results

During the project duration, innovative pseudoalloys are created in an additive process for the first time. Furthermore, material properties are adapted to YAG laser mediums in a single-step laser metal deposition process. An essential leap forward is the implementation of resource-efficient experiment designs. With them, parameter combinations are
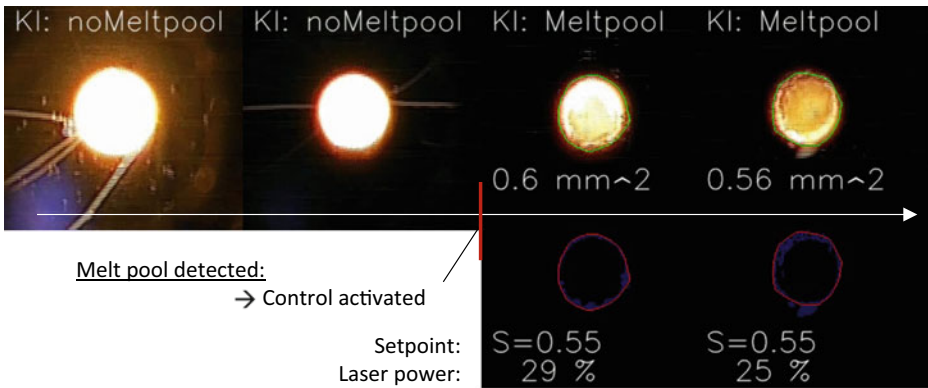
Fig. 14 Image recognition and laser power control [22]

found and material models are designed. The heights of the manufactured specimens are measured via a confocal microscope and analyzed via a semi-automatic feature extraction (Fig. 15). The data is used to create a model and a parameter profiler. Overall, data of more than 170 micro sections is acquired and used to refine the process. Regarding the measurement of the thermal expansion, larger dilatometer specimens are manufactured.

To ensure maximum reproducibility the process data is written to a database and the nozzle is inspected with every substrate change. Possible particle adhesions are removed throughout the experiment (see Fig. 16).
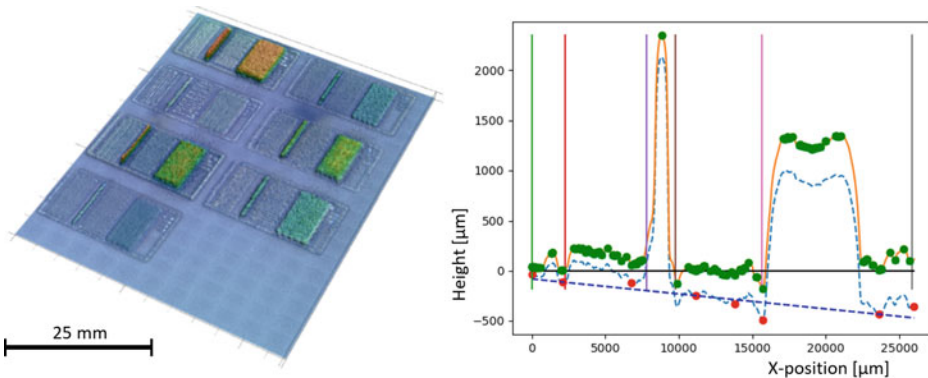
Fig. 15 Height measurements of 3D-printed specimen and semi-automatic profile measurement
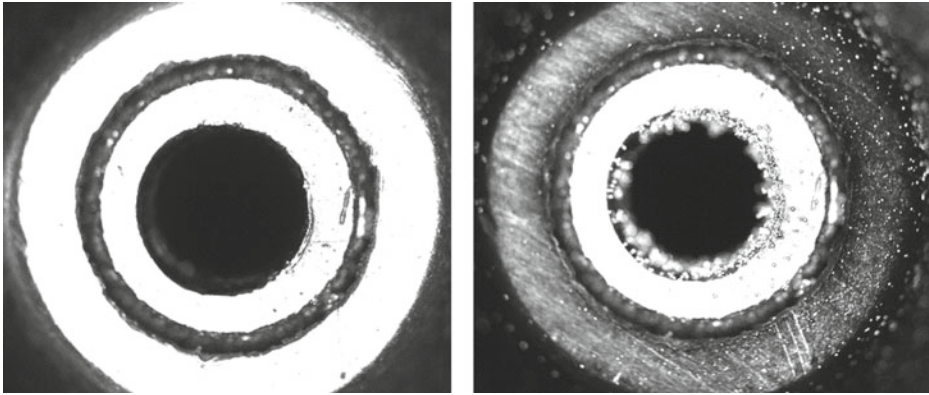
Fig. 16 Wear of the powder nozzle before and after finishing a substrate

5.1 Material Evaluation

In selected micro-sections with well-performing factor combinations, the deposited material shows molybdenum grains embedded inside a copper-colored matrix material. Copper phosphor phases and copper dendrites originate from the molybdenum grains (see Fig. 17). Compared to oven-based experiments the phosphor rich phases occur only in the carried out additive processes because of the steep temperature gradients during the solidification.

With a parameter set developed in the full factorial design, a larger 10 mm × 6 mm × 50 mmdilatometer specimen was generated. After the eight-hour additive laser process, a 40 mm cylindrical (Ø4 mm) dilatometer specimen was extracted by electrical discharge machining. Due to the increased thermal conductivity compared to the substrate, the cross
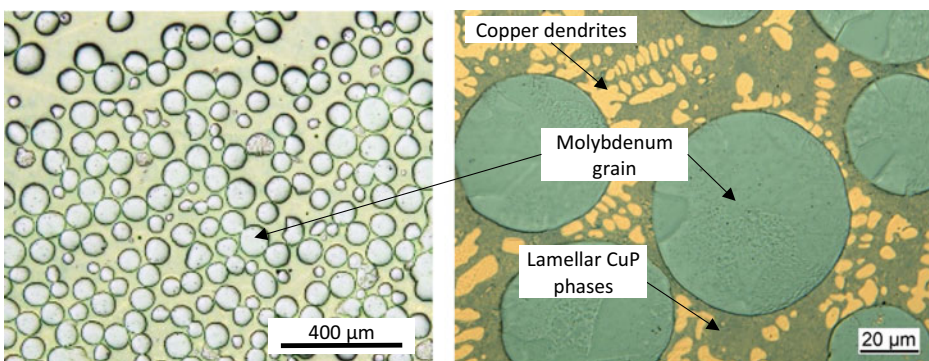
Fig. 17 Microsections of additively manufactured copper phosphor molybdenum pseudo alloys
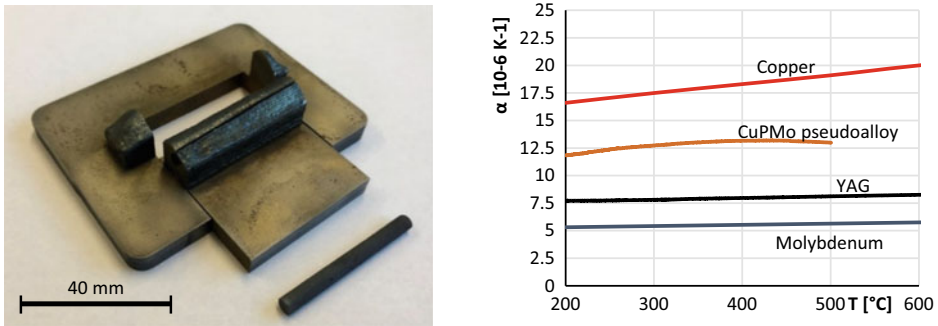
Fig. 18 Dilatometer specimen and the thermal expansion coefficient of the pseudoalloy compared to copper, molybdenum and YAG

section indicates some segregations. The results of the measured thermal expansion coefficient of the AM copper-phosphor-molybdenum pseudoalloy are compared to a YAG. Pure copper and molybdenum are added for reference. The final composition of that specimen was 70 $_{wt}$% molybdenum, 28.8$_{wt}$% copper and 1.8$_{wt}$% phosphor (Fig. 18).

The low melting point of the pseudoalloy inhibits dilatometer measurements above 500 °C. The graph shows a moderate rise from 11.8×10^{-6} K^{-1} at 200 °C to 13.0×10^{-6} K^{-1} at 500 °C. Consequently, the final thermal expansion results in between of copper and molybdenum. Even though the pseudoalloy does not match the YAG, it was possible to approximate the targeted values. Besides a physically limited molybdenum density of the spherical particles, the pseudoalloy lacks the sinter bonds between the molybdenum grains that would occur from conventionally sintering at higher temperatures.

5.2   Closed Loop Process Control

On average, the trained ResNet34 classifier shows a recognition rate of 95% in three unseen sets of 20 melt pool images. For testing, a superimposed translation of the melt pool is added. The recognition rate remained unchanged, which indicates a reliable classification. Therefore, the melt pool recognition is robust in respect to the camera orientation.

In order to analyze the weld tracks, height profiles are examined. A comparison of the new machine learning (ML) and the pyrometer-based control differences is present in Fig. 19. The pseudoalloy deposition of ML-assisted melt pool control is constant over the entire specimen. Non-critical powder adhesions are visible on the surface cladding. The temperature control, on the other hand, shows inconsistent and irregular material deposition especially at the transition from single track to surface cladding. The poor
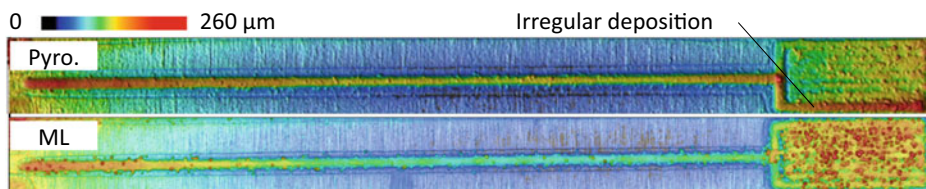
Fig. 19 Comparison of temperature and machine learning welds [22]

performance of the pyrometer-based control is due to the fluctuating emissivity of the molten metal and the heterogeneous powder. Therefore, it is not possible to keep the temperature constant of the copper-molybdenum material. In contrast, with the ML melt pool size control it is possible to reach the target melt pool size constantly. Furthermore, different geometries and movement speeds had a negligible impact. In conclusion, the intelligent process monitoring and control system based on a convolutional neural network provides an improved approach for more stable process control.

5.3 Multi-Material Combinations: Lasing Medium and Metal

For efficient parameter development and because of the high cost of YAG laser mediums alternative boron- and aluminum nitride ceramic specimens are used, which share the same thermal properties. In order to have a comparable surface, ceramic and YAG workpieces are coated with titanium via physical vapor deposition. A crucial part of the experiment is the toolpath planning. The multi-material combinations are successfully implemented by using the laser to preheat the substrate before the deposition. This is done by moving the process head up and off-axis. The substrate then rotates in the defocused for laser beam for 10 revolutions. The process head then moves back to the standoff distance and starts the weld process (see Fig. 20).

Dwell times and segmented welding reduce the heat input and circumvent damage to the YAG. The welding strategy is depicted in a cross-sectional and a top-down view in Fig. 21. The weld sequence for the inner two tracks is numbered. The substrate rotates counter clockwise while the laser stays stationary until it moves outward every second revolution. After the completed deposition of a layer, the process head moves up and closer to the YAG. The process is repeated for all 56 layers.

An X-ray analysis is used to show the integrity of the YAG and its ceramic substitute embedded inside the copper-phosphor-molybdenum. It hints at a successful imprinting and the creation of a multi-material component combining thermal, optical and structural properties (see Fig. 22).

| 1. Laser Preheating | 2. Material Deposition Layer 12 /56 | 3. Material Deposition Layer 56/56 |
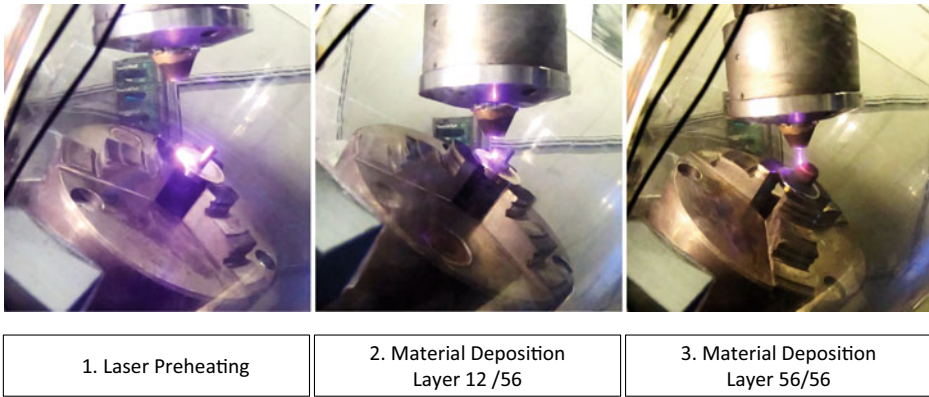
Fig. 20 YAG and laser metal deposition process steps
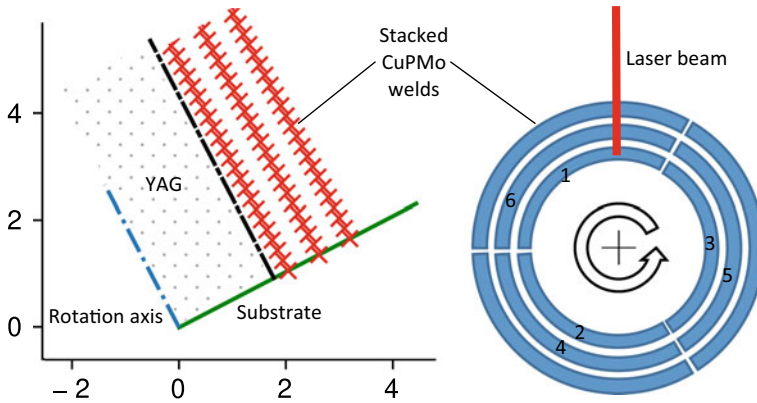
Fig. 21 Multi-material toolpath for YAG cross-section and top-down view
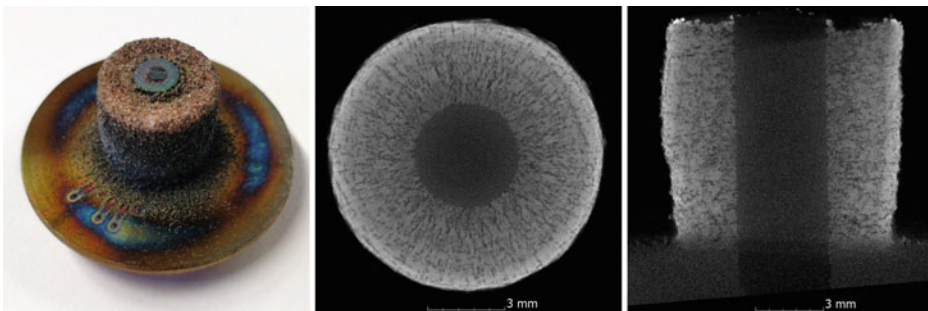
Fig. 22 Embedded YAG-substitute and two x-ray orthogonal cross-sections

6   Conclusion and Outlook

The results conclude with a successful additive manufacturing of an adaptive heatsink material. By processing the developed copper-molybdenum material with laser metal deposition, it is possible to adjust thermal and mechanical properties. These pseudoalloys are created in a single-stage additive process. Compared to conventional two-stage manufacturing by sintering, this yields improvements in thermal performance and process automation. The final thermal expansion is marginally higher than sintered molybdenum grains due to missing sinter bridges. To account for this effect in upcoming research, molybdenum powder with a smaller particle size could be added to increase the molybdenum percentage and reduce the thermal expansion of the pseudoalloy.

The achieved advancements in process control using machine learning and melt pool size control facilitate the manufacturing of the pseudoalloys. It directly influences the quality of the material deposition. Furthermore, it also allows for processing and qualification of inhomogeneous materials with inconsistent emissivity. Extensively collecting process data via a connected sensor network assisted in identifying irregularities and reducing process uncertainties. Overlaying the process head position with melt pool or temperature data can be used for on- and offline inspection. This creates a visual representation of the process comparable to a digital shadow.

Throughout the process development, the material was able to absorb enough laser energy so that process parameters are found. Statistically designed experiments lead to material and multi-material deposition. By using extensive characterizations of the deposited material via confocal microscopy, micro-sections and x-ray tomography, the main effects and the factor interactions can be modeled.

The results of the characterization using dilatometer experiments reflect the direct influence of the material composition on thermal expansion coefficients. There is still a discrepancy between the thermal expansion coefficients of the YAG structure and the CuPMo pseudoalloy. Nonetheless, it was possible to imprint a comparable YAG-substitute by laser preheating and segmented welding.

As an outlook, it is planned to realize a functional 3D-printed laser using a YAG embedded in the pseudoalloy soon.

Beyond multi-material applications, this pseudoalloy could also be used for customized cooling solutions of high-power integrated circuits and in other specialized heatsink applications.

All in all, this research emphasizes the potential of additive manufacturing for challenging material combinations.

References

1. Corbin, S., Khajepour, A., Toyserkani, E.: Laser Cladding. Boca Raton CRC (2004). ISBN 978-1-4200-3917-7
2. Metal additive manufacturing market 2018 and supplier forecast. Metal Additive Manufacturing Report (2019). https://am-power.de/en/insights/metal-additive-manufacturing-2/. Retrieved 05 Feb 2020
3. Bound metal additive manufacturing market outlook. SmarTech Analysis (2019). https://www.globenewswire.com/NewsRoom/AttachmentNg/d451cf16-bae6-417c-b291-3d93ea34554b. Retrieved 05 Feb 2020
4. Lachmayer, R., Lippert, R.B. (Hrsg.): Additive Manufacturing Quantifiziert: Visionäre Anwendungen und Stand der Technik. Springer Verlag, Deutschland Hannover (2017). ISBN: 978-3-662-54112-8
5. Bernhard, R., Neef P., Wiche, H., Wesling, V., Hoff, C., Hermsdorf, J., Kaierle, S.: Process development for additive multi-material components. Lasers in Manufacturing Conference Munich (2019)
6. P. Neef, R., Bernhard, H., Wiche, V., Wesling, F., Kranert, J., Budde, A., Wienke, J., Neumann, D., Kracht, M., Lammers, H., Ahlers, T., Grabe, K., Rettschlag, Lachmayer, R.: Generatives Fertigen optischer, thermaler und struktureller Komponenten für Lasersysteme. 3. Niedersächsisches Symoposisium Materialtechnik (2019)
7. Bernhard, R., Neef, P., Wiche, H., Wesling, V.: Additive Fertigungvon Kupfer-Molybdän und Eisen-Nickel Werkstoffen mittels Laserauftragschweißen. In: 41. WGF Assistentenseminar (2020)
8. Mahamood, R. M.: Laser Metal Deposition Process of Metals, Alloys, and Composite Materials (2018). Springer International Publishing. ISBN: 978-3-319-64984-9.
9. Gebhardt, A.: Generative Fertigungsverfahren: Additive Manufacturing und 3D Drucken für Prototyping—Tooling—Produktion. Carl Hanser Verlag, Munich (2013)
10. Griffiths, V., et al.: Cost-driven build orientation and bin packing of parts in selective laser melting (SLM). Eur. J. Oper. Res. **273**, 334–352 (2019)
11. Kaliudis Athanassios, Trumpf.com. "LMD reift zum starken generativen Verfahren für industrielle Anwendungen". https://www.trumpf.com/filestorage/TRUMPF_Master/Corporate/Press/Press_releases/2016_17/Laser_Technology/20161115_LMD_at_Formnext/LMD_Technique_EN.jpg. Accessed 10 Sept 2021
12. VDI Gesellschaft Produktion und Logistik: VDI 3405—Additive manufacturing processes, rapid manufacturing—Basics, definitions, processes. In: VDI Handbuch. Deutschland Berlin (2014)

13. Shields, J. A.: Applications of Molybdenum Metal and its Alloys. IMOA (2013). ISBN: 978-1-907470-30

14. Grabe, T., Budde, J., Kranert. F., Wienke, A., Neumann, J., Kracht, D., Lachmayer, R.: "Kühlkörper-Designansatz für einen in AlSi10Mg eingebetteten YAG-Laserkristall" in Konstruktion für die Additive Fertigung 2019. Springer Vieweg, Berlin Heidelberg (2020), pp. 159–175

15. Koen, W.: Middle-Infrared Laser Sources (2016). https://doi.org/10.13140/RG.2.1.3105.2565

16. Hardro, P. J.: Method of Forming a Part Made of a Molybdenum-Copper Composite Materal. United States Patent US7186369 (2007)

17. Rosalie, J.M., Guo, J., Pippan, R., et al.: On nanostructured molybdenum–copper composites produced by high-pressure torsion. J. Mater. Sci. **52**, 9872–9883 (2017)

18. Seiss, M., Mrotzek, T., Dreer, N., Knippscheer, S., Knabl, W.: Molybdenum-copper-composites for the advanced thermal. In: 19th Plansee Seminar (2020)

19. Song, L., Bagavath-Singh, V., Dutta, B., et al.: Control of melt pool temperature and deposition height during direct metal deposition process. Int. J. Adv. Manuf. Technol. **58**, 247–256 (2012). https://doi.org/10.1007/s00170-011-3395-2

20. Davis, T.A., Shin, Y.C.: Vision-based clad height measurement. Mach. Vision Appl. **22**(1), 129–136 (2011). https://doi.org/10.1007/s00138-009-0240-9

21. Bernhard, R., Neef P., Wiche, H., Wesling, V., Hoff, C., Hermsdorf, J., Kaierle, S.: Defect Detection in Additive Manufacturing via a Toolpath Overlayed Meltpool-Temperature Tomography. ICALEO Conference Orlando (2019)

22. Bernhard, R., Neef, P., Wiche, H., Wesling, V., Hoff, C., Hermsdorf, J., Kaierle, S.: Entwicklung einer intelligenten Prozessüberwachung und Regelung zum Laserauftragschweißen von Multimaterial-Verbindungen. Düren, Shaker (2021)

Development of System Technology for Coaxial Laser Material Deposition of Optical, Thermal and Structural Components

Marius Lammers⬤, Alexander Barroi, Jörg Hermsdorf, Stefan Kaierle, and Henning Ahlers

1 Introduction

1.1 Laser Material Deposition for Multi-Material Processing

Laser Material Deposition (LMD) is a manufacturing process for Additive Manufacturing (AM) based on wire and powder deposition materials. The materials to be processed are melted by the laser radiation and deposited accordingly, so that the generation of structures, the coating of surfaces and the repair of components are possible. The use of a coaxial setup of laser beams and deposition material results in the advantage of direction-independent machining and thus the possibility of producing complex structures with reduced handling requirements [1, 2].

M. Lammers (✉) · H. Ahlers
Hochschule Hannover University of Applied Sciences and Arts, Ricklinger Stadtweg 120, 30459 Hannover, Germany
e-mail: m.lammers@lzh.de

H. Ahlers
e-mail: henning.ahlers@hs-hannover.de

M. Lammers · A. Barroi · J. Hermsdorf · S. Kaierle
Laser Zentrum Hannover e.V. (LZH), Hollerithallee 8, 30419 Hannover, Germany
e-mail: a.barroi@lzh.de

J. Hermsdorf
e-mail: j.hermsdorf@lzh.de

S. Kaierle
e-mail: s.kaierle@lzh.de

The process can be used to process many fusible materials in the material classes of metals, ceramics/glass and polymers. Finished components therefore range from optical components such as lenses or fiber components made of glass, thermal structures such as heat sinks made of metal materials with a high thermal conductivity, and mechanical elements made of metal materials that serve to absorb mechanical stresses. This results in a wide range of possible applications for the technology. The LMD process is already being used today for the generation of mechanical metal structures. Typical fields of application are mold and tool making, where structures with complex geometries such as internal cooling channels or undercuts are generated or coatings are applied for wear and corrosion protection. The use of the process for processing glass materials is currently in the development stage and is subject to research. Due to the properties of the process, it has great potential in the field of optics manufacturing, for example beam guiding and shaping components [3, 4].

In order to map the processes and adapt them to the different materials, appropriate system technology is required. These requirements range from specialized laser sources and beam guidance systems to adapted material handling equipment.

1.2   Objectives of this Work

This work has the objective to summarize and describe the following points: Fundamentals of the LMD manufacturing process depending on the materials to be processed, possibilities and restrictions of the process, analysis of the current state of the art and research of the LMD process for the processing of glass fiber as well as metal powder and wire.

Also, this work shall give an overview of required and commercially available system technology, which is necessary for the process. In this context, the characteristics and requirements of the system technology are to be highlighted and foundations for the development of application-specific system technology are to be established.

In addition, a consideration of the application example for the combined processing of glass materials in fiber form as well as metal materials in wire and powder form in a machine environment for the generation of optical, thermal and structural components from the field of laser technology/optics will be carried out. The necessity as well as the focus of an application-specific development of laser system technology for the production of multi-material components by means of laser material deposition will be demonstrated and discussed.

2 Development of Laser System Technology

2.1 Definition and Methodology

The term system technology is widely used to summarize machine and system components for specific applications. As a rule, a combination of hardware and software is required for laser systems (machines that include at least one laser beam source) in order to perform special tasks or to map processes. The term laser system technology thus includes beam sources, optical elements, mechanical and control components, peripherals as well as their interconnection and application in material processing, taking a holistic view of the overall system. Furthermore, the term system technology describes the linking of several technical components to form an overall system that meets defined requirements, such as the mapping of a production or machining process. The development of system technology is referred to as systems engineering. It attempts to take a holistic approach to the design of complex overall systems rather than focusing on the development of subsystems. Therefore, the development of system technology, in contrast to the development of isolated products, requires the consideration of all components contained in the system (Fig. 1) [5].

The V-model of VDI 2206, originally intended to support the development of highly complex cyber-physical mechatronic systems [6], can be applied during the development of opto-mechatronic systems including the associated software [7–10]. This methodical approach has a similar sequential procedure as VDI 2221 "Design of technical products and systems—Model of product design" [11], but allows domain-specific design phases from the areas of mechanics, electrics, information technology and optics to run in parallel, so that development takes place under constant consideration of the overall system (Fig. 2). The basis for this form of development methodology is interdisciplinary (vertical integrity) as well as cooperation between different age, experience and hierarchy levels (horizontal integrity) [5].
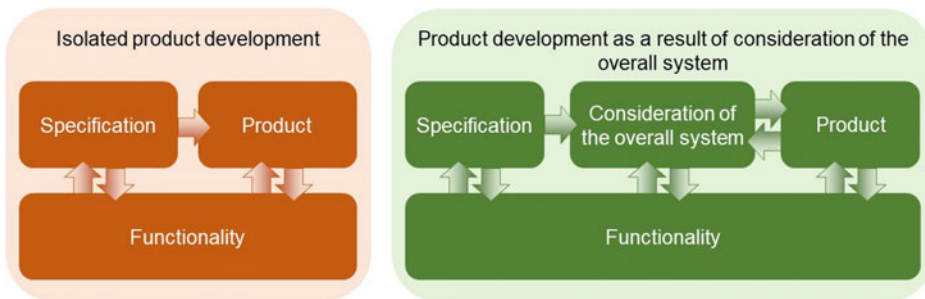
Fig. 1 Procedure model for the development of isolated products (left) and for the development of system technology (right), according to [5]
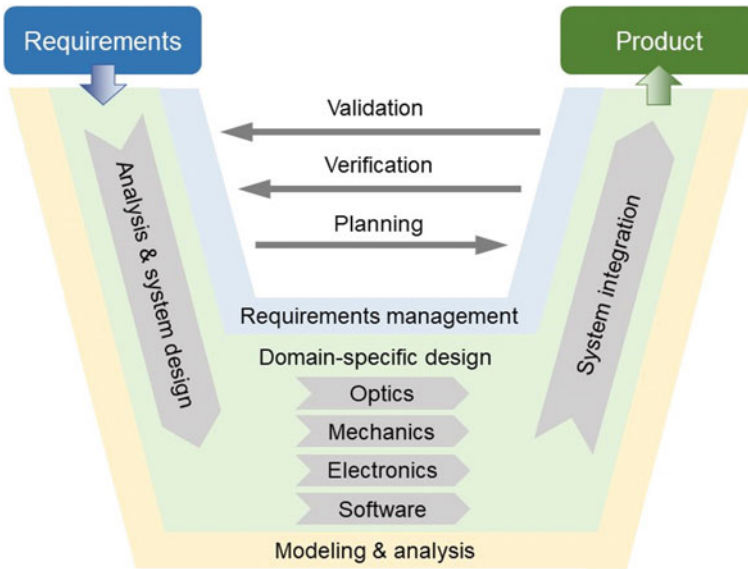
Fig. 2 V-model according to VDI 2206 modified for application on the development process of opto-mechatronic systems, based on [8, 9]

2.2   Target Criteria for the Development of System Technology

Machines and plants are always an overall system composed of components, consisting of hardware and software in the form of mechanics, electrical and fluid engineering, information technology and other elements. Composite systems therefore have interfaces between the individual elements. Target criteria for systems engineering as a whole therefore include criteria for individual elements, interfaces within the system, and the quality or performance of the entire system.

A good system technology is specially tailored to the respective application for which it is to be used and maps the requirements set by the application. The definition of requirements lays the foundation for the system technology to be developed and fundamentally determines its quality. In addition, a good system technology enables a repeatability of the process represented by it, is robust against disturbing influences and thus defines the quality of the products of the process. For the operator, good system technology is safe, ergonomic and easy to use. Furthermore, good system technology is characterized by high efficiency in terms of costs, energy and space requirements, as well as high availability and reasonable maintenance requirements and good serviceability. Last but not least, good system technology has a visual appearance that appeals to the target group for marketing reasons without being wasteful.

When developing system technology, the entire product life cycle must be taken into account: In addition to the intended operation, construction, transport and commissioning as well as the installation, maintenance and disposal must also be considered. The design and dimensioning of individual elements must be carried out in accordance with the intended service life of the system technology in order to ensure safe operation, without being wasteful with resources. An evaluation of system technology can be realized in the course of development by means of a utility value analysis. In this process, evaluation criteria are defined on the basis of which one or more concepts/designs are evaluated. The analysis results in the so-called utility value, which enables a qualitative comparison of several variants with each other as well as a rough quantitative assessment of the quality of the respective concept. [12]

Every machine used in industry serves a purpose. Accordingly, a corresponding manufacturing process is mapped on production systems for laser material processing. The quality of the process or the machine can be determined via a process or machine capability study [13]. The goal of a process or machine capability analysis is to determine the likelihood that a process or machine will produce results that meet defined specifications. Possible influencing factors on process or machine capability for laser additive manufacturing are shown in Fig. 3.
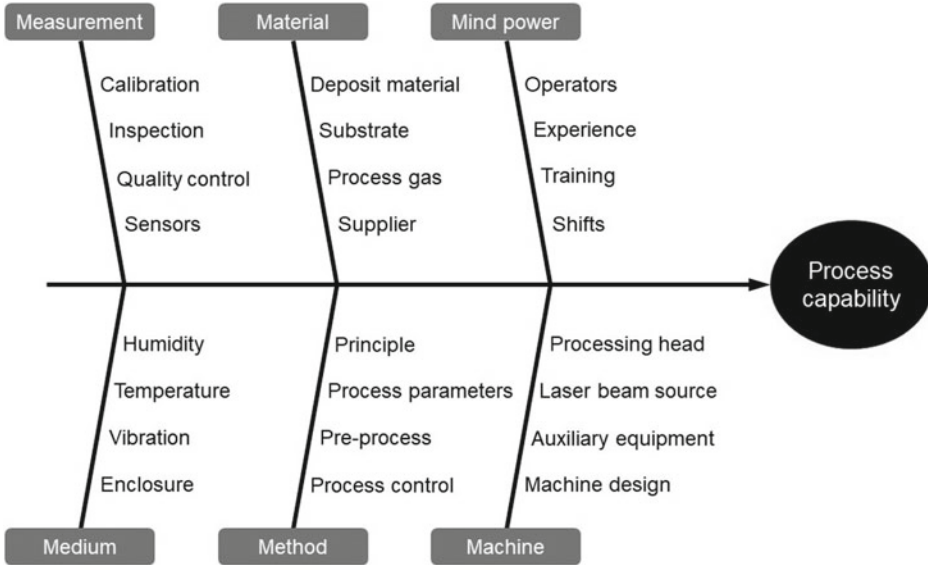
Fig. 3 Ishikawa-diagram: influencing factors on process capability for laser additive manufacturing

3   Laser Material Deposition for Optical, Thermal and Structural Components

3.1   Principle of Laser Radiation and Material Interaction

When a laser beam hits a medium (solid, liquid or gaseous), it interacts with it. Part of the incident laser radiation is reflected, part is absorbed by the medium and converted into thermal energy, and another part may radiate through the medium (Fig. 4). In total, the energy of the three parts corresponds to that of the entire incident radiation. [14]

The portion of reflected radiation can be diffuse, directional, or a mixture of the two. The same applies to the transmitted radiation. During the transition from one medium to another medium with a different refractive index, the transmitted radiation is deflected or "refracted". The absorbed (at the surface as well as inside the medium) part of the radiation produces various effects on the workpiece surface of fusible materials depending on the radiation intensity (Fig. 5). [15, 16]

In LMD, the aim is to achieve a molten pool and to avoid sublimation of filler metal and substrate material as far as possible. A decisive factor is the so-called degree of coupling. This describes the percentage of the incident laser radiation that is absorbed by the material, i.e. converted into thermal energy. The degree of coupling is dependent on the following properties (Table 1) [16, 17].

There are three possible principles of Direct Energy Deposition (DED):

(1) A melt pool on the substrate is generated by laser radiation and the deposition material is fed as a solid into the melt pool. The deposition material melts when entering the melt pool and is used for build-up. [18, 19]
(2) The deposition material is melted by laser radiation above the substrate and applied onto the solid surface. [20, 21]
(3) A hybrid of 1 and 2, where a melt pool is generated on the substrate surface and the deposition material is melted above the melt pool and fed into it. [22]

Fig. 4 Interaction between laser radiation and a medium [14]
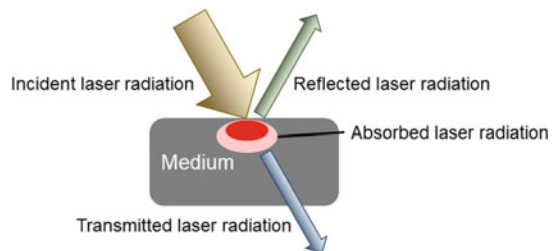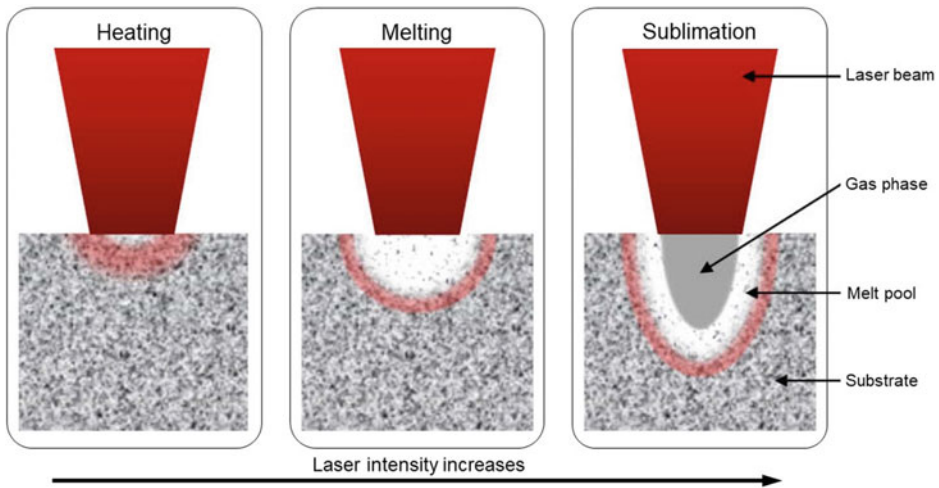
Fig. 5 Interaction between laser radiation and workpiece surface: degrees of coupling [16]

Table 1 Factors influencing the degree of laser coupling

Workpiece properties	Laser parameters
Material	Wavelength
Surface roughness	Intensity (dependent on spot size and power)
Temperature	Angle of incidence, polarization

3.2 Possible Deposition Materials

With regard to the deposition materials used in the additive process, a distinction can be made in three areas: Firstly, the material; by means of Laser Material Deposition, almost all fusible materials can be processed. These include metal materials such as nickel, titanium, aluminum, magnesium and iron-based alloys as standard, but metallic materials based on cobalt or copper can also be processed. For glass materials, for example, quartz glass can be processed, and for polymers, thermoplastics accordingly. Secondly, the deposition materials can be differentiated in terms of their shape: Here, powder and wire-shaped materials of the materials mentioned are used in build-up welding. Thirdly, it is also possible to subdivide into the different sizes of the respective weld metal: Typical diameters of the weld material in laser glass deposition are in the range of 0.1 to 0.5 mm for glass fibers and in the range of 0.1 to 1.6 mm for metal materials. In the case of powder, grain size distributions in the range 20 to 150 μm are generally used. [1, 23–30]

4 Laser System Technology for Multi Material Laser Material Deposition

4.1 Minimum Required Components of the System

A machine for laser material deposition consists of at least the following systems and components (Fig. 6):

(1) The laser system technology, consisting of a laser beam source, beam guidance and shaping, generates the laser radiation required for melting the deposition material, shapes the beam and guides it into the process zone.
(2) The deposition material handling system includes the material storage unit and a conveyor unit to feed the deposition material to the process zone.
(3) The handling system is used to move the substrate or the workpiece to be coated relative to the laser system technology and deposition material handling, whereby both the substrate and the other systems can be moved, depending on the embodiment.

In order to be able to map the requirements for the overall system, partial functions of a system for the laser material deposition process are often bundled in the form of so-called processing heads to precisely merge the deposition material and the laser radiation into the process zone: These comprise parts of the overall system. In LMD systems, beam shaping and parts of the beam guidance as well as elements of the material feed are usually integrated into a processing head. Since different solutions vary greatly due to their adaptation to specific applications, the other components of an overall system can also be integrated in the processing head. An example of this is the integration of laser beam sources directly in the processing head [31].

Fig. 6 Overview: minimum required system technology for laser material deposition (lateral process setup)
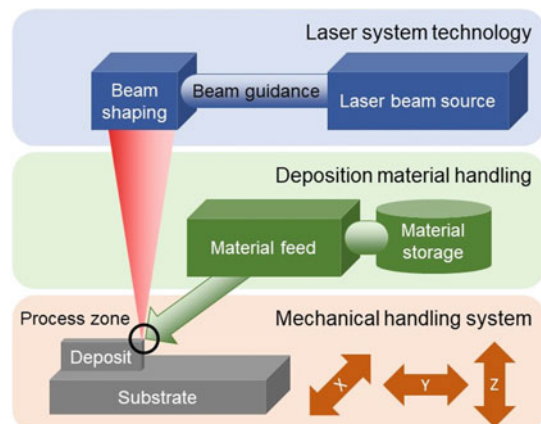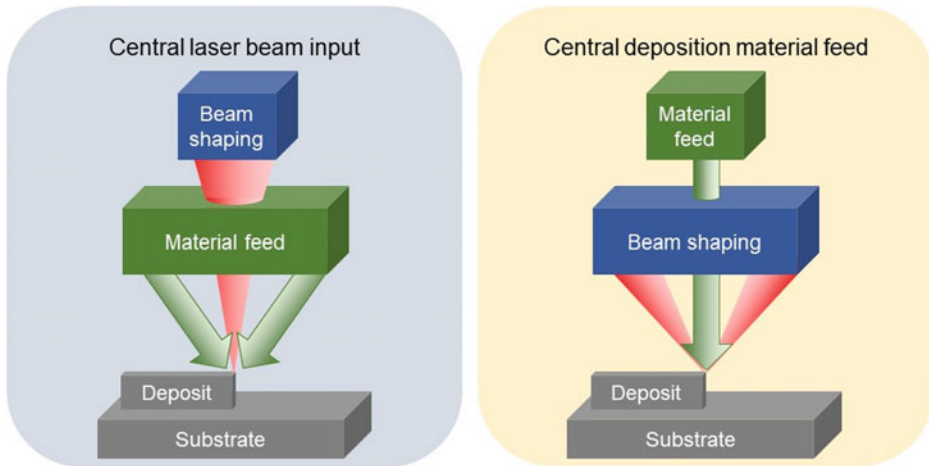
Fig. 7 Basic principles for coaxial laser material deposition heads: central laser beam input (left) and central deposition material feed (right)

4.2 Types of Coaxial Systems Technology

The design of beam guidance and feeding of the deposition material enables the energy input required for melting the weld metal to be more homogeneous. This means that the welding result is independent of the welding direction, which in turn offers advantages for handling in the process. However, the advantages of direction-independent machining are also accompanied by a number of challenges. First and foremost is the more complex design of the system technology, which will be discussed in the following.

In coaxial laser material deposition, the deposition material is fed in coaxially with the laser beam. Either the laser radiation or the filler material can be introduced centrally, while the other is fed from the outside (Fig. 7). With a central laser beam input and coaxial material feed, there must be room in the processing head for the beam path. With central material feed, there must be room for the material feed path. The coaxial material feed (central laser beam input) is typically used for powders, while the central material feed (coaxial laser beam input) is usually used for wire-shaped materials.

4.3 Laser Sources, Guidance and Shaping

4.3.1 Laser Sources

In laser material deposition, the laser source is primarily selected depending on the materials to be processed and the structure sizes to be manufactured. The selection of the materials to be processed fundamentally determines the possible laser wavelengths for

which the system technology must be designed. Solid-state lasers are typically used for laser cladding of metal materials. Laser sources in the near-infrared wavelength range around 1 µm are frequently used. With this wavelength, iron-based materials (steels), for example, can be processed very well, since they have a sufficiently high degree of coupling at this wavelength. For additive processing of glass materials or metals such as gold, silver or copper, beam sources with a wavelength in the 1 µm range are generally not suitable, since a large proportion of the radiation is transmitted in the case of glass materials and reflected in the case of precious metals. As a result, a comparatively small proportion of the incident laser radiation is converted into thermal energy in the material, not allowing an efficient process. Gas lasers in the mid-infrared range 5 µm (CO laser) to 10.6 µm (CO_2 laser) are therefore usually used for processing glass materials. For copper, on the other hand, solid-state laser sources with visible radiation in the green (approx. 530 nm) and blue (approx. 450 nm) exhibit much better material coupling. [16, 17, 23–25, 32, 33]

The minimal generated structure sizes correlate directly with the size of the projected laser spot on the workpiece surface. This in turn is significantly influenced by the beam quality of the laser beam source as well as by the properties of the optical systems used. For solid-state laser sources, the following variants are available: diode, disk and fiber lasers, which have different beam properties: Fiber lasers can achieve the best beam quality; accordingly, the smallest spots on the workpiece surface can be realized with them. Diode lasers have the lowest beam quality, while disk lasers are in between. The deposition rates achievable in the process are also fundamentally determined by the laser beam source used. The most important factor here (besides the wavelength) is the power of the laser beam source, followed by the size of the laser spot on the workpiece surface. For additive manufacturing of metal materials, laser power of up to 20 kW in continuous wave mode is usually used. For filigree components, on the other hand, pulsed beam sources are also used. [34]

4.3.2 Coaxial Beam Guidance with Central Material Feed

In order to realize a coaxial beam guidance around a central material feed, there are two different possibilities (Fig. 8):

First, the laser radiation from a single beam source can be used. To achieve coaxiality, the beam must be split by a beam splitter and fed to the process zone. The beam splitter can be either reflective or transmissive or diffractive. Typically, these systems generate either three to four individual beams that converge at a point in the process zone, or a circular ring-shaped beam is generated in the center of which the material feed is located. Further information on this topic (beam shaping) is given in Sect. 4.3.3. The design with the beam splitter has the advantage that one commercially available laser beam source is required per system, which can usually be procured quickly and comparatively inexpensively. A disadvantage, however, is the complex beam splitting and guiding. [28, 35–39]
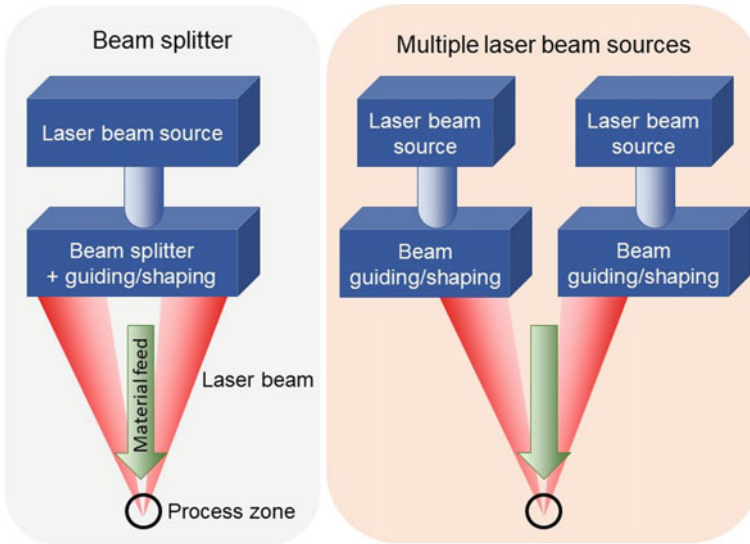
Fig. 8 Laser system technology for coaxial laser material deposition with central deposition material feed using a beam splitter (left) or multiple laser beam sources (right)

Also, when using a beam splitter, in some systems the material feed path is formed like an S-curve. If the radii of this curve are too small, the wire can be plastically deformed and is therefore not fed straight into the process zone. As a result, the positioning of the weld metal relative to the incident laser radiation is no longer centric and the directional independence of the coaxial process is lost. [40]

Instead of splitting a single beam, several beam sources can be used which are aligned such that the emitted individual beams coaxially surround the central material feed and converge at one point in the process zone. This variant offers the advantages that the material feed is straight and comparatively short, which leads to a more direct feed. In addition, the beams can be switched individually, so that different or dynamic intensity distributions are possible. [31, 41]

In general, the design of laser beam guidance depends primarily on the wavelength of the laser radiation used. Almost all typically used wavelengths can be guided reflectively via mirrors in a comparatively simple way, whereas transmissive guidance requires more effort for certain wavelengths: Radiation emitted by solid-state lasers, for example, can be guided very well by fibers and transmissive optics (such as lenses) made of inexpensive glass materials, while the radiation from gas lasers can be guided transmissively only via expensive special materials such as zinc selenide or germanium. For this reason, the radiation from gas lasers is often guided reflectively via metal mirrors (e.g. made of copper).

4.3.3 Beam Shaping

The beam profile of the laser spot in the process zone can be circular or annular by using an appropriate beam shaping (Fig. 9). In the case of the circular beam profile, there can also be different intensity distributions within the circular spot: for example, the intensity can be Gaussian or normally distributed. The variant with the normally distributed intensity profile is also referred to as a Top Hat profile. [42, 43]

In addition to the total incident laser power, a descriptive key figure for beam profiles is the beam diameter, which describes the outer diameter of the spot. With an ideal normally distributed radiation intensity (Top Hat) the determination of the outer diameter is trivial. For Gaussian distributions, however, this is not the case, so that certain parameters have to be used. One of these parameters is the 1/e2-intensity-threshold, which was historically defined for the description of Gaussian distributed circular beam distributions and is still used today. The diameter according to this method describes a circular area containing 86.5% of the total incident laser power. Another descriptive figure is called Full Width at Half Maximum (FWHM). This index describes the width of a laser spot where the boundaries correspond to half the maximum intensity of the Gaussian profile. Accordingly, the diameter with the width corresponding to FWHM contains approximately 76% of the total incident laser power. For ring profiles, the inner and outer diameters of the spot are used as parameters. According to ISO 11146, the beam diameter is defined by so-called moments. The characteristic D4σ (second moment width) is calculated numerically and is also applicable for non-Gaussian and non-circular intensity profiles. For an ideal Gaussian distributed beam, the characteristic values $1/e^2$ and D4σ are identical. [44–46]

If several individual beams are used, as is the case with beam splitter systems or systems with several beam sources, further shapes can be created by superimposing several
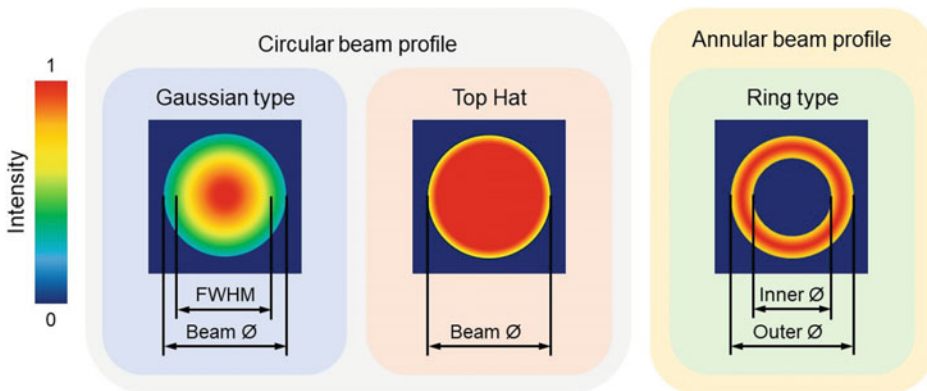
Fig. 9 Typical beam profiles used for LMD processes: Gaussian (left), Top hat (middle) and Ring type (right)

spots, or the beam profile can deviate from a perfectly round circle. Special shapes represent elliptical or rectangular beam profiles, which are sometimes used in powder LMD processes [47].

4.4 Deposition Material Handling

4.4.1 Types of Deposition Material Feed

Figure 10 shows the three types of material feed in LMD: Central single channel feed, coaxial multiple channel feed and coaxial annular gap feed.

Round nozzle cross sections (Fig. 10 left) are typically used for central single channel feed. This has the advantage of being simple and therefore inexpensive to manufacture since only one feed channel is required. Furthermore, very small diameters can be realized, resulting in small powder-gas flow diameters during coaxial powder build-up welding, which increases powder efficiency [48].

Round multiple nozzles (Fig. 10 middle) are also typically used with a centered laser beam delivery and coaxial multi-channel delivery for the material. These can be manufactured cost-effectively and have advantages when the system technology is used in a constrained position. In addition, only one laser beam is needed, which can be realized via off-the-shelf components. The disadvantage is that this results in larger powder-gas flow diameters, which leads to poorer powder efficiency. [49]

Annular gap nozzles with central delivery of the laser beam (Fig. 10 right) also have the advantage that only one laser beam is required. This results in a clear cost advantage for the beam guidance. The annular form of powder supply has a disadvantageous effect on the achievable minimum powder focus diameters. In addition, this variant allows smaller deviations in the welding position (in relation to the optimum flat position). [49]

Fig. 10 Nozzle design for coaxial laser material deposition and typical applications: central single channel feed for use of wire or powder (left), coaxial multiple channel feed (middle) and coaxial annular gap feed (right), both used for powder only

Combinations of the three feed types shown in Fig. 10 are also possible: For example a central feed for the wire-shaped material together with a coaxial annular gap nozzle enclosing it and laser beam guidance introduced coaxially from the outside [41].

In addition to the supply of laser radiation and the deposition material, a process gas is usually fed to the process zone. This can be a protective gas which prevents oxidation of the deposited material when processing materials with an affinity for oxygen. Alternatively, an active gas can be used, for example, to reduce spatter or to cause targeted oxidation.

When processing glass filaments, they are often coated with a polymer coating (e.g. acrylate). This coating enables better handling of the glass fibers during production and later use, as they do not break as easily as they do without the coating. During the deposition welding of these coated glass fibers, the coating must be burned off completely before entering the melt pool to avoid contamination. For this reason, air or oxygen is used as the process gas in the Laser Glass Deposition process. [24, 50]

In the case of coaxial powder nozzles, an additional so-called shape-gas stream can be applied, in order to compress the gas-powder stream and reduce its diameter [48].

4.4.2 Handling of Wire Materials

The wire-shaped material is conveyed from the material storage, usually a spool, to the processing head by means of roller drives for both metal and glass materials, similar to the fusion welding process [51, 52]. In wire conveying technology, roller drives with a total of two or four rollers are typically used, whereby the material to be conveyed (metal wire, polymer filament or glass fiber) is conveyed in each case by a pair of rollers pressed together (Fig. 11). If all rollers are rotationally driven, which is usually done by an electric motor, the system is referred to as a 2-roller or 4-roller drive (a roller pair consists of two driven rollers). Alternatively, only one roller of a pair of rollers can be driven and the designation 1 + 1- or 2 + 2-roller drive is used (a pair of conveyor rollers consists of a drive roller and a pressure roller). [52, 53]

The design of the rollers is adapted to the material to be conveyed: For steel materials, one roller with a V-groove or trapezoidal groove and one roller with a flat surface are usually used per roller pair, with both rollers made of steel. For softer materials such as aluminum, one roller with a semicircular groove corresponding to the wire diameter and
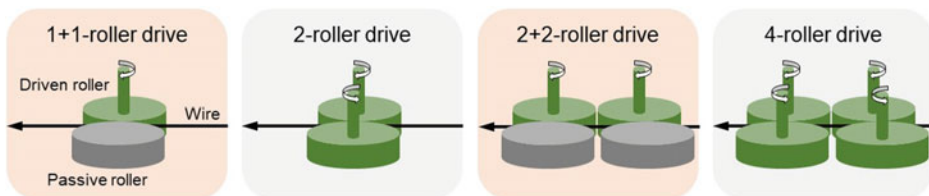
Fig. 11 Roller drive setups for conveying and feeding wire-shaped materials

one roller with a flat surface are used. To prevent the rollers from slipping, the groove can also be textured [53–55]. Glass fibers are usually conveyed in additive manufacturing using a 1 + 1 roller conveyor with rollers made of an elastic material [51, 56, 57].

In the case of metal wires, the conveying path between the wire spool, the roller drive and the nozzle takes place via cores, which can consist of a metal spiral or a polymer hose. Typical core materials are steel, brass, polyamide (PA), and polytetrafluoroethylene (PTFE). For metal materials, the tribological properties when conveying through various conveyor sections are sufficiently well known. When larger conveying distances in excess of 5 m are present, the conveying of metal wires typically requires a push–pull system in which one roller drive is located directly at the weld metal storage and another roller drive is located near the processing head. Another solution for reducing friction in long conveying distances is the use of roller hoses. [53, 58–60]

In order to achieve process control or regulation during wire feeding, force-controlled wire feeding systems are used. The actual feed device is located on the carriage of a linear guide, which allows a degree of freedom in the direction of the feed. The core is fixed at a holder, which is not on the carriage of the linear guide, so that the feeder pushes away from the core during feeding. To absorb the pushing force, a load cell or force sensor is mounted between the core holder and the movable carriage on which the feed unit is mounted. During conveying, this can be used to measure the corresponding force that the feed unit has to overcome in order to convey the wire-shaped material (Fig. 12). [61]

Since the wire-shaped material can have a curvature, which can have a negative effect on the process because the weld metal cannot be introduced exactly into the process zone, wire straightening units are used in laser wire additive manufacturing. Straightening units are usually used with metal wires, since with these the bending radius, which leads to plastic deformation, is often undershot during spooling. When processing glass materials, on the other hand, straightening units are not required due to the mechanical properties of
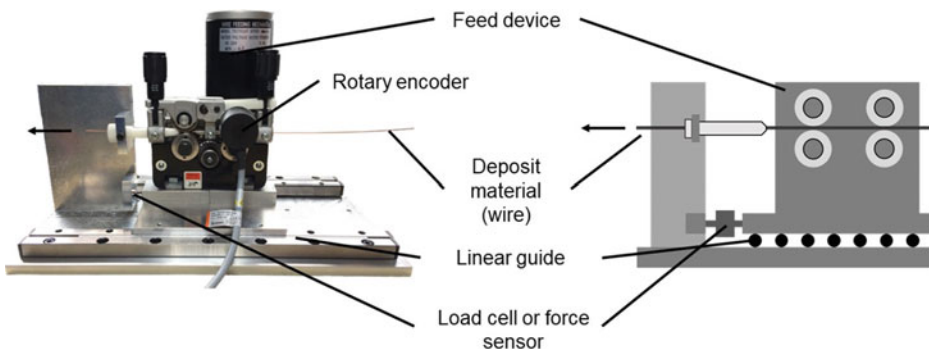
Fig. 12 Closed loop forced-controlled wire feed: setup used for trials (left) and principle (right) [40]
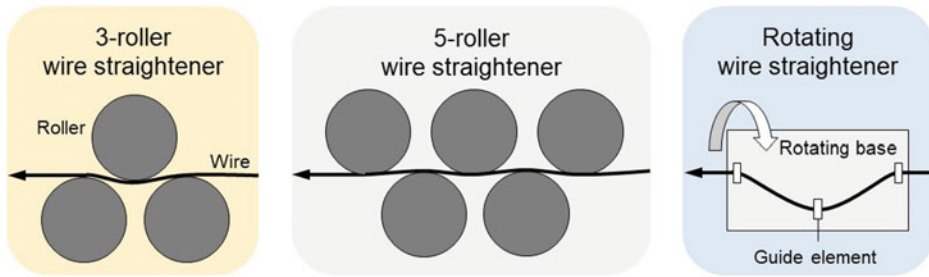
Fig. 13 Typical setups used for wire straightening: 3-/5-roller wire straightener (left/middle) and rotating wire straightener (right)

glass: The glass fibers are elastically deformed by handling or, if the radii are too small, the fibers break, but plastic deformation does not usually occur.

Roller straightening units or rotating straightening units are used as straightening units (Fig. 13). The roller straightening units can straighten the wire in only one direction at a time, so that two straightening units connected in series are required for straightening in two axes. The advantages of roller straightening units are the simple and compact design, whereby variants with 3 rollers are correspondingly more compact than 5-roller systems. The advantage of rotating straightening units is the ability to straighten very thin wires (diameter less than 100 μm). The disadvantage is the need for a drive and a bearing for the rotation. Rotating straightening units are currently commercially available only for discontinuous operation (spool to spool or wire sections), since continuous operation causes problems with regard to torsion. However, initial trials with an alternating rotating straightening unit for microwires show great potential. [62]

4.4.3 Handling of Powder Materials

The powder handling system has the task of storing, conveying, dosing and feeding the powder to the process.

For the storage of the powder material, powder containers are used, which can be closed gas-tight. The powder containers usually have funnel-shaped connections on the bottom, to enable the powder flow out of the container due to gravity. When storing powder, clumping due to moisture must be prevented. In larger or higher powder containers clumping can also occur due to the powders own weight. This solidification is avoided by relief elements which are inserted into the container. In addition, fire and explosion protection must be ensured when handling powder materials with an affinity for oxygen (e.g. certain titanium or magnesium alloys). In the first place, explosive atmospheres must be avoided by the use of inert gas. As a second measure, effective ignition sources are to be avoided, e.g. by grounding all components that could be statically charged and are prone to sparking. The third measure is to limit the extent of possible damage, e.g., by
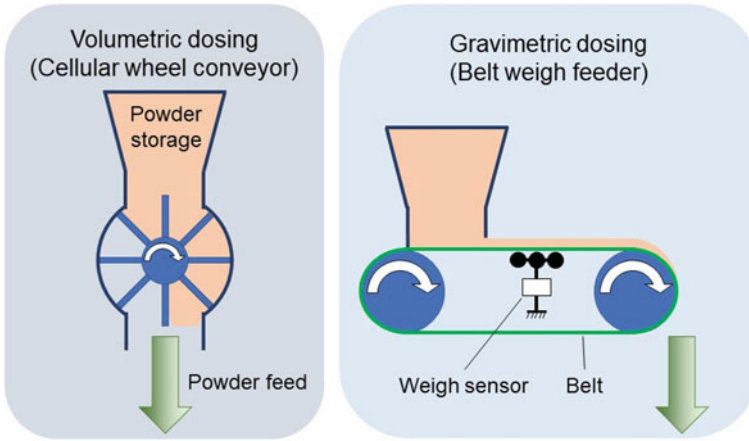
Fig. 14 Examples for volumetric dosing (left) and gravimetric dosing (right)

personal protective equipment, fire doors or extinguishing systems. Any emissions and the toxicity of certain powder materials must also be considered. [63–66]

The powder is conveyed from the powder container to the process head via a hose. In some cases, the complete system is also referred to as the powder conveyor, which comprises one or more powder containers and the conveying equipment including the control system. Dosing in additive manufacturing is often volume-based, since this principle is comparatively simple and therefore cost-effective. The volume is limited by individual areas or chambers, as for example with the so-called chamber feeder or with disc feeders. Due to the principle, the metering has a pulsation that varies in intensity depending on the respective individual or chamber volume. As an alternative to volume-based metering, gravimetric metering systems are used in which the weight of the material conveyed is measured and controlled (Fig. 14). One example of these systems is the so-called belt weigh feeder. [63, 67, 68]

To convey the powder through the hose a gas stream is used. For this gas-stream, inert gases such as argon are typically used. Conveying is based almost exclusively on the principle of pneumatic flight conveying. This principle is primarily characterized by the high flexibility of the system, e.g. with varying delivery rates. In addition, it can be used well for long conveying distances and requires only simple components which need little maintenance. [63, 68, 69]

4.4.4 Automatic Deposition Material Changeover

In hybrid processing of wire and powder materials, three scenarios of a material change are possible:

- Change from wire material A to wire material B [41, 70]

- Change from powder material A to powder material B [41, 63]
- Change from wire material to powder material or vice versa [31, 41].

The material changes considered refer to the use of a processing head. An alternative would be a change to a different processing head, e.g. when changing from wire to powder and vice versa. In addition to a material change, some systems can also process two different (wire and powder) materials simultaneously to alloy in-situ or produce graded components. In this case, the feeding of the different materials is realized via separate feeders: For example, the wire can be fed centrally, while the powder is introduced simultaneously via a coaxial annular gap nozzle. [31, 41]

Commercially available systems for changing the deposition material in additive manufacturing exclusively provide for the use of metal materials in wire or powder form. Systems for changing from metal to glass materials are not available on the market.

4.5 Mechanical Handling Systems

The mechanical handling systems used in LMD have the task of moving the process head relative to the workpiece. The movements take place in linear or rotational axes. The drives used are mainly electric motors, rarely hydraulic systems. A corresponding control system (Numerical Control, NC) is required for the movement. In addition, measuring systems, gears and brakes are often integrated in the mechanical handling system. [71, 72]

Typical systems for LMD processes are translational axis systems and articulated robots. For axis systems, 3-axis systems (3 linear axes: XYZ) or 5-axis systems (usually 3 linear axes XYZ + two rotary axes) are often used. Articulated arm robots usually have 6 rotary axes. In order to always be able to weld in the tub position, rotary/swivel units are used for handling the substrates or components in addition to the articulated arm robot, which usually handles the processing head. Combinations of linear and jointed-arm robots are also used in laser build-up welding, such as moving the whole articulated arm robot on a linear system. Special shapes such as parallel kinematics or other robot shapes are used less frequently. Mobile systems are used for large workpieces that are difficult to transport and handle. [73]

4.6 Commercially Available Processing Heads

Processing heads available on the market for laser wire additive manufacturing are shown in Fig. 15. These are intended exclusively for processing metal materials. The maximum usable laser power ranges from 1 kW to a maximum of 6 kW. Solid-state lasers at a wavelength around 1 µm are used as beam sources. The ProFocus system from Oscar PLT has six diode laser beam sources built directly into the head, while the other systems

	LZH CoaxKopf Mk II	COAXwire	COAXwire mini	N/A	CoaxPrinter	ProFocus	M450
Trade name	LZH CoaxKopf Mk II	COAXwire	COAXwire mini	N/A	CoaxPrinter	ProFocus	M450
Manufacturer	Laser Zentrum Hannover	Fraunhofer IWS	Fraunhofer IWS	Fraunhofer ILT	Precitec	Oscar PLT	Meltio
Image							
Material feed	Central	Central	Central	Central	Central	Central	Central
Priciple	Reflective beam splitter	Beam splitter	Beam splitter	Beam splitter, Reflective optics	Beam splitter, Axicon based	Multiple direct diode beam sources	Multiple fiber coupled beam sources
Number of beams	4	3	3	1 (ring shaped)	1 (ring shaped)	6	6
Maximum Laserpower	4 kW	4 kW	1 kW	N/A	6 kW	1 kW	1,2 kW
Wavelength range	800 nm – 1,100 nm	890 nm – 1,100 nm	450 nm - 550 nm 890 nm – 1,100 nm	N/A	900 nm – 1,080 nm	N/A	976 nm
Processible materials	Metals (e.g. 1.4718, 100Cr6, Ti64)	Metals	Metals	Metals (e.g. Ti6242)	Metals	Metals	Metals (e.g. steel, Ti64, In718)
Material shape	Wire	Wire	Wire	Wire	Wire	Wire, powder	Wire & powder simultanously
Wire diameter	0,5 mm – 1,6 mm	0,4 mm – 1,6 mm	0,1 mm – 0,6 mm	N/A	1,0 mm – 1,6 mm	0,8 mm – 1,2 mm	0,8 mm – 1,2 mm
Weigth	5 kg	13 kg	10 kg	5 kg	12 kg	13 kg	N/A
Other	Hot wire	Integrated collision protection, hot Wire	N/A	N/A	N/A	Hot wire	Hot wire, automatic wire changing

Fig. 15 Overview: commercially available coaxial welding heads for wire-based laser material deposition, specifications of the respective manufacturer [30, 31, 35–41]

use external beam sources. The special feature of the M450 system from Meltio is that up to 6 individual diode laser beam sources are connected to the system via their own optical fiber, each of them emits one of the 6 beams fed coaxially to the material into the process zone. The other processing heads use the laser radiation of a single beam source. The beam is either split and deflected to the common process zone accordingly and in some cases the beam is formed to a ring profile. This is done to be able to insert the material coaxially in the center of the processing zone. The wire diameter is typically in the range 0.4–1.6 mm. An exception is the Fraunhofer IWS processing head COAXwire mini, which can process wire diameters in the range of 0.1–0.6 mm. Special features are the systems from Oscar PLT and Meltio, which, in addition to the use of wire-shaped weld metal, can also process powder as a build-up material. Other additional functions integrated into the heads include the use of hot wire as well as an integrated collision protection with the Fraunhofer IWS COAXwire. [30, 31, 35–41]

Figure 16 shows commercially available processing heads for powder build-up welding. Most systems use a central supply of the laser radiation, while the powdered weld metal is supplied coaxially from the outside. In these systems, beam sources with different wavelengths (solid-state lasers with approx. 1 μm wavelength up to CO_2 lasers with 10.6 μm wavelength) can generally be used. Only metal alloys are used as welding material. Typically, spherical metal powders with a powder particle size distribution of 20–150 μm are used. The diameter of the powder-gas flow is between 0.3 and 3 mm for the heads. Structure sizes or wall thicknesses that can be produced vary from 0.1 to 12 mm, depending on the system. The given powder efficiency reads up to 98% at a seam width of 3 mm. The processing heads from Oscar PLT and Meltio are hybrid systems that can process deposition material in both powder and wire form. [31, 41, 74–77]

5   Laser Material Deposition Processing Head for Glass and Metal Materials

5.1   Objective and Principle

Within the mGROTESK subproject, the system technology for additive processing of integrated laser optics is to be developed. The work objective fundamentally involves the development of system technology for additive manufacturing of optical, thermal and structural components. The machine should enable the manufacturing of integrated optical parts in a single machine environment. For this purpose, additive manufacturing processes must be combined within the machine environment in order to generate, for example, structural and thermal functional elements of the component from a metal material. Furthermore, it should be possible to manufacture the optical elements from polymers or glass materials in the same environment. The materials used can be in powder form, but also as wire (metal) or fiber (glass). The focus is on the development of a machine head

Trade name	COAX-40/50-S/F	COAXn	3-JET-SO12/16-S/F	HIGHNO	YC30 | YC52	ProFocus	M450
Manufacturer	Fraunhofer ILT	Fraunhofer IWS	Fraunhofer ILT	Harald Dickler	Precitec	Oscar PLT	Meltio
Material feed	Coaxial annular gap	Coaxial annular gap/coaxial multiple channel	coaxial multiple channel	Coaxial annular gap/coaxial multiple channel	Coaxial annular gap/coaxial multiple channel	Central single channel	Central annular gap
Maximum Laserpower	5 kW	10 kW	5 kW	20 kW	6 kW	1 kW	1,2 kW
Wavelength range	Solid state, diode, CO_2-laser	Solid state and CO_2-laser	Solid state, diode, CO_2-laser	Solid state and gas laser	Solid state laser	N/A	976 nm
Processible materials	Metals	Metals	Metals	Metals	Metals	Metals	Metals
Material shape	Powder	Powder	Powder	Powder	Powder	Wire, powder	Wire & powder simultanously
Powder distribution	20 μm - 100 μm	20μm - 125 μm	20 μm - 100 μm	20 μm - 100 μm		45 μm - 150 μm	
Powder-Gas-Diameter	0,3 mm - 1,5 mm	0,9 mm bis 3 mm	1 mm - 3,0 mm	1,8 mm - 2,5 mm	0,7 mm - 2 mm		
Seam width	0,1 mm - 5 mm		1 mm - 6 mm	1 mm - 12 mm	Up to 6 mm		
Weigth	3 kg	3 kg	3 kg	1 kg	3,5 kg - 5,5 kg	13 kg	
Powder efficiency	Max. 98% @ 3mm seam width	Max. 95% @ 3mm seam width	Max. 95% @ 5 mm seam width	Max. 98% @ 3mm seam width			85%
Other		Mixing of up to 4 different powders				Hot wire	Hot wire, automatic wire changing

Fig. 16 Overview: commercially available coaxial welding heads for powder-based laser material deposition, specifications of the respective manufacturer [31, 41, 74–77]

Fig. 17 Principle of the developed multi-wavelength laser deposition head [28]
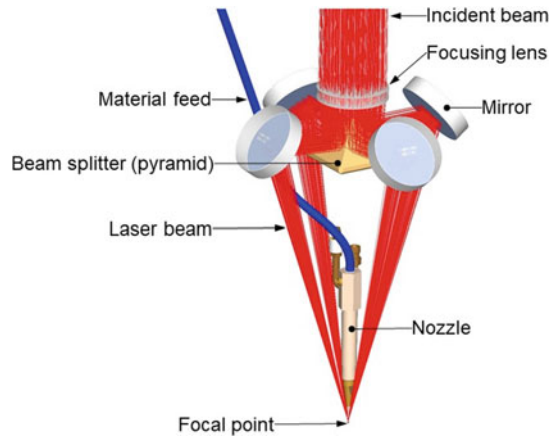
that maps the corresponding processes and enables processing of the selected application materials, metal and glass, in powder and wire/fiber form. The required deposition handling technology for the use of the machine head is also being developed as part of this project. Figure 17 shows the working principle of the developed processing head.

The central element of the processing head is a beam splitter in the form of a four-sided pyramid with a broadband reflective coating. This beam splitter divides a converging laser beam into four partial beams. Each four beams are deflected by a mirror and thus meet below the processing head at a common focal point. The reflective beam guiding elements allow a wide range of laser wavelengths to be used. For example, the system technology for processing metal materials can be operated with a laser wavelength in the 1 μm range, while a CO_2 laser with a wavelength of 10.6 μm is used for processing glass. Also, a CO laser with a wavelength of approx. 5 μm can be implemented. Due to the design of the processing head, the weld metal can be fed between the partial beams and is introduced coaxially and centrically to the beams into the common focal point of the partial beams. This permits a direction-independent welding. The feed of the respective weld material follows an S-shaped curve.

An overview of the system technology for processing powder and wire glass and metal materials is shown in Fig. 18. A system is shown, which can switch between a total of four different materials: Two materials are in powder form, the other two in wire form. The materials used are metals for the powder and glass materials or metals for the wires.

Switching between wires is done by retracting the unused wire to above the y-piece. The wire to be used for surfacing at this time is fed through the y-piece to the processing head through the welding nozzle into the process zone. The change between the two powders takes place directly via the powder feeder: The volumetric feeder therefore has two separate powder containers and two separately controllable metering units. A slider device can be used to change between wire and powder materials in the material feed.
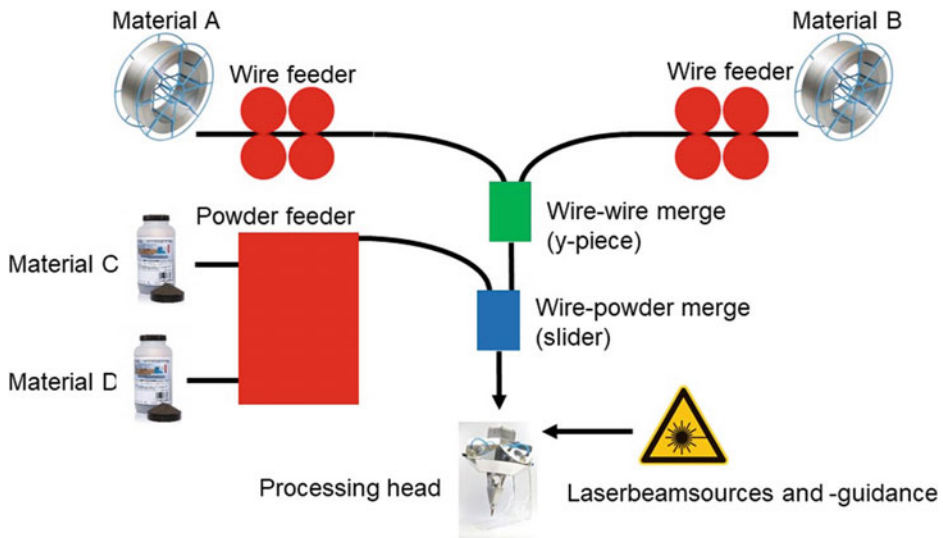
Fig. 18 Principle of the system technology

5.2   Design of Systems Technology

Pure copper is used as the basic material for the beam splitter, which is coated with a gold layer as well as a protective layer. This form of beam delivery enables the use of a laser power of up to 4 kW at a wavelength of around 1 µm in cw mode. Due to the reflective design, other wavelengths can also be used. For the processing of glass, for example, mid to far IR lasers with wavelengths from 5 to 10.6 µm and powers up to more than 500 W can be used. With conductive preheating of the wire, the amount of laser power can be reduced with the same welding result. The system can process metal wires with diameters from 0.6 to 1.6 mm, which can be preheated with a current intensity of up to 200 A. [28]

In order to control the temperature of the processing head as effective as possible, it has a total of six cooling water zones including fiber connector, collimating unit and welding nozzle (Fig. 19). The processing head has a total weight of approx. 10 kg without peripherals like holder, wire feed unit and collimator. [28]

5.3   Tests Performed and Results

As part of the development of the system technology, various tests were carried out to determine unknown requirements and design specifications of the hardware. The experiments include welds of metal materials in powder and wire form and glass materials in fiber form. Two setups were used: One for use with solid-state laser beam sources in the
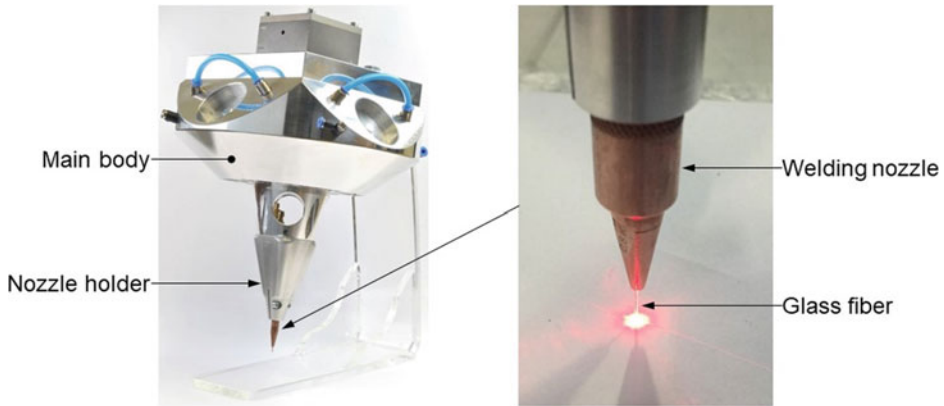
Fig. 19 Coaxial multi-wavelength processing head (left) and close up of its welding nozzle with a fused silica fiber and a red laser pointer showing (right) [28, 50]

1 µm wavelength range for processing metals, and another one for use with gas lasers in the 5–10.6 µm range to process glass materials. Subsequently, a combined system was developed that maps both processes. Furthermore, two wire feeding units as well as a merging unit were implemented so that metal wires and glass fibers can be fed to the deposition process and changed automatically. Commercially available system technology was used for powder conveying. The tests demonstrate the feasibility of the project and show the potential of the system technology. The results are presented below.

5.3.1 Laser Metal Deposition

Figure 20 shows the processing head (left) during the processing of a round bar made of mild steel to which structures made of martensitic chromium-silicon steel are applied using laser wire deposition. The wire diameter used is 0.8 mm and the alloy used is
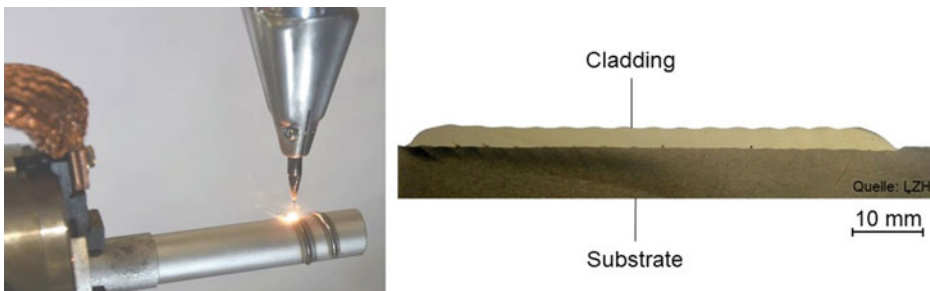
Fig. 20 Cladding of martensitic chromium-silicon steel on a mild steel substrate by coaxial laser-wire deposition: process photo (left) and cross section of the manufactured part (right) [78]

1.4718 (X45CrSi9-3). The diameter of the round bar used as a substrate is 30 mm and is made of the mild steel 1.0402 (C22). A diode laser with a wavelength in the range 1020–1060 nm was used and a laser power of 1400 W was set. The cross-section of the finished part (right) shows good adhesion of the applied layer to the base material without critical cracks or pores. The result is a homogeneous weld penetration depth and a degree of dilution of less than 5% as well as a surface hardness of approx. 59 HRC. By means of the welding head, cladding processes, repairs as well as the generative manufacturing of structures with wall thicknesses in the range of millimeters can be generated using the wire-based process. [78]

A process photograph (left) and the result of the coaxial laser powder weld process (right) are shown in Fig. 21. A copper-molybdenum powder with 80% pure copper content is used as the cladding material. The particle sizes of the spherical powder particles are between 45 and 125 µm. A nozzle with a capillary tube with 600 µm inner diameter is used as the powder feed. A fiber laser with a wavelength of 1070 nm is used as the beam source and a laser power of 200 W is set. The axis feed rate is set to 600 mm/min. The laser spot diameter and thus the approximate diameter of the melt pool on the workpiece surface is 0.6 mm. Coaxial laser powder deposition with central powder feed via a capillary tube shows great potential with regard to powder utilization of up to 30% at a wall thickness of about 600 µm. The high powder utilization is achieved by the reduction of the free jet-length of the exiting powder gas stream, even with small laser
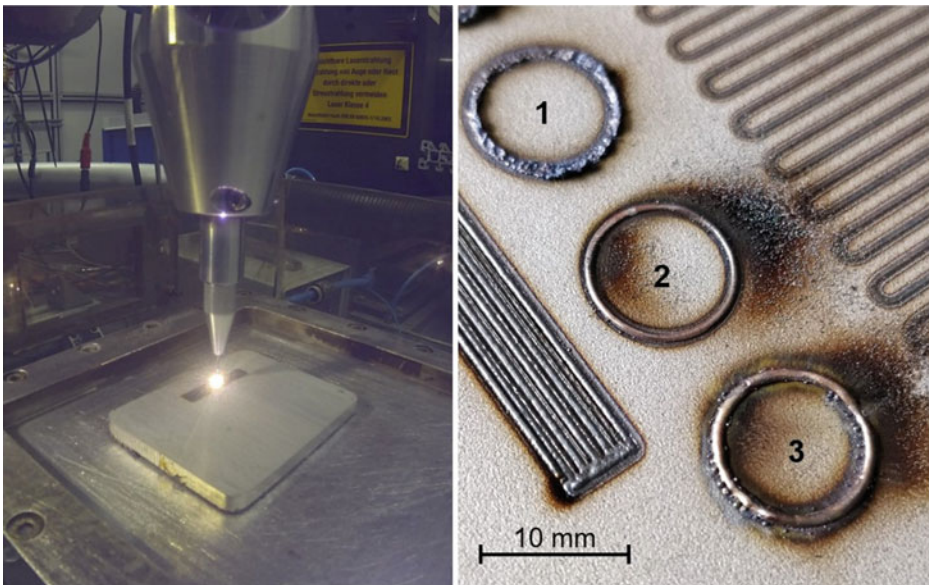
Fig. 21 Powder LMD process using central material feed via a capillary nozzle: process photo (left) and deposited structures (right) [48]

spot diameters and thus small melt pool dimensions. The process can be used to produce filigree structures from materials with good thermal conduction properties. For example, heat sinks and holders for optical elements can be manufactured. [48]

5.3.2 Laser Glass Deposition

A CO_2 laser beam source with a wavelength of $10.6\,\mu m$ is used for the experiments on coaxial additive manufacturing of glass materials. A quartz glass fiber (SiO_2) with a diameter of 400 μm and a polymer coating with a thickness of 50 μm is used as the deposit material. This results in a total diameter of the fiber of 500 μm. An oxygen gas stream is supplied via the welding nozzle. The combination of the oxygen and the laser radiation burns and therefore removes the polymer coating from the fiber. Compressed air is used as a sealing gas to protect the optics in the processing head. A 1 + 1 roller wire conveyor (see Sect. 4.4.2) driven by a stepper motor is used to convey the fiber. The fiber is fed via a PTFE core, which connects the wire conveyor to the welding nozzle. [28]

In the course of the experiments, a welding layer of quartz glass can be deposited on a glass substrate by means of the coaxial processing head. For this purpose, a laser power of 67.5 W, a wire feed speed of 600 mm/min and a feed speed of the processing head over the substrate of 100 mm/min are used. The weld result is shown in Fig. 22. Small cracks and pores can be seen in the area of the starting point (top right in the picture). After the process has stabilized, a uniform seam geometry is created (top center). At the end of the seam (top left), a superelevation is created. Indentations appear at the edges of the deposited seam, which are caused by sublimation of the glass material by the laser radiation. For further tests, a larger focal diameter of the laser beam should therefore be
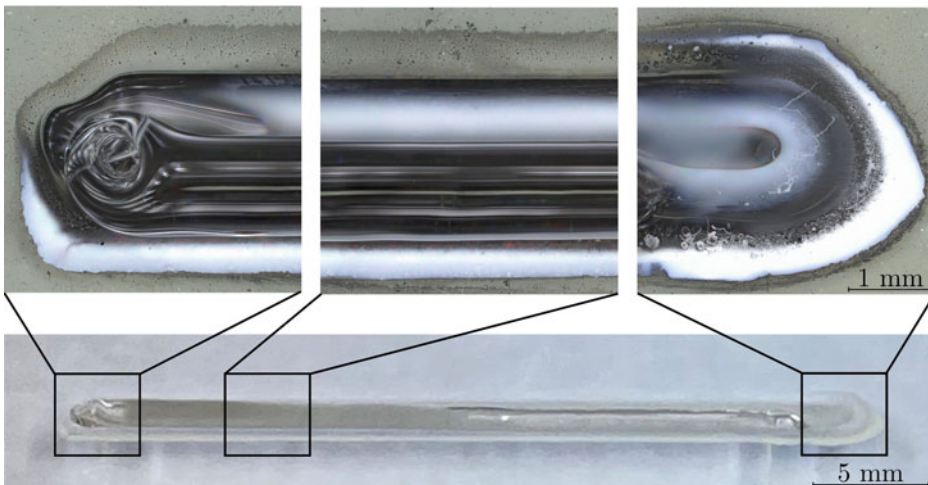
Fig. 22 Quartz glass substrate with a deposited fused silica glass fiber: the manufacturing process proceeded from right to left [50]

selected to counteract this effect. In general, the tests show that coaxial processing of quartz glass fibers by means of coaxial laser cladding is possible. [50]

5.3.3 Feeding of Deposition Material

Appropriate material handling system technology is required to introduce the deposition material into the process zone (see Sect. 4.4). The deposition material includes metal wire and powder, and glass fiber. Since appropriate technology is commercially available for the conveying of metal wires and powder materials, the conveying of glass fibers is primary elaborated here. A setup as shown in Fig. 12 was used to determine the feeding specifications of a glass fiber compared to a metal wire.

In the tests, the maximum conveying force achieved by the feed unit is to be determined first. Subsequently, measurements are carried out to determine which forces are required for conveying from the material storage (wire or fiber spool) and for transporting through the conveyor section to the processing head (core). For an acrylate-coated quartz glass fiber with an outer diameter of 0.5 mm, a maximum conveying force of 14 N can be achieved with a 2 + 2 roller drive (see Sect. 4.4.2) and pressure rollers made of polyurethane. On one hand, this has to overcome the force required to unwind the fiber from the roller in the amount of up to 0.28 N, as well as the force required for a further conveying of the fiber through the core to the process zone. The tests showed that both tested cores made of PA and PTFE can be used. PTFE is the preferred material for small bending radii of the core (100 mm) due to the specific conveying force required. Another aspect is the fact that PA has a significantly higher water absorption, which can result in different material properties under different environmental conditions. For the PTFE core with a bending radius of 100 mm, the specific conveying force is 0.0714 N/m (with a standard deviation of 0.00470 N/m for this series of measurements). If this value is compared with the achievable conveying force minus the force required for unwinding, this results in a theoretical maximum conveying distance (PTFE core) of pprox. 192 m. With a 1 + 1 roller drive, this distance is reduced to pprox. 109.5 m. Since in practice further elements such as welding nozzles or connecting pieces must also be overcome, this value will effectively be lower. In addition, the lifting work resulting from height differences may have to be included in the calculation for long distances. However, since typical welding systems have conveying distances in the range of up to several meters, conveying glass fibers to a processing head is feasible with the presented experimental setup. [40]

The maximum conveying force achieved with a 1 + 1 roller drive for steel wires with an outer diameter of 1 mm is 98.2 N, which is significantly higher compared to glass fibers. However, with metal wires, the conveying force of 4.55 N required for unwinding is also significantly higher. When conveying through tight radii, a PTFE core is also preferable due to the lower specific conveying force of 3.97 N/m at a bending radius of 100 mm. Here, the conveying length theoretically achievable with the setup is pprox. 23.6 m. [40]

For precise, uniform and, if necessary, force-controlled conveying of glass fibers, it is advisable to position the feed unit as close as possible to the processing head. However, compared to wire, longer conveying distances can be realized without the need for a push–pull system. In addition, a 1 + 1 roller drive with a polyurethane pressure roller as well as a steel drive roller is sufficient for conveying glass fibers. Also, with small bending radii of 100 mm, no plastic deformation occurs with glass fibers in opposite to metal wires. [40]

5.3.4 Changing of Deposition Material

Since appropriate system technology is commercially available for the changing between powder materials, the changing of glass fibers to metal wires and vice versa is elaborated here. With the system developed in the mGROTESK subproject it is also possible to switch between different metal wires and/or between different glass fibers. The changing system can be used to create hybrid components with areas made of different materials (Fig. 23).

The first changing tests were carried out at a feeding speed of 4 m/min, resulting in a changeover time from one material to the other of 21 s. The first test was aborted after 53 cycles because the wire was no longer transported through the system to the pneumatic shears. The reason for this was wear of the welding nozzle tip. Cutting the wire with the pneumatic shears leads to a burr on the wire. This damaged the tip on every cycle and little chips are released from it. Therefore the wire is being blocked and further transport to the pneumatic shears is no longer possible. This results in a breakage of the glass fiber, which means that no further change is possible. Due to this, another proximity sensor, which is placed in front of the Y-piece and only allows the medium to be fed into the system when no wire or fiber is detected by the sensor. The test was repeated with a new welding nozzle tip. In this case, the test was aborted again after 60 cycles, since
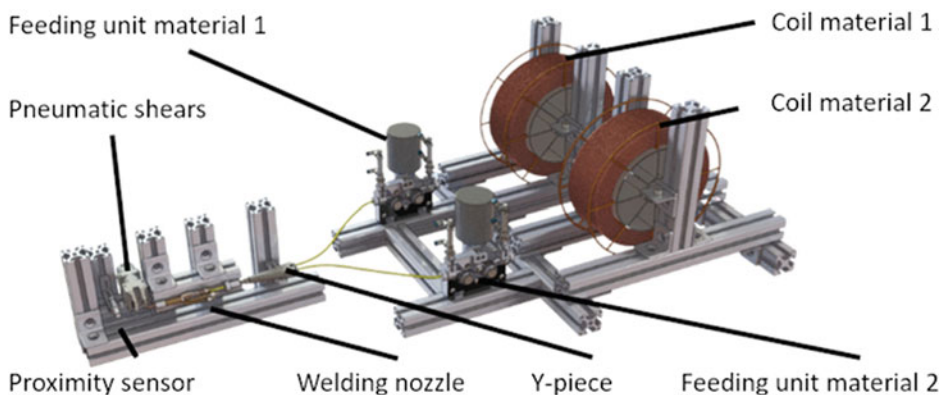
Fig. 23 Trial-setup for automated changing of wire-shaped deposition materials [70]

once again the wire was no longer transported to the shears due to the same error. It can be concluded that the nozzle tip, which is a wearing part, must be replaced when using metal wire material after approximately 50 changes in order to prevent an error. Observations have revealed another weak point of the system: When pulling the weld material backwards, the wire and fibers are only fed out of the feeder and not rewound, which allows the material to slip off the side of the coil. This is another possibility for a failure, especially when the distance between the y-piece and the welding nozzle is high. [70]

6   Summary and Outlook

6.1   Summary

The chapter "Development of system technology for coaxial laser material deposition of optical, thermal and structural components" describes the fundamentals of laser system technology for the build-up welding of multi-materials, primarily metal and glass materials. The system technology required for processing is considered holistically, with a special focus on the processing heads used. Commercially available solutions are analyzed and characteristics are summarized for a better overview. In this context, a differentiation is made between laser technology, weld metal handling and the mechanical handling system. Systems that enable the conveying of metal powders as well as wire-shaped metal and glass materials are examined, as these are of particular importance for the production of optical, thermal and structural components. In addition, corresponding beam sources are described that enable the processing of suitable metal alloys and glass materials.

Furthermore, the development of a processing system is described, which allows the processing of glass and metal materials within one manufacturing environment. Since the application is the fabrication of integrated opto-mechanical systems, this system has the capability to produce filigree metal structures from powder as well as highly transparent structures from quartz glass. With the special coaxial beam guidance and four individual beams generated via a reflexive beam splitter, both, solid-state lasers in the 1 μm wavelength range and gas lasers in the 5 μm (CO) to 10.6 μm (CO_2) wavelength range can be used. The system consists, among other things, of a processing head in which elements for beam guidance and for handling deposition materials in wire and powder form are implemented. Furthermore, a wire handling system was developed, which consists of several wire conveyors as well as an exchange device, so that it can be used to switch between metal wires and glass fibers. The potential of the whole system was successfully demonstrated in initial tests.

6.2 Outlook

In the further course, the developed system technology consisting of processing head with appropriate beam guidance for the use of gas and solid-state lasers with integrated multi-material welding nozzle and the developed wire conveyor technology will be used for experiments. As part of the trials, other structures made of glass and metal materials will be created using the system. The processing of the two groups of materials within a single component, i.e. the welding of glass on metal and vice versa, is also to be tested. Also, trials regarding the change between powder and wire materials will be carried out. The knowledge gained from the trials is to be incorpoeted to an improved design for the system technology. In addition, the system technology is to be offered commercially and thus made available to a large circle of end users.

EUROPÄISCHE UNION
Europäischer Fonds für
regionale Entwicklung

References

1. Kaierle, S., Barroi, A., Noelke, C., Hermsdorf, J., Overmeyer, L., Haferkamp, H.: Review on laser deposition welding: From micro to macro. Physics Procedia **39**(2012), 336–345 (Lane 2012, Elsevier B.V, 2012).
2. Rafiee, M., Farahani, R. D., Therriault, D.: Multi-material 3D and 4D printing: A survey. Adv. Sci. **7**, 1902307 (WILEY-VCH Verlag GmbH & Co. KGaA, Weinheim, 2020)
3. Schneberger, J.-H., Häfele, T., Kaspar, J., Vielhaber, M.: Hybrid Additive manufacturing—requirements engineering framework for process chain considerations. In: Proceedings of the 22nd International Conference on Engineering Design (ICED19), Delft, The Netherlands, 5–8 August 2019 (2019). https://doi.org/10.1017/dsi.2019.372
4. Aversa, A., Fino, P.: Special issue on materials development by additive manufacturing techniques. Appl. Sci. 2020, **10**, 5119 (MDPI, Basel, Switzerland, 2020). https://doi.org/10.3390/app10155119

5. Frigger, M., Müller-Czygan, G.: Was ist Systemtechnik? Einer zukunftsweisenden Methodik auf der Spur. Whitepaper der HST Systemtechnik GmbH & Co. KG, Meschede (2019)
6. VDI 2206: VDI-Richtlinie: Entwicklungsmethodik für mechatronische Systeme (2004)
7. Gräßler, I., Hentze, J., Bruckmann, T.: V-models for interdisciplinary systems engineering. In: Marjanovic, D. (Hrsg.), Storga, M. (Hrsg.), Pavkovic, N. (Hrsg.), Bojcetic, N. (Hrsg.), Skec, S. (Hrsg.) Proceedings of the DESIGN 2018 15th International Design Conference, S. 747–756 (2018). https://doi.org/10.21278/idc.2018.0333
8. Knöchelmann, M., Ley, P.-P., Kloppenburg, G., Mozgova, I., Lachmayer, R.: Methodische Entwicklung eines opto-mechatronischen Systems am Beispiel eines hochadaptiven Fahrzeugscheinwerfers. In: Tagungsband der VDI Fachtagung Mechatronik 2019. Universität Padeborn, Paderborn (2019)
9. Ley, P.-P. et al.: Development methodology for optomechatronic systems using the example of a high-resolution projection module. In Proceedings of the 22nd International Conference on Engineering Design (ICED19), Delft, The Netherlands, 5–8 August 2019 (2019). https://doi.org/10.1017/dsi.2019.261
10. Ley, P., August, J., Lachmayer, R.: Design tool to develop highly efficient optomechatronic systems. Proc. Des. Soc. Des. Conf. **1**, 305–314 (2020). https://doi.org/10.1017/dsd.2020.270
11. VDI 2221: VDI-Richtlinie: Design of technical products and systems—Model of product design (2019)
12. VDI 2225 Blatt 3, VDI-Richtlinie: Design Engineering Methodics—Engineering Design at Optimum Cost—Valuation of Costs (1998)
13. REFA: Industrial Engineering—Standardmethoden zur Produktivitätssteigerung und Prozessoptimierung, Carl Hanser (2011). ISBN-10 3-46-43062-8
14. Xu, X.F., Bates, P.J., Zak, G.: Effect of glass fiber and crystallinity on light transmission during laser transmission welding of thermoplastics. Optics Laser Technol. **69**(June 2015), 133–139 (2014). https://doi.org/10.1016/j.optlastec.2014.12.025
15. Reza, F., Katayoun, K.A.M., Farzaneh, A., Nikoo, T.: Laser in orthodontics. In: Principles in Contemporary Orthodontics (InTech, 2011). https://doi.org/10.5772/20204
16. Patschger, A.: Grundlegende Untersuchungen zum Prozessverständnis des Laserstrahl-Mikroschweißens von metallischen Folien. In: Bergmann, J.P.: Fertigungstechnik – aus den Grundlagen für die Anwendung, Schriften aus der Ilmenauer Fertigungstechnik Band 3, Universitätsverlag Ilmenau (2016)
17. Hipp, D.: Einkopplung von Laserstrahlung unter Prozessbedingungen der Materialbearbeitung - Entwicklung einer Bestimmungsmethodik und Ergebnisse, Technische Universität Dresden (201). https://nbn-resolving.org/urn:nbn:de:bsz:14-qucosa2-724992
18. Prasad, H.S.: Phenomena in material addition to laser generated melt pools. Luleå University of Technology, Luleå, Sweden (2019)
19. Murr, L. E., Johnson, W. L.: 3D metal droplet printing development and advanced materials additive manufacturing. Brazilian Metallurgical, Materials and Mining Association. Published by Elsevier Editora Ltd. (2016). https://doi.org/10.1016/j.jmrt.2016.11.002
20. Da Silva, A., Frostevarg, J., Volpp, J., Kaplan, A.F.H.: Additive Manufacturing by laser-assisted drop deposition from a metal wire. Mater. Des. **209**(2021), 109987 (2021). https://doi.org/10.1016/j.matdes.2021.109987
21. Halisch, C., Radel, T., Tyralla, D., Seefeld, T.: Measuring the melt pool size in a wire arc additive manufacturing process using a high dynamic range two-colored pyrometric camera. Welding World (2020). https://doi.org/10.1007/s40194-020-00892-5
22. Eimer, E., Suder, W., Williams, S., Ding, J.: Wire laser arc additive manufacture of aluminium zinc alloys. Welding World (2020). https://doi.org/10.1007/s40194-020-00872-9

23. Kotz, F., Helmer, D., Rapp, B.E.: 3D printing of transparent glasses. In: Heinrich, A. (ed.) 3D printing of optical components. Springer series in optical sciences, vol. 233 (Springer Nature, Switzerland AG, 2021). https://doi.org/10.1007/978-3-030-58960-8

24. Rettschlag, K., Kranert, F., Hohnholz, A., Wienke, A., Suttmann, O., Neumann, J., Kracht, D., Lachmayer, R.: Laser deposition of fused silica coreless fibers to generate functional waveguides. In: Lasers in Manufacturing Conference 2019 (2019)

25. Grabe, T., Rettschlag, K., Wang, S., Lachmayer, R. (eds.): Modellierung und Evaluation thermischer Effekte für die laserbasierte Additive Fertigung von funktionalen Glaswellenleitern, Konstruktion für die Additive Fertigung 2020 (Springer Vieweg, Berlin, Heidelberg, 2020)

26. Pohl, L., von Witzendorf, P., Chatzizyrli, E., Suttmann, O., Overmeyer, L.: CO_2 laser welding of glass: Numerical simulation and experimental study. Int. J. Adv. Manuf. Technol. **90**(1–4), 397–403 (2017)

27. von Witzendorf, P., Pohl, L., Suttmann, O., Heinrich, P., Heinrich, A., Zander, J., Bragard, H., Kaierle, S.: Additive manufacturing of glass: CO_2-Laser glass deposition printing in [Procedia CIRP 74], **74**, 272–275 (2018)

28. Lammers, M., Hermsdorf, J., Kaierle, S., Ahlers, H.: Entwicklung von Laser-Systemkomponenten für das koaxiale Laser-Draht-Auftragschweißen von Metall- und Glaswerkstoffen, in Konstruktion für die Additive Fertigung 2019, 245–260. Springer, Berlin Heidelberg (2020)

29. Luo, J., Gilbert, L.J., Bristow, D.A., Landers, R.G., Goldstein, J.T., Urbas, A.M., Kinzel, E.C.: Additive manufacturing of glass for optical applications. In: Gu, B., Helvajian, H., Piqué, A. (eds.) Laser 3D Manufacturing III, SPIE Proceedings, 97380Y, SPIE (2016)

30. Kelbassa, J., Gasser, A., Pirch, N.: Wire vs. Powder in LMD, Presentation at LAM 2018, 29 March 2018 (Fraunhofer ILT, Schaumburg, 2018)

31. Brocke, N.: 3D-Generieren mit ProFocus Direktdioden- Laser für Pulver und Draht, https://oscar-plt.de/wp-content/uploads/2020/07/Flyer_ProFocus.pdf (OSCAR PLT GmbH). Date of last access 20 Sept 2021

32. Hummel, M., Schöler, C., Häusler, A., Gillner, A., Poprawe, R.: New approaches on laser micro welding of copper by using a laser beam source with a wavelength of 450 nm. J. Adv. Joining Process. **1** (2020). https://doi.org/10.1016/j.jajp.2020.100012

33. Serafini, V., Riva, M., Pippione, G., Mirigaldi, A., Coriasso, C., Codato, S., Gotta, P., Maina, A., Paoletti, R., Perrone, G.: Compact high-brightness and highly manufacturable blue laser modules. In: Proceeding of SPIE 11668, High-Power Diode Laser Technology XIX, 116680J (10 Mar 2021) (2021). https://doi.org/10.1117/12.2583229

34. Lee, H., Lim, C.H.J., Low, M.J., Tham, N., Murukeshan, V.M., Kim, Y.J.: Lasers in additive manufacturing: A review. Int. J. Precision Eng. Manuf. Green Technol. **4**(3), 307–322 (2017). https://doi.org/10.1007/s40684-017-0037-7

35. Fraunhofer IWS COAXwire. https://www.iws.fraunhofer.de/de/technologiefelder/thermische_oberflaechentechnik/auftragschweissen/systemtechnik/COAXwire.html. Date of last access 20 Sept 2021

36. Fraunhofer IWS COAXwire mini. https://www.iws.fraunhofer.de/de/technologiefelder/thermische_oberflaechentechnik/auftragschweissen/systemtechnik/COAXwire_mini.html, Date of last access 20 Sept 2021

37. Walters, C., Hay, J., Ream, S.: Fully reflective, coaxial laser wire additive manufacturing, A focusing optic in development enables very high laser power capability in wire additive manufacturing. https://www.iws.fraunhofer.de/de/technologiefelder/thermische_oberflaechentechnik/auftragschweissen/systemtechnik/COAXwire_mini.html, Date of last access 20 Sept 2021

38. Fraunhofer ILT. https://www.ilt.fraunhofer.de/content/dam/ilt/en/documents/annual_reports/AR16/TF2/AR16_P64_coaxial-wire-feed-laser-metal-deposition.pdf, Date of last access 20 Sept 2021
39. Precitec coax printer. https://www.precitec.com/de/laserschweissen/produkte/bearbeitungskoepfe/coax-printer/, Date of last access 20 Sept 2021
40. Lammers, M., Biester, K., Hermsdorf, J., Kaierle, S., Ahlers, H.: Förderung von stabförmigen Schweißzusatzstoffen für das koaxiale Laserauftragschweißen von Glas- und Metallwerkstoffen, in: Tagungsband 4. Symposium Materialtechnik, 25. Bis 26. Februar 2021, Band 10, Clausthaler Zentrum für Materialtechnik, TU Clausthal (2021).
41. Meltio M450. https://meltio3d.com/technology/, Date of last access 20 Sept 2021
42. Eppich, B.: Laser beam characterization, Präsentation LA3NET—Workshop Aachen 2013, Leibniz Ferdinant-Braun-Institut (2013)
43. Rung, S., Barth, J., Hellmann, R.: Characterization of laser beam shaping optics based on their ablation geometry of thin films. Micromachines **2014**(5), 943–953 (2013). https://doi.org/10.3390/mi5040943
44. Eichler, J., Dünkel, L., Eppich, B.: Die Strahlqualität von Lasern, Wie bestimmt man Beugungsmaßzahl und Strahldurchmesser in der Praxis? www.laser-journal.de (LTJ, 2004)
45. Kroyan, A., Lalovic, I., Farrar, N.: Effects of 95% integral vs. FWHM bandwidth specifications on lithographic. In: Imaging, September 2001 Proceedings of SPIE—the international society for optical engineering (2001). https://doi.org/10.1117/12.435661
46. ISO 11146: Lasers and Laser-Related Equipment—Test Methods for Laser Beam Parameters—Beam Widths, Divergence Angle and Beam Propagation Factor (International Standard, 1998)
47. Liu, S., Zhang, Y., Kovacevic, R.: Numerical simulation and experimental study of powder flow distribution in high power direct diode laser cladding process. Springer, New York (2015)
48. Lammers, M., Bernhard, R., Neef, P., Wiche, H., Hoff, C., Hermsdorf, J., Kaierle, S., Ahlers, H., Wesling, V.: Koaxiales Laser-Pulver-Auftragschweißen mit zentraler Schweißgutzufuhr über ein Kapillarröhrchen zur Steigerung der Pulverausnutzung, erschienen. In: Konstruktion für die Additive Fertigung 2020 (Springer, 2020)
49. Arrizubieta, J.I., Ruiz, J.E., Martinez, S., Ukar, E., Lamikiz, A.: Intelligent nozzle design for the laser deposition process in the industry 4.0. In: Manufacturing Engineering Society International Conference 2017, MESIC 2017, 28–30 June 2017, Vigo (Pontevedra) Spain (2017)
50. Grabe, T., Lammers, M., Wang, S., Wang, X., Rettschlag, K., Sleiman, K., Barroi, A., Biermann, T., Ziebehl, A., Röttger, J., Ley, P.-P., Wolf, A., Jaeschke, P., Hermsdorf, J., Kaierle, S., Ahlers, H., Lachmayer, R.: Additive anufacturing of fused silica using coaxial laser glass deposition: experiment, simulation and discussion. In: Proceeding of SPIE 11677, Laser 3D Manufacturing VIII, 116770Z (8 Mar 2021) (2021). https://doi.org/10.1117/12.2577205
51. Luo, J.: Additive manufacturing of glass using a filament fed process. Dissertation, Missouri, USA (2017)
52. Schuler, V., Twrdek, J.: Praxiswissen Schweißtechnik. Werkstoffe, Prozesse, Fertigung. 6. Aufl. Springer Vieweg Verlag. Wiesbaden 2019, S. 56 (2019)
53. Matthes, K.-J., Schneider, W. (Hrsg.): Schweißtechnik. Schweißen von metallischen Konstruktionswerkstoffen. 6. Aufl. Carl Hanser Verlag. München 2016, S. 87ff. (2016)
54. Jeffus, L.: Welding. Principles and Applications. 9. Aufl. Cengage Learning 2020, S. 297 (2020)
55. Dilthey, U.: Schweißtechnische Fertigungsverfahren 1. Schweiß- und Schneidtechnologien. 3. Aufl. Springer Verlag Berlin Heidelberg, S. 83 (2006)
56. Von Witzendorff, P., Pohl, L., Suttmann, O., Heinrich, P., Heinrich, A., Zander, J., Bragard, H., Kaierle, S.: Additive manufacturing of glass: CO_2-Laser glass deposition printing. In: Procedia CIRP 74, S. 272–275 (2018)

57. Rettschlag, K., Kranert, F., Hohnholz, A., Wienke, A., Suttmann, O., Neumann, J., Kracht, D., Lachmayer, R.: Laser deposition of fused silica coreless fibers to generate functional waveguides. Lasers Manuf. 2019 (LiM 2019) (2019)
58. Dzelnitzki, D.: Schweißen von Leichtmetallen verlangt modifizierte Prozesse. Was ein Drahtvorschub-System zum Laserschweißen leisten muss. Laser Technik J **5**(5), S. 36–39 (2008)
59. Klingbeil, N.: Untersuchung des Drahtsystems zur Prozessstabilisierung für das drahtbasierte Laserauftragschweißen in der additiven Fertigung, Dissertation, Aachen (2019)
60. DVS Media GmbH (Hrsg.): Drahtförderschlauch Rolliner mindert Reibung und Verschleiß. In: SCHWEISSEN UND SCHNEIDEN, S. 656–657 (2007)
61. EUTECT GmbH: Sensitive Wire Feeder (SWF), https://eutect.de/modulare-loetautomation/verbindungstechnik/drahtvorschuebe/swf/. Date of last access 21Sept 2021
62. Pamin, S., Grafe, M., Lammers, M., Hermsdorf, J., Kaierle, S., Overmeyer, L.: Rotary straightening of fine wire for LMD-W applications. In: Lasers Manufacturing Conference 2021 (2021)
63. GTV Verschleißschutz GmbH: Pulverförderer Serie Pf, Für jede Anwendung die passende Lösung, https://www.gtv-mbh.com/cms/upload/downloads/pulverfoerderer-de.pdf. Date of last access 27 Sept 2021
64. Schweitzer-Karababa, Iris: Explosionsschutz an Staubarbeitsplätzen, baua: Bundesanstalt für Arbeitsschutz und Arbeitsmedizin (Hrsg.), Aktuelles zum Gefahrstoffrecht—September 2015 (2015)
65. Jacob, H.-J.: Pulververarbeitung unter Staub- und Gas-Ex-Bedingungen. In: Technische Sicherheit Bd. 9 (2019) Nr. 07/08 - Juli/August. Special: Explosionsschutz, Ballrechten-Dottingen (2019)
66. SuvaArbeitssicherhei (Hrsg.): Explosionsschutz – Grundsätze, Mindestvorschriften, Zonen, Bereich Chemie, 5., überarbeitete Auflage – Juli 2008 (2008)
67. Vetter, G.: Handbuch Dosieren. Vulkan-Verlag, Essen (1994)
68. Schopphoven, T.: Experimentelle und modelltheoretische Untersuchungen zum Extremen Hochgeschwindigkeits-Laserauftragschweißen, Dissertation, FRAUNHOFER VERLAG (2019)
69. Zeppelin Systems GmbH (Hrsg.): DER WEG IST UNSER ZIEL, Innovative Fördersysteme, Werbebroschüre. https://www.zeppelin.com/content/dam/zeppelin/anlagenbau/footer/downloads/04_prozessl%C3%B6sungen/Zeppelin-Systems-06-F%C3%B6rdertechnik.pdf, Date of last access 27 Sept 2021
70. Lammers, M., Biester, K., Schwarz, N., Hermsdorf, J., Kaierle, S., Ahlers, H.: Automatic changing of weld deposit for additive manufacturing of hybrid metal-glass components using direct laser deposition, Lasers in Manufacturing Conference 2011, München, Wissenschaftliche Gesellschaft Lasertechnik e. V. (2021)
71. Infineon Technologies AG (Hrsg.): Grundlagen der Robotik, Website: https://www.infineon.com/cms/de/discoveries/grundlagen-robotics/. Date of last access 27 Sept 2021
72. VDI 2860: Assembly and handling; handling functions, handling units; terminology, definitions and symbols, VDI-Gesellschaft Produktion und Logistik (1990)
73. Picum, M.T., GmbH (Hrsg.): Maschinensysteme für die mobile Präzisionsbearbeitung, Website: https://picum-mt.com/de/home-de/, Date of last access 27Sept 2021
74. Jung, S., Backes, G.: Koaxiale Pulverdüsen Präzise und effizient, Fraunhofer ILT (Hrsg.). https://www.ilt.fraunhofer.de/content/dam/ilt/de/documents/Leistungsangebote/lasermaterialbearbeitung/HZ_Koaxiale%20Pulverdu%CC%88sen_de.pdf. Date of last access 30 Sept 2021
75. Hillig, H.: Modulares Pulverdüsensystem COAXn, Fraunhofer IWS (Hrsg.). https://www.iws.fraunhofer.de/de/technologiefelder/thermische_oberflaechentechnik/auftragschweissen/systemtechnik/COAXn.html. Date of last access 30Sept 2021

76. Dickler, H.,Tharmakulasingam, S.: HIGHNO 4.0 – KOAXIALE PULVERZUFUHRDÜSE, HD Sonderoptiken für die Lasertechnik (Hrsg.). http://www.hd-sonderoptiken.de/de/documents/Produktblatt%20-%20HighNo%204.0.pdf. Date of last access 30 Sept 2021
77. Precitec GmbH & Co. KG (Hrsg.): Laserauftragschweißen mit Metallpulver – Fokussieroptiken YC30|YC52, https://www.precitec.com/de/laserschweissen/produkte/bearbeitungskoepfe/yc30/. Date of last access 30 Sept 2021
78. Lammers, M., Budde, L., Barroi, A., Hermsdorf, J., Kaierle, S.: Entwicklung von Laser-Systemkomponenten optimiert für die additive Fertigung mittels SLM. In: Konstruktion für die Additive Fertigung 2018, ISBN: 978-3-662-59057-7 (Springer Berlin Heidelberg, 2019)

Index